DYNAMICS AND SECURITY OF COMPLEX CLUSTERED NETWORK SYSTEMS

by

Liang Huang

A Dissertation Presented in Partial Fulfillment
of the Requirements for the Degree
Doctor of Philosophy

ARIZONA STATE UNIVERSITY

December 2008

DYNAMICS AND SECURITY OF COMPLEX CLUSTERED NETWORK SYSTEMS

by

Liang Huang

has been approved

October 2008

Graduate Supervisory Committee:

Ying-Cheng Lai, Chair
Juan M. Lopez
Tolga M. Duman
Junshan Zhang
Richard Akis

ACCEPTED BY THE GRAUDATE COLLEGE

ABSTRACT

Networks with a community (or cluster) structure underlie many social and biological phenomena. In such a network, individuals tend to form sparsely linked local communities, each having dense internal connections. This dissertation explores the different dynamics of complex clustered networks, revealing a new set of rules that show how the dynamic properties are affected by the clustered structures.

The dynamics of information propagation on clustered networks is studied by using a three-state epidemic model with a unit spreading rate. A resonance-like phenomenon is uncovered: the information lifetime on the network can be maximized by the number of clusters.

Synchronization in complex, clustered random networks is found to be determined by the interplay between inter-cluster and intra-cluster links. The network is most synchronizable when the numbers of the two types of links are approximately equal. In the presence of a mismatch, increasing the number of intra-cluster links, while making the network distance smaller, can suppress or even destroy the synchronization. For clustered networks with regular subnetworks, as the density of intra-cluster links is increased, the network exhibits strong and weak synchronizability in an alternating manner. A theory based on analyzing the eigenvalues and eigenvectors of the coupling matrix is provided to explain this phenomenon. For gradient clustered networks, the synchronizability can be optimized by the strength of the gradient field. A remarkable finding is that, if the gradient field is sufficiently strong, synchronizability of the network is mainly determined by the properties of the subnetworks in the two largest clusters.

A model of cascading in complex clustered networks based on physical analysis and numerical computations is developed for the key ingredients of traffic dynamics in typical clustered networks. An effective strategy is proposed for preventing cascading breakdown.

By focusing on network synchronizability, it is found that globally coupled networks and random networks are scalable, but locally coupled regular networks are not. Scale-free networks are scalable for certain types of node dynamics. For a typical clustered network, as its size is increased, the synchronizability can be maintained or even enhanced but at the expense of deterioration of the clustered characteristics.

This dissertation is dedicated to my family

ACKNOWLEDGMENTS

I would like to thank my advisor, Dr. Ying-Cheng Lai, for his insights on selecting topics, and for his persistent help and support that made everything that I have achieved toward my PhD degree possible. Also, his open mind, precise insights and meticulous attitude on doing research have educated me with good disciplines that would help a lot in my future works.

I also owe a lot of thanks to Qingfei Chen, Kwangho Park, Rui Yang, Xiaojuan Ma, Yan Wang, Lin Du, Wenxu Wang, Xingang Wang, Jesús M. Seoane, and Mary Ann F. Harrison for fruitful collaborations and discussions that broadened the scope of my knowledge. With all these friends' encourage and help, life was much easier and abounded with joyful memories.

I thank Dr. Junshan Zhang for his insights and discussions that made our collaboration productive. Special thanks are due to Dr. Juan M. Lopez, Dr. Tolga M. Duman, Dr. George Pan, Dr. Dieter K. Schroder *et al.* for their illuminating instructions which lifted my knowledge on the specific topics significantly. They have already benefited me in my research projects.

I would like to thank Dr. David K. Ferry, Dr. Richard Akis, and Dr. Stephen M. Goodnick among others in the Center for Solid State Electronics Research for their constructive suggestions recently on my project of graphene.

I would also like to thank all my committee members, for their precious time reading and commenting on my dissertation.

My wife Tianming's constant love and pleasant mood bring me joy and confidence, which renew me to be ready for next day's work.

I would like to thank my parents for their unconditionally love and support that have shaped me to the man that I am now.

There are many many others, some of those whose names I even don't know, helped me and enlightened me in both daily living and academic through my studies. I owe them a lot of thanks too.

TABLE OF CONTENTS

Page

LIST OF TABLES

LIST OF FIGURES

Figure Page

1 . INTRODUCTION

1.1. Concept of complex clustered networks

Networks with a community structure, or clustered networks, are relevant to many social and biological phenomena [1–6]. A clustered network consists of a number of groups, where nodes within each group are densely connected but the linkage among the groups is sparse. Such is indeed the case in many social networks, where individuals in a society tend to form groups according to their social characteristics. Within a group, each member is directly connected to most other members, but connections among different groups are relatively rare.

Viewing biological cells in terms of their underlying network structure is a useful concept and has attracted much attention recently [7–11]. Over the past several years, network science has been developed and mathematical treatments have been employed to understand the relation between the topological structure of networks and their functions [11–15]. Organizing biological information using the network idea has been fundamental to utilizing various systems-level approaches to understanding biological function. A key organizational feature in many biological systems is the tendency to form a clustered network structure [2,3,5,16]. For example, proteins with a common function are usually physically associated via stable protein-protein interactions to form larger macromolecular assemblies. These protein complexes (or clusters) are often linked together by extended networks of weaker, transient protein-protein interactions to form interaction networks that integrate pathways mediating the major cellular processes [3,16]. As a result, a protein-protein interaction network can be viewed naturally as an assembly of interconnected functional clusters, or a complex clustered network. Another example is the metabolic network of organisms. It has been found that various metabolic networks are organized into many small, highly connected clusters that combine in a hierarchical manner into larger, less cohesive units. For example, within the *Escherichia coli*, the uncovered hierarchical modularity is highly correlated with known metabolic functions. It is possible that the clustered network architecture is generic to system-level cellular organization [2].

Complex multicellular organisms such as the human body require multi-scale organizational structures, including formation of organs from large numbers of cells and integration of many organs into the systemic structure necessary for individual survival and proliferation. The organs typically consist of large numbers

of multicellular functional units such as crypt in the colon, nephron in the kidney, lobule in the liver, and alveolus in the lung, etc. While extensive recent work has focused on the structure and dynamics of intracellular molecular networks [17–21], there has been little effort to extend this kind of analysis to the interactions among cells within functioning multicellular organs which allow, for example, the human liver to synchronize as many as 10^{12} individual cells into a single functioning unit. There are two general methods by which cells can communicate with each other. Locally, cells usually establish their mutual communication channels through transmembrane pathways such as gap junctions that allow small molecules to pass between two cells in both directions. At a larger scale, cells communicate with each other through diffusing signals with cell-specific receptors. The interaction is usually directed in the sense that signals such as growth factors are produced by some, but not all cells, and can be received only by other cells that express the appropriate receptors. Despite the fact that many of the specific pathways by which cells communicate have been reasonably well characterized, remarkably little is known about the organizational principles that govern communications among large numbers of cells and permit synchronized function over substantial distances [22, 23].

Since cells communicate with each other using the two general methods described above, an intercellular-information network contains two essential features: a *locally regular* topology based on local communication with neighbors via membrane structures such as gap-junction and integrins [24] and *globally random*, directional couplings based on long-range diffusing signals and the corresponding cell membrane receptors. To better distinguish between local and global interactions, it is useful to assume that local interactions are confined within clusters, and global interactions occur among the clusters. The result is a class of complex clustered networks with a regular subnetwork in each cluster but with random, sparse couplings among clusters.

The above considerations assume identical cluster size and uniform interactions between clusters. In particular, we assume that in these works all clusters in a network are on the equal footing in the sense that their sizes are identical and the interactions between any pair of clusters are symmetrical. In realistic applications the distribution of the cluster size can be highly uneven. For example, in a clustered network with a hierarchical structure, the size of a cluster can in general depend on the particular hierarchy to which it belong.

More importantly, the interactions between clusters in different hierarchies can be highly asymmetrical. For instance, the coupling from a cluster at a top hierarchy to a cluster in a lower hierarchy can be much stronger than the other way around. An asymmetrically interacting network can in general be regarded as the superposition of a symmetrically coupled network and a directed network, both being weighted. A weighted, directed network is a *gradient network* [25, 26], a class of networks for which the interactions or couplings among nodes are governed by a gradient field. Our interest is then the synchronizability and the actual synchronous dynamics on complex clustered networks with a gradient structure.

Given the above clustered network topologies, we will focus on spreading dynamics, synchronization of coupled oscillators with such clustered structures, and the issue of security due to traffic jamming caused cascadings.

Research on epidemic in networks started with the work of Sudbury [27] on completely random networks and has received increasing attention [13, 28–41] after the discoveries of complex networks such as the small-world [42] and the scale-free [43] networks. The problem of epidemic deals with whether an initially localized seed infection can spread to a substantial part of the network [44, 45]. The pioneering work by Pastor-Satorras and Vespignani [28] considered a two-state model, where nodes can be either susceptible (S) or infected (I). A susceptible node can become infected and an infected node can recover and return to the susceptible state - hence the SIS model. They found that for scale-free networks, there is no intrinsic epidemic threshold in the thermodynamic limit. The result was extended by May and Lloyd [29] to the SIR model, a three-state model where a node in the network can be in one of the three states: susceptible, infected, and refractory (R), and an infected node can become refractory and is no longer susceptible to the infection. In Chapter 2, we investigate the SIR dynamics on clustered networks. Our interest is in information propagation, which may be particularly important for social networks. The information can be, for instance, rumor, news, or facts. In general, once an "ignorant" is contacted with a piece of information, there is a high probability that the individual will spread the information. In the SIR framework, a convenient way to model this situation is to set the spreading rate to be one, which is the probability that a susceptible node is infected when contacted. This situation also applies to a very virulent epidemic where a contacted individual

is almost certainly infected. In the SIR framework, the work of Zanette [30] and Newman *et al* [35] suggested the existence of propagation threshold for small-world networks but clustered networks typically possess the small-world feature [1–3]. Our focus here is on for how long a piece of information on a clustered network may last. A key parameter characterizing a clustered network is the number of modules, M. Intuitively, one would expect the information lifetime to increase with M. However, we find, surprisingly, that the lifetime can be maximized for a specific value of M. In particular, as M is increased initially, the time increases but reaches a maximum for some value of M, and then decreases as M is increased further, which is basically a *resonant phenomenon* [46]. The implication can be quite striking: the information lifetime is relatively short for clustered networks having either small or large number of modules. In the case of the spread of an extremely virulent disease in a human society, assuming the size of a city is proportional to the number of modules in the underlying social network, the epidemic may last long not for cities of small or large size, but for those of medium size! In the remaining of this Chapter we shall present analysis and numerical evidence to substantiate our finding.

Recent years have witnessed a growing interest in the synchronizability of complex networks [47–59]. Generally, complete synchronization is considered for coupled identical oscillators on a network, where each node is an oscillator and the coupling is via the network links. Using the master stability function formalism, Pecora *et al* [60] showed that under certain conditions, the synchronization problem, where dynamics and topological connections interweaved together, can be separated into two parts: the dynamic part and the topological part. Then whether the oscillator network is synchronizable is determined by the conditions relating these two parts. Thus for a given local dynamic, only examining the connection topology will yield the synchronizability of the oscillator network. Earlier works [47–53] suggest that small-world [42] and scale-free [43] networks, due to their small network distances, are generally more synchronizable than regular networks. It has been found, however, that heterogeneous degree distributions typically seen in scale-free networks can inhibit their synchronizability [54], but adding suitable weights to the network elements can enhance their chances to synchronize with each other [55–58]. In Chapters 3-5, we will study systematically the synchronizability of complex clustered networks. In Chapter 3, we present a new set of rules that govern

the synchronizability in clustered networks when each cluster is a random graph [61]. Chapter 4 provides validation of this set of rules under more general conditions, such as different coupling schemes and different local dynamics, and also examines different network structures in each cluster [62]. Chapter 5 reveals a new phenomena of alternating synchronizability in clustered networks when each cluster is a regular network [63]. In Chapter 6, we investigate synchronization in complex gradient clustered networks, where the size of the clusters can be different and a coupling gradient from one cluster to its neighboring cluster may exist [64].

Cascading breakdown [65–67] in complex networks has received considerable attention recently [68–71]. The phenomenon is referred to as an avalanching type of process, where the failure of a single or of a few nodes can result in a large-scale breakdown of the network. In particular, in a physical network nodes carry and process certain loads, such as electrical power, and their load-bearing capacities are finite. When a node fails, the load that it carries will be redistributed to other nodes, potentially triggering more failures in the network as a result of overloading. This process can propagate through the entire network, leading to its breakdown. Indeed, cascading breakdown appears to be particularly relevant for large-scale failures of electrical power grids, and efforts have been made to understand the dynamical origin of such failures [72]. From the standpoint of network security, scale-free networks [43], where a small subset of nodes (hubs) possess substantially more links than those of an average node and therefore carry disproportionally more loads, are especially vulnerable to cascading breakdown, as attack on one of the hub nodes can cause a significant load redistribution [66, 69]. In this regard, a strategy for protecting scale-free networks against cascading breakdown has been proposed [70], where a selective set of "unimportant" nodes that process little but contribute relatively large loads to the network are pre-emptively removed so as to reduce the overall load in the network. In Chapter 7, we investigate cascading breakdown in complex clustered networks. We uncover a specific pattern of traffic flow, based on which we propose a control strategy to prevent global scale cascading.

The above issues focus on certain particular network properties. Next we consider the scalability problem of functional networks, for both clustered networks and network without clustered structures. In particular, if a dynamical phenomenon of interest occurs in networks of size N_1, can the same phenomenon be

anticipated in networks of size N_2, where N_2 is substantially larger than N_1? More importantly, does the scalability so defined depend on the network topology? To address the issue of network scalability, we focus on synchronization, a fundamental type of collective dynamics in biological systems [73], and investigate the interplay between synchronization-based scalability and network topology. Chapter 8 discusses the scalability of networks without clustered structures, say, regular networks including full-connected network and ring network, and random network and scale-free networks. Scalability of clustered networks is discussed in Chapter 9.

Finally, to justify the master stability function approach employed in the dissertation and also many recent papers, we provide in Appendix A the master stability functions for several the typical chaotic oscillators with different single-component couplings. The results ascertain the generality of the interested class of coupled dynamics, where the master stability function is negative only in a finite interval of the normalized coupling parameter.

1.2. Linear stability analysis for coupled identical oscillators

Here we briefly review the techniques of linear stability analysis, which provides criteria of synchronization for coupled identical oscillators.

1.2.1. Coupled discrete map system

The diffusively coupled maps on networks can be generally written as [74]

$$\begin{aligned} \mathbf{x}_{m+1}^{i} &= \mathbf{f}(\mathbf{x}_{m}^{i}) + \epsilon \frac{1}{k_i} \sum_{j} A_{ij} \mathbf{H}(\mathbf{f}(\mathbf{x}_{m}^{j}) - \mathbf{f}(\mathbf{x}_{m}^{i})) \\ &= \mathbf{f}(\mathbf{x}_{m}^{i}) - \epsilon \sum_{j} G_{ij} \mathbf{H}(\mathbf{f}(\mathbf{x}_{m}^{j})). \end{aligned} \tag{1.1}$$

where $\mathbf{x}_{m+1} = \mathbf{f}(\mathbf{x}_m)$ is a k-dimensional discrete dynamical system, $\mathbf{H}$ is a linear coupling function, $\mathbf{G}$ is the coupling matrix such that $G_{ij} = -A_{ij}/k_i$ for $j \neq i$, and $G_{ii} = 1$. k_i is the degree (number of links) of node i, and $\mathbf{A}$ is the adjacent matrix of the network that $A_{ij} = 1$ if node i is connected to node j and$A_{ij} = 0$ otherwise. Since the rows of the coupling matrix $\mathbf{G}$ have zero sum, Eq. (1.1) permits an exact synchronized solution: $\mathbf{x}_m^1 = \mathbf{x}_m^2 = \ldots = \mathbf{x}_m^N = \mathbf{s}_m$, where $\mathbf{s}_{m+1} = \mathbf{f}(\mathbf{s}_m)$. The variational equations governing the time

evolution of the set of infinitesimal vectors $\delta\mathbf{x}^i \equiv \mathbf{x}^i - \mathbf{s}$ are

$$\delta\mathbf{x}^i_{m+1} = \mathbf{Df}(\mathbf{s})\delta\mathbf{x}^i_m - \epsilon\sum_j G_{ij}\mathbf{DH}(\mathbf{f}(\mathbf{s}_m))\mathbf{Df}(\mathbf{s}_m)\delta\mathbf{x}^j_m, \tag{1.2}$$

where $\mathbf{DF}$ and $\mathbf{DH}$ are the Jacobian matrices of the corresponding vector functions evaluated at $\mathbf{s}_m$ and $\mathbf{f}(\mathbf{s}_m)$ respectively. Diagonalizing the Laplacian matrix G yields a set of eigenvalues $\lambda_i, i = 1, \cdots, N$. Since $G_{ij} \leqslant 0$ for $j \neq i$ and $G_{ii} = 1 = -\sum_{j\neq i} G_{ij}$, the eigenvalues of G are nonnegative (by Gerschgorin Theorem). Thus we can sort the eigenvalues as $0 = \lambda_1 \leq \lambda_2 \leq \ldots \leq \lambda_N$ and the associated normalized eigenvectors $\mathbf{e}_1, \mathbf{e}_2, \ldots, \mathbf{e}_N$. The transform $\delta\mathbf{y} = O^{-1} \cdot \delta\mathbf{x}$, where O is a matrix whose columns are the set of eigenvectors, leads to the block-diagonally decoupled form of Eq. (1.2):

$$\delta\mathbf{y}^i_{m+1} = [\mathbf{I} - \epsilon\lambda_i\mathbf{DH}(\mathbf{f}(\mathbf{s}_m))]\mathbf{Df}(\mathbf{s}_m)\delta\mathbf{y}^i_n. \tag{1.3}$$

The system is stable if for any i, $2 \leq i \leq N$, that

$$\lim_{m\to\infty}\frac{1}{m}\ln\frac{|\delta\mathbf{y}^i_m|}{|\delta\mathbf{y}^i_0|} = \lim_{m\to\infty}\frac{1}{m}\ln\prod_{j=0}^{m-1}\frac{|\delta\mathbf{y}^i_{j+1}|}{|\delta\mathbf{y}^i_j|} < 0. \tag{1.4}$$

Usually, $\mathbf{H}$ is a linear function, thus $\mathbf{DH}$ is a constant matrix. If the system is one dimensional, $\mathbf{DH} = H'$ is just a constant, say, γ. The above equation becomes:

$$\ln|1 - \epsilon\lambda_i\gamma| + \lim_{m\to\infty}\frac{1}{m}\ln\prod_{j=0}^{m-1}|f'(s_j)| < 0. \tag{1.5}$$

Recall that the second term of the above equation is just the Lyapunov exponent μ of a single map, thus

$$\ln|1 - \epsilon\lambda_i\gamma| + \mu < 0, \tag{1.6}$$

which is

$$|e^\mu(1 - \epsilon\lambda_i\gamma)| < 1, i = 2, \ldots, N. \tag{1.7}$$

For coupled logistic maps, $f(x) = 1 - ax^2$, $H(f) = f$, $\gamma = 1$, Eq. (1.7) reads (Ref. [74]):

$$|e^\mu(1 - \epsilon\lambda_i)| < 1, i = 2, \ldots, N. \tag{1.8}$$

The above inequality will hold for all the is if it holds for $i = 2$ and $i = N$. For the above coupling matrix $\mathbf{G}$, $0 < \lambda_2 \leq 1$ and $1 \leq \lambda_N \leq 2$, thus the condition (1.8) can be further simplified as:

$$\lambda_2 > \frac{1}{\epsilon}(1 - e^{-\mu}), \tag{1.9}$$

$$\lambda_N < \frac{1}{\epsilon}(1 + e^{-\mu}). \tag{1.10}$$

The boundary of the synchronization region in the phase diagram can be determined by setting $\lambda_2 = \frac{1}{\epsilon}(1 - e^{-\mu})$ and $\lambda_N = \frac{1}{\epsilon}(1 + e^{-\mu})$. In our simulation in the dissertation, we use $a = 1.9$, and the corresponded Lyapunov exponent of the logistic map is $\mu = 0.55$, thus $\lambda_2 = 0.423/\epsilon$, and $\lambda_N = 1.577/\epsilon$. If the coupling function $\mathbf{H}$ is nonlinear, $\mathbf{DH}[\mathbf{f}(\mathbf{s}_m)]$ will depend on the value of $\mathbf{f}(\mathbf{s}_m)$ and it is difficult to obtain explicit boundaries for λ_2 and λ_N.

1.2.2. Continuous-time oscillators

We consider the synchronization condition of coupled continuous-time identical chaotic oscillators [60]. Each oscillator, when isolated, is described by:

$$\frac{d\mathbf{x}}{dt} = \mathbf{F}(\mathbf{x}), \tag{1.11}$$

where $\mathbf{x}$ is a d-dimensional vector and $\mathbf{F}(\mathbf{x})$ is the velocity field. The parameters of the oscillator are chosen such that it oscillates chaotically. The dynamics of N coupled oscillators are described by

$$\frac{d\mathbf{x}_i}{dt} = \mathbf{F}(\mathbf{x}_i) - \epsilon \sum_{j=1}^{N} G_{ij}\mathbf{H}(\mathbf{x}_j), \tag{1.12}$$

where $\mathbf{H}(\mathbf{x})$ is a linear coupling function, ϵ is global coupling parameter, and $\mathbf{G}$ is the coupling matrix describing the connection topology. The matrix $\mathbf{G}$ satisfies the condition $\sum_{j=1}^{N} G_{ij} = 0$ for any i, where N is the network size, therefore the system permits an exact synchronized solution: $\mathbf{x}^1 = \mathbf{x}^2 = \ldots = \mathbf{x}^N = \mathbf{s}$, where $d\mathbf{s}/dt = \mathbf{F}(\mathbf{s})$.

For the system described by Eq. (1.12), the variational equations governing the time evolution of the set of infinitesimal vectors $\delta\mathbf{x}_i(t) \equiv \mathbf{x}_i(t) - \mathbf{s}(t)$ are

$$\frac{d\delta\mathbf{x}_i}{dt} = \mathbf{DF}(\mathbf{s}) \cdot \delta\mathbf{x}_i - \epsilon \sum_{j=1}^{N} G_{ij}\mathbf{DH}(\mathbf{s}) \cdot \delta\mathbf{x}_j, \tag{1.13}$$

where $\mathbf{DF}(\mathbf{s})$ and $\mathbf{DH}(\mathbf{s})$ are the $d \times d$ Jacobian matrices of the corresponding vector functions evaluated at $\mathbf{s}(t)$. Diagonalizing the connection matrix G yields a set of eigenvalues $\{\lambda_i, i = 1, \cdots, N\}$ and the corresponding normalized eigenvectors are denoted by $\mathbf{e}_1, \mathbf{e}_2, \ldots, \mathbf{e}_N$. The eigenvalues are real and nonnegative and can be sorted as $0 = \lambda_1 < \lambda_2 \leq \cdots \leq \lambda_N$ [74]. The transform $\delta\mathbf{y} = O^{-1} \cdot \delta\mathbf{x}$, where O is a matrix whose columns are the set of eigenvectors, leads to the block-diagonally decoupled form of Eq. (1.13):

$$\frac{d\delta\mathbf{y}_i}{dt} = [\mathbf{DF}(\mathbf{s}) - \epsilon\lambda_i\mathbf{DH}(\mathbf{s})] \cdot \delta\mathbf{y}_i.$$

Letting $K = \epsilon\lambda_i$ $(i = 2, \ldots, N)$ be the normalized coupling parameter, we can write

$$\frac{d\delta\mathbf{y}}{dt} = [\mathbf{DF}(\mathbf{s}) - K\mathbf{DH}(\mathbf{s})] \cdot \delta\mathbf{y}. \tag{1.14}$$

The largest Lyapunov exponent from Eq. (1.14) is the master-stability function $\Psi(K)$ [60]. If $\Psi(K)$ is negative, a small disturbance from the synchronization state will diminish exponentially, thus the system is stable and can be synchronized; if $\Psi(K)$ is positive, a small disturbance will be magnified and the system cannot be synchronized.

2 . INFORMATION PROPAGATION ON CLUSTERED NETWORKS

2.1. Background

Networks with a community structure, or clustered networks, are relevant to many social and biological phenomena [1–6]. A clustered network consists of a number of groups, where nodes within each group are densely connected but the linkage among the groups is sparse. Such is indeed the case in many social networks, where individuals in a society tend to form groups according to their social characteristics. Within a group, each member is directly connected to most other members, but connections among different groups are relatively rare. Among the many outstanding problems concerning clustered networks, the propagation of information, such as rumor, news, or facts, is of great interest.

Research on epidemic in networks started with the work of Sudbury [27] on completely random networks and has received increasing attention [13, 28–41] after the discoveries of complex networks such as the small-world [42] and the scale-free [43] networks. The problem of epidemic deals with whether an initially localized seed infection can spread to a substantial part of the network [44, 45]. The pioneering work by Pastor-Satorras and Vespignani [28] considered a two-state model, where nodes can be either susceptible (S) or infected (I). A susceptible node can become infected and an infected node can recover and return to the susceptible state - hence the SIS model. They found that for scale-free networks, there is no intrinsic epidemic threshold in the thermodynamic limit. The result was extended by May and Lloyd [29] to the SIR model, a three-state model where a node in the network can be in one of the three states: susceptible, infected, and refractory (R), and an infected node can become refractory and is no longer susceptible to the infection. For comprehensive review on epidemic in complex networks, see Refs. [13, 41].

In this Chapter we investigate the SIR dynamics on clustered networks [46]. Our interest is in information propagation, which may be particularly important for social networks. The information can be, for instance, rumor, news, or facts. In general, once an "ignorant" is contacted with a piece of information, there is a high probability that the individual will spread the information. In the SIR framework, a convenient way to model this situation is to set the spreading rate to be one, which is the probability that a susceptible node is infected when contacted. This situation also applies to a very virulent epidemic where a contacted individual is almost certainly infected. In the SIR framework, the work of Zanette [30] and Newman *et al* [35] suggested

the existence of propagation threshold for small-world networks but clustered networks typically possess the small-world feature [1–3]. Our focus here is on *for how long a piece of information on a clustered network may last*. A key parameter characterizing a clustered network is the *number of modules*, M. Intuitively, one would expect the information lifetime to increase with M. However, we find, surprisingly, that the lifetime can be maximized for a specific value of M. In particular, as M is increased initially, the time increases but reaches a maximum for some value of M, and then decreases as M is increased further, which is basically a *resonant phenomenon*. The implication can be quite striking: the information lifetime is relatively short for clustered networks having either small or large number of modules. In the case of the spread of an extremely virulent disease in a human society, assuming the size of a city is proportional to the number of modules in the underlying social network, the epidemic may last long not for cities of small or large size, but for those of medium size! In the remaining of this Chapter we shall present analysis and numerical evidence to substantiate our finding.

2.2. Model setup

We consider a clustered network with $N \gg 1$ nodes and M modules, where $M \ll N$. Each module is thus a subnetwork of $n = N/M \gg 1$ nodes, which can be either scale-free, small-world, or random. For convenience, each module is assigned an integer, say, from 1 to M, and all modules are placed on a topological ring with the periodic boundary condition. For each pair of adjacent modules, one node is chosen randomly from each module and a link is added between the two nodes. At this stage all modules are connected through next-neighbor type of links. Links of short-cut type are generated by randomly selecting pairs of modules of distance l apart along the ring according to the probability $P(l) \sim e^{-\alpha l}$ and linking them, where α is a control parameter. For $\alpha \sim 0$, random long-range links are highly probable, making the whole clustered network small-world like. Since the linkage among the modules is sparse comparing with the linkage within each module, and since for α not close to zero the links among modules are mostly local or diametrical, large-scale propagation is more unlikely in these cases. It thus makes sense to focus attention on networks with $\alpha \sim 0$.

The SIR dynamics for information propagation is implemented on the network, as follows. Initially all

nodes are susceptible. At $t = 0$, a piece of information is generated at a randomly chosen node (seed). At the next time step, one of its neighbors is randomly picked up, and becomes "infected " with the information if it is susceptible; otherwise, the original infected node itself becomes refractory. This process continues until there is no longer any infected node in the network, and the time the whole process takes is the information lifetime T. The number of refractory nodes for $t \geq T$ thus represents the number of nodes in the network that have been infected.

2.3. Critical spreading depending on the intercluster link densities

For a piece of information to spread on a clustered network, the number of links among the modules needs to be large. The minimally required average number of intercluster links can be estimated, as follows. First, recall that each module is effectively a subnetwork that can be random, small-world, or scale-free. For a random network, the mathematical theory of SIR dynamics with unit spread rate [27] indicates that the fraction of nodes that can be infected approaches a universal constant of about 0.8 as the number of nodes goes to infinity. For scale-free networks and more general networks that contain both random and scale-free components, there is numerical evidence that the fraction is slightly below 0.8 [38]. In any case, given a network of reasonably large size, the fraction of nodes that can be infected under the SIR dynamics is approximately a constant $r_0 \lesssim 0.8$. Next, let k_M be the average number of short-cut type of links. Taking into account the next-neighbor type of connections between the modules and the fact that $n \gg k_M$, the average number of nodes in a module with links going outside is $k_e = 2k_M + 2$. Thus, within an infected module, the average number of such nodes that carry the information is $r_0 k_e$. Finally, let $\langle k \rangle$ be the average number of internal links per node in the subnetwork. If a node with an outgoing link is infected, the probability that the link is chosen to spread the information is $1/(\langle k \rangle + 1)$. Thus, on average, the number of nodes that carry the information *and* spread it to a different module is $r_0 k_e/(\langle k \rangle + 1)$. For information to spread over the entire network, we must have $r_0 k_e/(\langle k \rangle + 1) \geq 1$, yielding $k_M^{min} = (\langle k \rangle + 1)/(2r_0) - 1$. For instance, if $\langle k \rangle = 10$, using $r_0 = 0.8$ we obtain $k_M^{min} = 6$. This agrees quite well with numerics, as shown in Fig. 1, where the fraction of infected nodes on the whole clustered network is calculated as a function of k_M, for 6 different

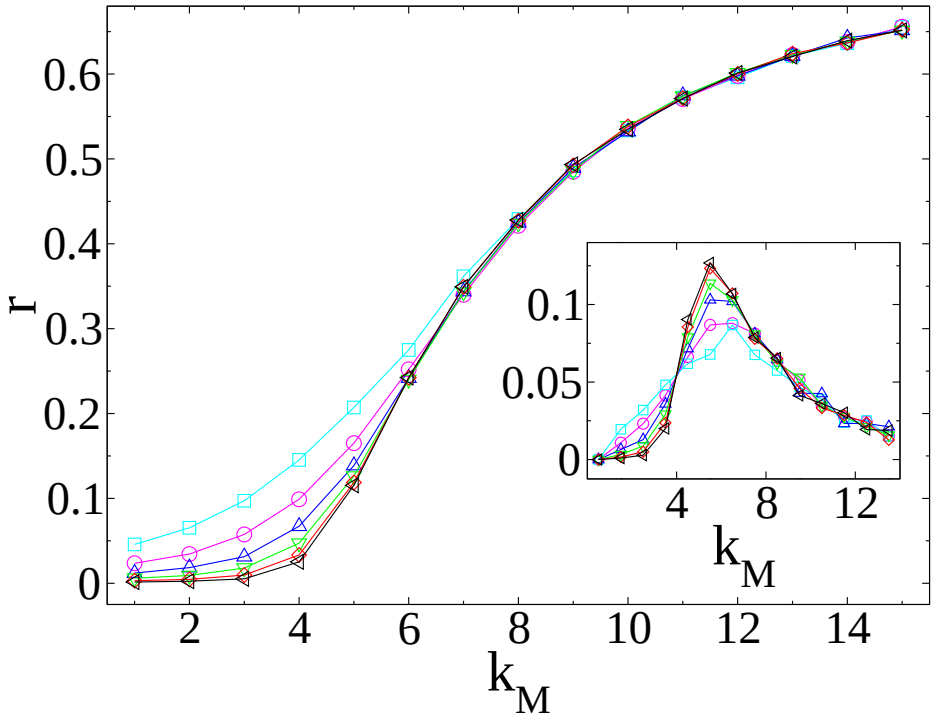

Fig. 1. For clustered network with a ring topology, the fraction of infected nodes versus k_M. Parameters are $\alpha = 0$, $\langle k \rangle = 10$, and $n = 200$. The six curves correspond to network size of $N = 5 \times 10^3$ (squares), 10^4 (circles), 2×10^4 (up triangles), 4×10^4 (down triangles), 8×10^4 (diamonds), and 16×10^4 (left triangles), respectively. Each data point is the result of averaging over 10^4 random realizations of the network. The inset shows the dr/dk_M versus k_M, which is indicative of a continuous phase transition.

values of N. Apparently, the fraction becomes substantial for $k_M \geq 6$, indicating a large scale information spread on the clustered network.

2.4. Resonant behavior of information lifetime

2.4.1. Resonant phenomena

We now examine the dependence of the lifetime T on the number of modules. Figures 2(a) and 2(b) show, for a network of $N = 4 \times 10^4$ nodes, the fraction r of infected nodes and T versus M, respectively. The subnetwork in each module is random. We see that as M varies over two orders of magnitude (from 10 to 1000), r remains approximately constant (about 0.54). Since r is substantially above zero, a large-scale

information spread on the network occurs. The surprising phenomenon is that the lifetime T, as shown in Fig. 2(b), is apparently nonmonotonic and in fact exhibits a bell-shape behavior. There exists a value of M for which the time reaches maximum, indicating a resonance-type of phenomenon. The phenomenon persists when each subnetwork is scale-free as shown in Figs. 2(c) and 2(d).

In Fig. 2, squares are the data for fixed $\langle k\rangle$ and k_M. As the number of module M is increased, the average degree of the network $\overline{k} = \langle k\rangle + 2(k_M+1)M/N$ also increases. One may wonder whether the resonance is caused by this increase. To address this issue, we fix the value of $\overline{k}$ by reducing $(k_M+1)M$ inner edges, i.e., edges that connect nodes in the same module, while keeping the network fully connected. The results for fixed $\overline{k}$ and k_M are also shown in Fig. 2 (circles). We see that the results for fixed $\langle k\rangle$ and for fixed $\overline{k}$ are essentially the same, indicating that the observed resonant phenomenon is not a numerical artifact, but more likely an intrinsic property of clustered networks.

2.4.2. Theory

To establish the credence and the generality of the observed resonant phenomenon, we seek for a theoretical explanation. To gain insight, we consider the spread of information from a seed node on a two-dimensional square lattice. By the assumptions of the SIR dynamics, once a node is infected, it will become refractory or stay infected, and cannot be infected again. Assume that a node at the point $\mathbf{r} = (x, y)$ is infected at time $t-\tau$ from the node at $(x, y-a)$, where τ and a are the time step and lattice constant, respectively. At time t this newly infected node infects one of its nearest-neighbor nodes, if it is susceptible. If all nearest-neighbor nodes of the newly infected nodes are susceptible except for the node at $(x, y-a)$, the probability for any of these susceptible nodes to be infected at time $t+\tau$ is 1/3. Let $P(\mathbf{r}, t)$ be the probability that a node at the point $\mathbf{r}$ is infected at time t. We have $P(\mathbf{r}, t) = (1/3)[P(x+a, y, t+\tau)+P(x-a, y, t+\tau)+P(x, y+a, t+\tau)]$. Subtracting $P(\mathbf{r}, t+\tau)$ from both sides and dividing by τ, we get, in the continuum limit $a \to 0$ and $\tau \to 0$, $\partial P(\mathbf{r}, t)/\partial t = D\partial^2 P(\mathbf{r}, t)/\partial x^2 + \mu\partial P(\mathbf{r}, t)/\partial y$, where $D = -a^2/3\tau$ and $\mu = -a/3\tau$. Since $|D| \ll |\mu|$, the diffusion term can be neglected, yielding $\partial P(\mathbf{r}, t)/\partial t \approx \mu\partial P(\mathbf{r}, t)/\partial y$. In this equation, the term on the right-hand side is derived by taking into account only the unidirectional spreading of the information along the y-axis. Since unidirectional spreading can also occur in the x-direction, the equation governing the

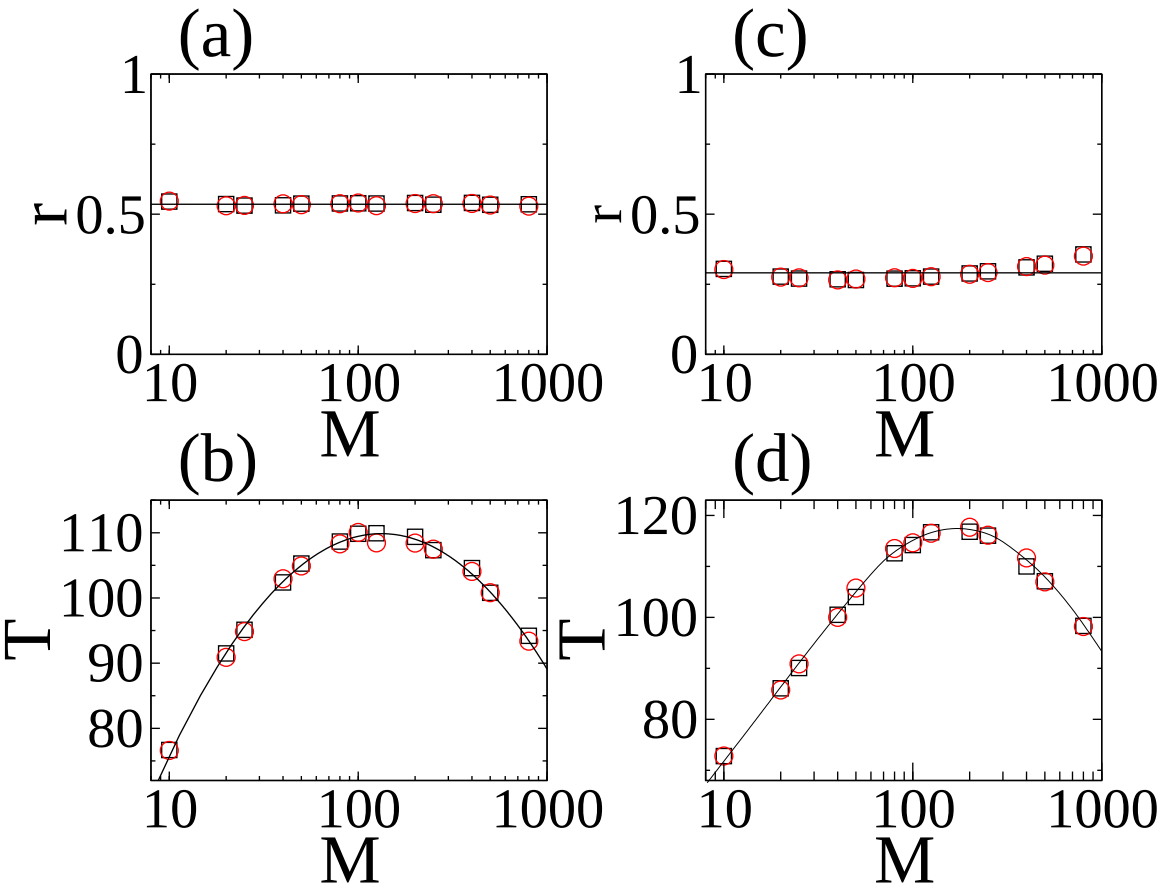

Fig. 2. For clustered network with a ring topology, (a) the fraction of infected nodes and (b) the information lifetime T versus the number of modules, for random subnetworks. Squares: $\langle k \rangle = 10$, the average degree $\overline{k}$ varies as M increases; circles: $\overline{k} = 10$. Other parameters are $\alpha = 0$, $N = 4 \times 10^4$, and $k_M = 10$. Each data point is the average over 10^4 random network realizations. (c) and (d) are the corresponding plots when the subnetwork within each module is scale-free.

propagation of infection in the two-dimensional lattice is

$$\frac{\partial P(\mathbf{r},t)}{\partial t} = \nu\big[\frac{\partial P(\mathbf{r},t)}{\partial x} + \frac{\partial P(\mathbf{r},t)}{\partial y}\big], \tag{2.1}$$

where ν is a constant. Equation (2.1) is invariant under the scaling transformation $\mathbf{r} = (x,y) \to l\mathbf{r} = (lx, ly), t \to l^z t$ and $P(\mathbf{r},t) \to l^\alpha P(\mathbf{r},t)$, where l is a dilatation factor. Comparing all terms in Eq. (2.1) under the transformation, we have $z = 1$. This means that, if the seed node is at $\mathbf{r} = \mathbf{0}$ and $t = 0$, there is a nonzero probability that a node at distance L will be infected at time T, where $T \sim L$. For a complex network, although we were not able to derive a similar equation, the basic dynamical process for infection spreading is the same. Since the relevant distance is the network diameter d, we expect the information lifetime to be proportional to d: $T \sim d$, which has been confirmed numerically for both random and scale-free networks, as shown in Fig. 3(a).

Now consider a clustered network of M modules, where the subnetwork of n nodes within each module is either random or scale-free. The average network diameter of each subnetwork is of the order of $\ln n$ [75, 76]. Assume that the links among the modules are randomly distributed. If each module is regarded as a node in a network, the network diameter is of the order of $\ln M$. For two randomly selected nodes in the clustered network, on average their distance is of the order of $D_M(a_1 + a_2 \ln n)$, where D_M is the average number of modules that the shortest path between the two nodes passes, which is of the order of $\ln M$, and a_1 and a_2 are constants. The diameter of the clustered network can thus be written as $d = (a_3 + a_4 \ln M)(a_1 + a_2 \ln n)$, where a_3 and a_4 are constants. Since $n = N/M$, we have

$$d = a + b \ln M + c(\ln M)^2, \tag{2.2}$$

where a, b, and c are constants. A numerical verification of Eq. (2.2) is shown in Fig. 3(b). The quadratic dependence of the network diameter d on M, together with the linear relation between the information lifetime and the diameter, suggests a quadratic relation (resonant behavior) between the lifetime and the number of modules, as observed numerically.

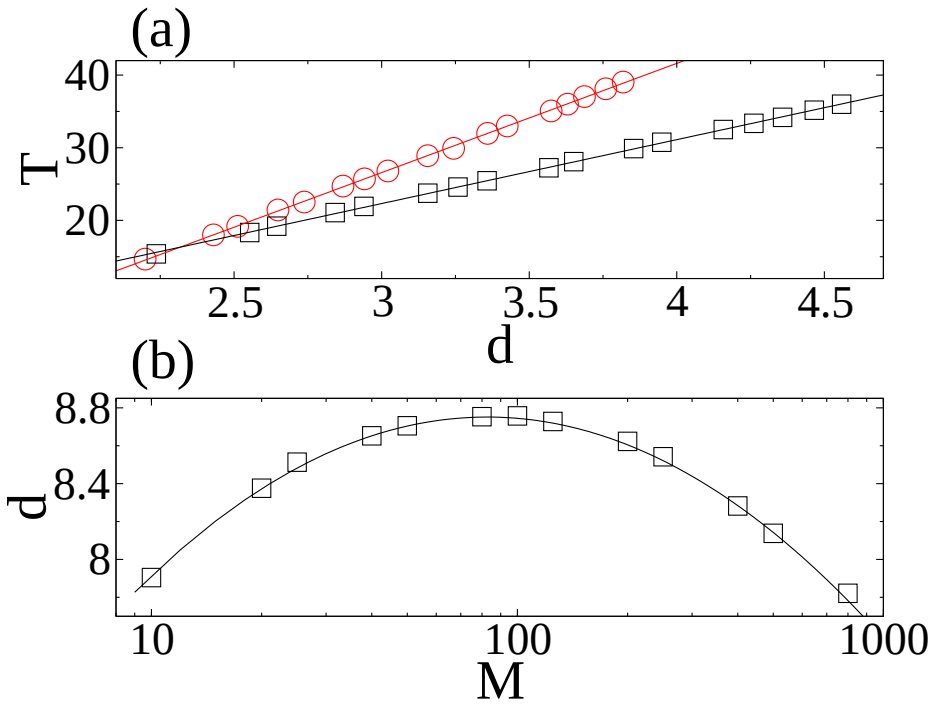

Fig. 3. (a) Relation between information lifetime T and network diameter d for both random (lower trace) and scale-free (upper trace) networks. For both networks, the average degree is 10 and the size varies from 100 to 2×10^4. Each value of d is obtained from 10 network realizations and each value of T is the average over 10^5 realizations. (b) For a ring clustered network of $N = 4 \times 10^4$ nodes, the relation between the network diameter and the number of modules. Parameters are $\alpha = 0$, $\langle k \rangle = 10$, and $k_M = 10$. Each data point is the average over 10 random network realizations. The solid curve is the theoretical fit.

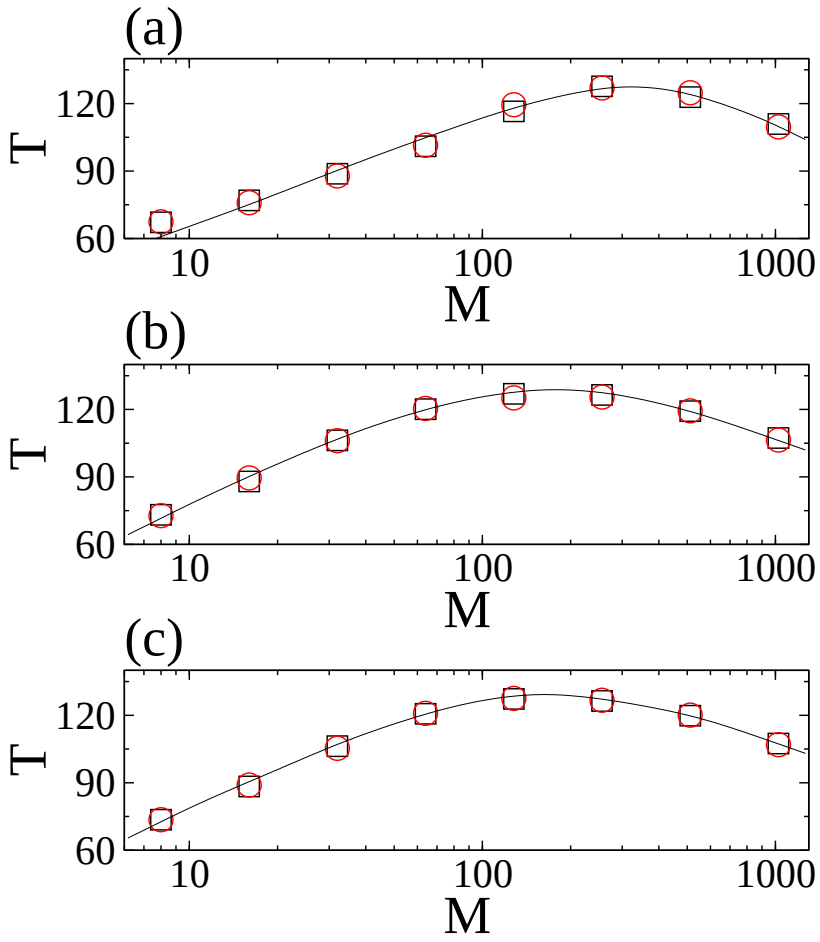

Fig. 4. For Zachary network of $N = 52000$ nodes, the resonant behavior between the information lifetime and the number of modules for three cases: (a) scale-free subnetworks and preferential intercluster links, (b) random subnetworks and preferential intercluster links, and (c) random subnetworks and random intercluster links. In each subgraph, squares: $\langle k \rangle = 10$, the average degree $\overline{k}$ varies as M increases; circles: $\overline{k} = 10$. Other parameters are $\beta = 0$ and $k_M = 10$. Each data point is obtained by averaging the lifetime over 10^4 random network realizations.

2.4.3. Resonance on more realistic clustered networks

Can the resonant behavior occur in more realistic clustered networks? To address this question we have also studied another class of clustered networks, the Zachary networks [77], which were originally proposed as a model of social networks. To construct a Zachary network of N nodes, we first divide all nodes into M modules, each having $n \gg 1$ nodes. Next, the modules are organized into levels, where each group in level 1 consists of two modules, and each level-2 group consists of two level-1 groups, and so on. Finally, random links among modules are added according to the probability $P(l) \sim e^{-\beta l}$, where $l \geq 0$ is the level distance between two random nodes in the network and $\beta \geq 0$ is a control parameter. In particular, a node (say, node i) is chosen randomly and a link is added between this node and another node from a *different* module (target module) according to $P(l)$. Once the target module is determined, the node (say, node j) in the module to which node i will connect is determined either randomly or by a preferential attachment rule within the target module. For the latter, the probability that node j is picked up is proportional to k_j, the number of links this node already has within the module. The process is repeated until the number of links among modules reaches the prescribed number $k_M M$. Implementing the SIR dynamics on the Zachary network, we have again observed the resonant phenomenon, as shown in Fig. 4, where squares are for fixed $\langle k \rangle$ and circles are for fixed $\overline{k}$. Note that there is essentially no difference between the two cases, suggesting that the resonant phenomenon is generic for clustered networks.

In summary, our investigation of the SIR dynamics on complex, clustered networks leads to the finding of an interesting resonance-like phenomenon: the information lifetime typically exhibits a quadratic dependence on the number of modules. Thus, a piece of information will last shorter for networks having either a small number or a large number of modules. The same result holds for extremely virulent epidemics. In particular, our result may be useful for a social network where such an epidemic has just emerged. Knowing for how long the epidemic can potentially last can help in key decision making such as resources distribution in order to suppress the epidemic.

3 . ABNORMAL SYNCHRONIZATION IN COMPLEX CLUSTERED NETWORKS

3.1. Background

There has been a growing interest in the synchronizability of complex networks [54, 78, 79]. Earlier works [78] suggest that small-world [42] and scale-free [43] networks are generally more synchronizable than regular networks. While heterogeneous degree distributions can inhibit synchronization [54], adding suitable weights to the network elements can enhance their chances to synchronize with each other [79]. In general, given a complex network with a fixed number of nodes, its synchronizability can be improved by increasing the number of links. This is intuitive as a denser linkage makes the network more tightly coupled or, "smaller," thereby facilitating synchronization.

In this Chapter, we present a counterintuitive finding about the synchronizability of clustered networks [61]. A clustered network consists of a number of groups, where nodes within each group are densely connected, but the linkage among the groups is sparse [80]. These networks have recently been discovered in important areas of biological physics [2, 81]. A complex clustered network is typically small-world so that its average distance is small. Moreover, its degree distribution can be made quite homogeneous. The surprising phenomenon is that more edges (links), which make the network smaller, do not necessarily lead to stronger synchronizability. There can be situations where more edges can even suppress synchronization if placed improperly. In particular, we find that the synchronizability of a clustered network is determined by the interplay between the inter-connections (links among clusters) and intra-connections (links within clusters) of the network. Strong synchronizability requires that the numbers of the inter-links and intra-links be approximately matched. In this case, increasing the number of links can indeed enhance the synchronizability. However, if the matching is deteriorated, synchronization can be severely suppressed or even totally destroyed.

Our finding can have potential impacts on real network dynamics. In particular, there is mounting evidence that several types of biological networks possess a clustered structure, such as the metabolic networks [2] and the protein interaction graphs [81]. In biology, synchronization is fundamental, on which many biological functions rely. Our result implies that, in order to achieve robust synchronization for a clustered biological network, the characteristics of the links are more important than the number of links. Simply counting the number of links may not be enough to determine its synchronizability. Instead, links should be

distinguished and classified to predict synchronization-based functions of the network. Clustered structure has also been identified in technological networks such as electronic circuit and computer networks [82]. Suppose a large-scale, parallel computational task is to be accomplished by a computer network, for which synchronous timing is of paramount importance. Our result can provide clues as to how to design the network to achieve the best possible synchronization and consequently optimal computational efficiency.

Our approach is to introduce nonlinear dynamics on each node in the network and then perform stability and eigenvalue analyses [60, 74]. The theoretical derivation yields the stability regions for synchronization in the two-dimensional parameter space defined by the numbers of the two types of links. The analytic predictions are verified by numerical simulations.

3.2. Abnormal synchronization

We consider a random clustered network model: N nodes are classified into M groups, where each group has $n = N/M$ nodes. In a group, a pair of nodes is connected with probability p_s, and nodes belonging to different groups are connected with probability p_l. For a clustered network, the number of inter-connections is typically far less than the number of intra-connections. As a result, the parameter region of small p_l values is more relevant. To be concrete, we first study the following general class of coupled-map networks: $\mathbf{x}_{m+1}^i = \mathbf{f}(\mathbf{x}_m^i) - \varepsilon \sum_j G_{ij}\mathbf{H}[\mathbf{f}(\mathbf{x}_m^j)]$, where $\mathbf{x}_{m+1} = \mathbf{f}(\mathbf{x}_m)$ is a d-dimensional map, ε is a global coupling parameter, $\mathbf{G}$ is the Laplacian matrix, and $\mathbf{H}$ is a coupling function. For convenience we choose $G_{ij} = -A_{ij}/k_i$ for $j \neq i$ and $G_{ii} = 1$, where k_i is the degree of node i and A_{ij} is an element of the adjacent matrix $\mathbf{A}$ of the network. Since the rows of the coupling matrix $\mathbf{G}$ have zero sum, the system permits an exact synchronized solution: $\mathbf{x}_m^1 = \mathbf{x}_m^2 = \ldots = \mathbf{x}_m^N = \mathbf{s}_m$, where $\mathbf{s}_{m+1} = \mathbf{f}(\mathbf{s}_m)$. To gain insight, we set $\mathbf{f}(\mathbf{x})$ to be the logistic map $f(x) = 1 - ax^2$ ($0 < a \leq 2$) and choose $\mathbf{H}(\mathbf{x}) = x$. If the system is synchronizable, starting from a random initial condition, it will approach the synchronization state. In the simulation, synchronization is defined as $\langle |x_i - \langle x_i \rangle| \rangle < 10^{-10}$, where $\langle \cdot \rangle$ denotes average over the network. The average time T required for the system to become synchronized can be used to characterize the ability of the system to synchronize. If the system is unsynchronizable, T is infinite. Figure 5 shows the behavior of T in the two-dimensional parameter space (p_l, p_s) for networks with 2 clusters (a) and 10 clusters (b). This gives the synchronizable

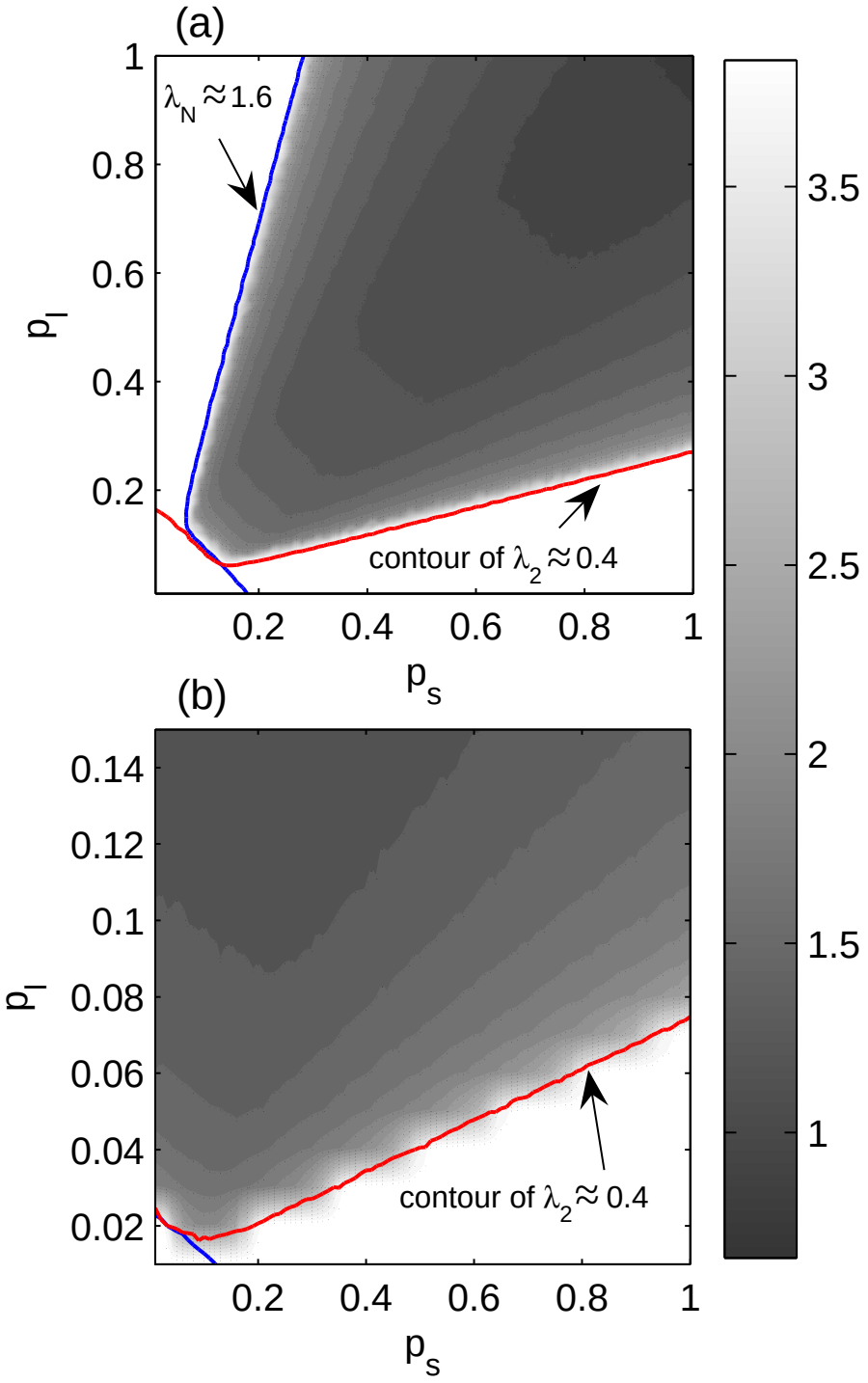

Fig. 5. Contour plot of the synchronization time T (on a logarithmic scale $\log_{10} T$) in (p_l, p_s) space for coupled logistic-map network with (a) $N = 100$, $M = 2$, and (b) $N = 500$, $M = 10$. $\varepsilon = 1$, $a = 1.9$. The line segments defining the boundaries between the synchronizable and unsynchronizable regions are determined by theory. Each data point is the result of averaging over 100 network realizations.

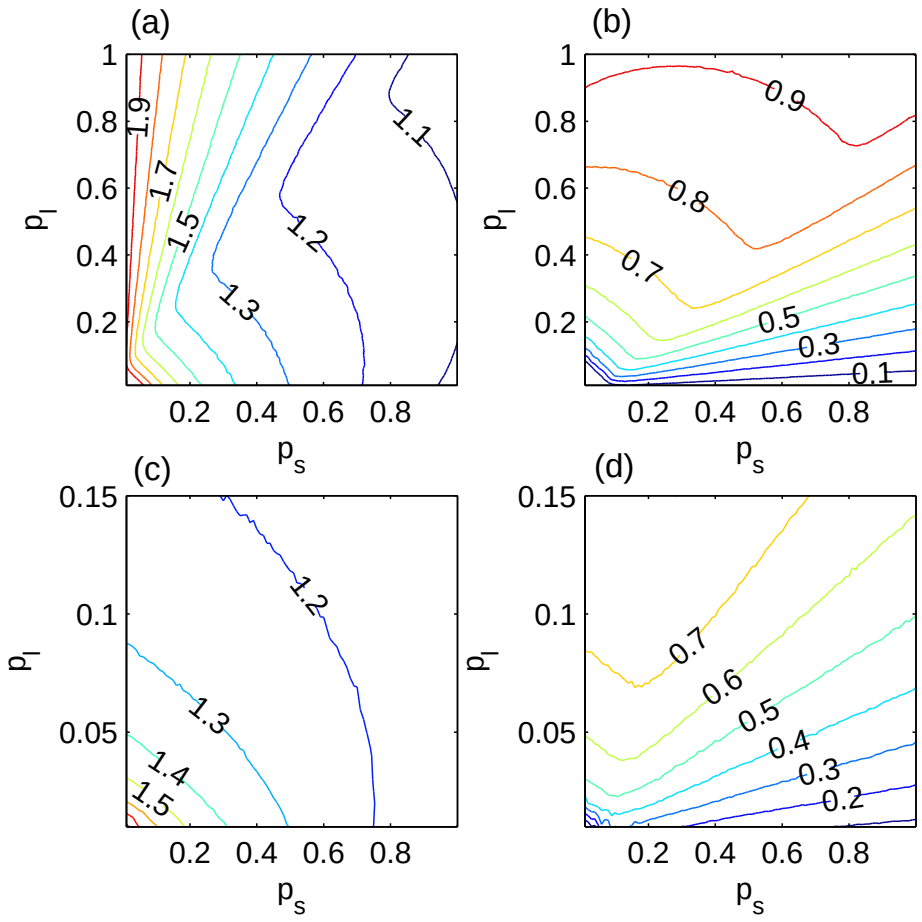

Fig. 6. Contour plot of λ_N (a)(c) and λ_2 (b)(d) in the (p_l, p_s) plane, for $N = 100$ and $M = 2$ (a)(b) and $N = 500$ and $M = 10$ (c)(d).

region (grey regions in Fig. 5) in the parameter space that the system is able to synchronize within a certain time, and the unsynchronizable region (white regions in Fig. 5). The shape of the figure depends on the coupling strength ε and on the contour lines of λ_2 and λ_N (see Fig. 6). For 2-cluster networks, if $\varepsilon = 1$, the shape appears to be symmetric, while if $\varepsilon < 1$, the boundary is asymmetric. Figure 5(a) demonstrates that for a given p_l (e.g., 0.2), as p_s is increased from 0.2, synchronization time T is also increased. At a certain point (about 0.75 in this case), the system becomes unsynchronizable. That is, too many intra-links tend to destroy the global synchronization [83].

For the coupled-map network, the synchronization condition is $\lambda_2 > \frac{1}{\varepsilon}(1-e^{-\mu})$ and $\lambda_N < \frac{1}{\varepsilon}(1+e^{-\mu})$ [Eqs. (1.9) and (1.10)]. The boundaries of the synchronization regions in the parameter space can be determined by setting $\lambda_2 = (1-e^{-\mu})/\varepsilon$ and $\lambda_N = (1+e^{-\mu})/\varepsilon$. In our simulations, we have used $a = 1.9$ ($\mu \approx 0.55$). Thus we have $\lambda_2 \approx 0.4$ and $\lambda_N \approx 1.6$ for $\varepsilon = 1$, the contour lines of which are shown in Fig. 5. There is a good agreement between the theory and numerics.

3.3. Eigenvalue analysis

To better understand the abnormal behavior of the dependence of synchronizability on p_s, we analyze the eigenvalues of the Laplacian matrix of a general clustered network. Figure 6 shows the contour plots of the λ_N and λ_2 in the parameter space, for 2 (a,b) and 10 (c,d) clusters. There is an apparent similarity between some of the contour lines and the stability boundaries in Fig. 5. From Fig. 6 we can see that, for a given value of p_l, λ_N decreases as p_s increases, so it is easier to synchronize the network. However, for large values of p_s, λ_2 decreases as p_s increases, thus synchronization becomes more difficult. We see that the behavior of λ_2 accounts for the abnormal synchronizability behavior shown in Fig. 5. In the following, we shall derive a theoretical formula to understand the dependence of λ_2 on p_l and p_s for small values of p_l (typical parameter regime of clustered networks).

For a clustered network, the components of the eigenvector $\mathbf{e}_2$ have approximately the same value within any cluster, while they can vary among clusters, as demonstrated in Fig. 7. Thus, we can write $\mathbf{e}_2 \approx [\widetilde{e}_1, \widetilde{e}_1, \cdots, \widetilde{e}_1, \widetilde{e}_2, \cdots, \widetilde{e}_2, \widetilde{e}_3, \cdots, \widetilde{e}_M]^T$, where $[*]^T$ denotes the transpose, and for each I, $1 \leqslant I \leqslant M$, there are n $\widetilde{e}_I$'s in $\mathbf{e}_2$. By definition, $\mathbf{G}\cdot\mathbf{e}_2 = \lambda_2\mathbf{e}_2$ and $\mathbf{e}_2\cdot\mathbf{e}_2 = 1$, we have $\lambda_2 = \mathbf{e}_2^T\cdot\mathbf{G}\cdot\mathbf{e}_2 = \sum_{i,j=1}^{N} e_{2i}G_{ij}e_{2j}$, where e_{2i} is the ith component of $\mathbf{e}_2$. Expanding the summation in j yields $\lambda_2 = \sum_{i=1}^{N} e_{2i}\{G_{i1}\widetilde{e}_1 + G_{i2}\widetilde{e}_1 + \cdots + G_{in}\widetilde{e}_1 + G_{in+1}\widetilde{e}_2 + \cdots + G_{iN}\widetilde{e}_M\}$. If i and j belong to the same cluster, G_{ij} equals $-1/k_i$ with probability p_s and 0 with probability $1-p_s$; while if i and j belong to different clusters, G_{ij} equals $-1/k_i$ with probability p_l and 0 with probability $1-p_l$. We thus have $\lambda_2 = \sum_{i=1}^{N} e_{2i}[N(p_l/k_i)\widetilde{e}_I - n(p_l/k_i)\sum_{J=1}^{M}\widetilde{e}_J]$, where $\widetilde{e}_I$ is the component associated with the cluster that contains node i, and the equality $1 - np_s/k_i = (N-n)p_l/k_i$ has been used. For a randomly clustered network, the degree distribution has a narrow peak centered at $k = np_s + (N-n)p_l$, implying $k_i \approx k$. This

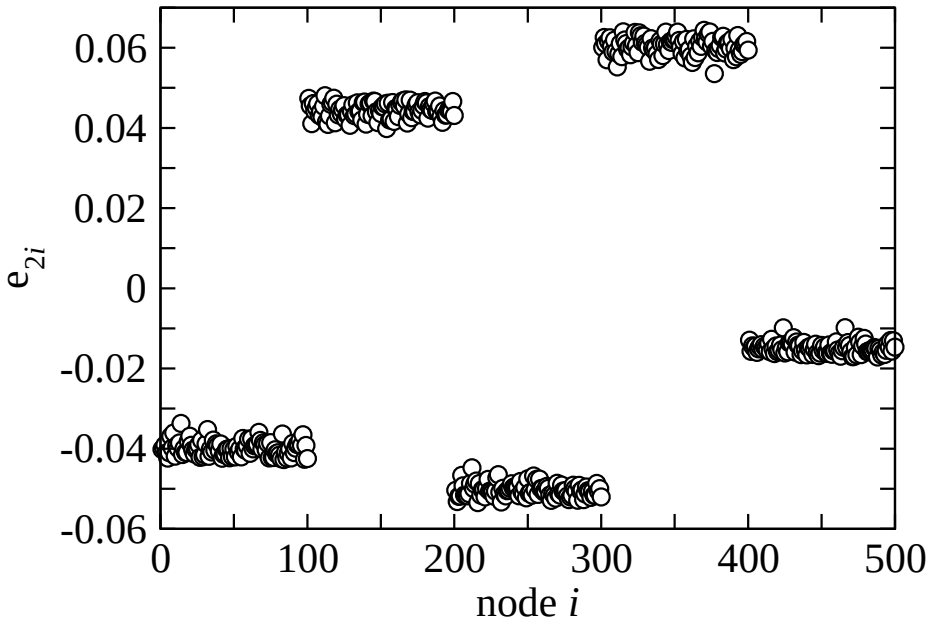

Fig. 7. A typical profile of components of the eigenvector $\mathbf{e}_2$. Parameters are $N = 500$, $M = 5$, $p_l = 0.01$, and $p_s = 0.8$.

allows us to carry out the summation over i. We obtain $\lambda_2 \approx N(\sum_{I=1}^{M} n\widetilde{e}_I^2)p_l/k - (n\sum_{J=1}^{M}\widetilde{e}_J)^2 p_l/k$. Since $\sum_{I=1}^{M} n\widetilde{e}_I^2 \approx \sum_{i=1}^{N} e_{2i}^2 = 1$, and $n\sum_{J=1}^{M}\widetilde{e}_J = \sum_{i=1}^{N} e_{2i}$, we have

$$\lambda_2 = \frac{Np_l}{np_s + (N-n)p_l} - (\sum_{i=1}^{N} e_{2i})^2 \frac{p_l}{k}. \tag{3.1}$$

As the normalized eigenvector $\mathbf{e}_1$ associated with λ_1 describes the synchronized state, its components are identical: $\mathbf{e}_1 = [1/\sqrt{N}, \cdots, 1/\sqrt{N}]^T$. If $\mathbf{G}$ is symmetric, its eigenvectors are orthogonal to each other: $\mathbf{e}_i \cdot \mathbf{e}_j = \delta_{ij}$, where $\delta_{ij} = 1$ for $i = j$ and 0 else. Taking $i = 1$, $j = 2$ we have $\sum_{i=1}^{N} e_{2i} = 0$. If $\mathbf{G}$ is slightly asymmetric (as for a weighted network), $\sum_{i=1}^{N} e_{2i}$ is nonzero but small, and the second term in Eq. (3.1) can be neglected. These approximations lead to

$$\lambda_2 \approx \frac{Np_l}{np_s + (N-n)p_l}. \tag{3.2}$$

For $p_l \ll p_s$, the above equation agrees well with the numerics. This provides an analytic explanation for the

observed abnormal behavior. Furthermore, the fact that λ_2 depends only on the ratio of p_l/p_s explains the straight-line patterns in Fig. 5 and in Fig. 6 (b)(d) for $p_s > p_l$.

The above analysis can be extended to more general clustered networks, i.e., those with different cluster sizes or heterogeneous degree distributions in each cluster, by replacing n with n_I—the size of the Ith cluster—for each I, and using the degree distribution $P_I(k)$ in the summation over $1/k$. In this case, p_s and p_l can be regarded as effective parameters, and may vary for different clusters. A formula similar to Eq. (3.2) can be obtained, because even in such a case, the contribution of the second term in Eq. (3.1) is small.

In conclusion, we have uncovered a phenomenon in the synchronization of complex clustered networks, namely, the balance between the numbers of the inter-cluster and intra-cluster links plays a key role in the global synchronizability of the network [84]. The network has the strongest synchronizability only when these numbers match. Mismatch can weaken and even destroy the synchronizability. Clustered networks have been increasingly recognized to be important for real network systems. Our work may provide fresh insight into the functionings of such networks.

4 . OPTIMIZATION OF SYNCHRONIZATION IN COMPLEX CLUSTERED NETWORKS

4.1. Background

Recent years have witnessed a growing interest in the synchronizability of complex networks [47–59]. Earlier works [47–53] suggest that small-world [42] and scale-free [43] networks, due to their small network distances, are generally more synchronizable than regular networks. It has been found, however, that heterogeneous degree distributions typically seen in scale-free networks can inhibit their synchronizability [54], but adding suitable weights to the network elements can enhance their chances to synchronize with each other [55–58]. Synchronizability of complex clustered networks has begun to be studied only recently [61, 85]. In particular, the dependence of synchronizability on the number of clusters in the network has been investigated in Ref. [85], with the result that a network can become more synchronizable with the number of clusters if there are random, long-range links. In the absence of such links, the synchronizability would deteriorate continuously as more clusters appear in the network.

Viewing biological cells in terms of their underlying network structure is a useful concept and has attracted much attention recently [7–11]. Over the past several years, network science has been developed and mathematical treatments have been employed to understand the relation between the topological structure of networks and their functions [11–15]. Organizing biological information using the network idea has been fundamental to utilizing various systems-level approaches to understanding biological function. A key organizational feature in many biological systems is the tendency to form a clustered network structure [2,3,5,16]. For example, proteins with a common function are usually physically associated via stable protein-protein interactions to form larger macromolecular assemblies. These protein complexes (or clusters) are often linked together by extended networks of weaker, transient protein-protein interactions to form interaction networks that integrate pathways mediating the major cellular processes [3,16]. As a result, a protein-protein interaction network can be viewed naturally as an assembly of interconnected functional clusters, or a complex clustered network. Another example is the metabolic network of organisms. It has been found that various metabolic networks are organized into many small, highly connected clusters that combine in a hierarchical manner into larger, less cohesive units. For example, within the *Escherichia coli*, the uncovered hierarchical modularity is highly correlated with known metabolic functions. It is possible that the clustered network architecture is

generic to system-level cellular organization [2]. Recent works have also revealed that the clustered topology is fundamental to many types of social and technological networks [1, 4, 6].

In biology, synchronization is one of the most fundamental dynamics [73]. For examples, fireflies in Southeast Asia, stretching for miles along the river bank, by adjusting the rhythms on receiving signals from others, can flash synchronously [86]. The heart's pacemaker, the so-called sinoatrial node, consists of about 10000 synchronous cells, and generates the electrical rhythm that commands the rest of the heart to beat [87]. Other examples include the rhythmic activity of cells of the pancreas [88] and of neural networks [89]. As the complex, clustered network topology is necessary for describing and understanding the dynamics and function of some key biological systems, it is important to study the synchronizability of such networks.

Given a complex network with a fixed (large) number of nodes, it is believed that its synchronizability can be improved by increasing the number of links. This is intuitive as a denser linkage makes the network more tightly coupled or, "smaller," thereby facilitating synchronization. However, in Chapter 3 we have presented a phenomenon that apparently contradicts this intuition. In particular, a complex clustered network is typically small-world so that its average distance is small. Moreover, its degree distribution can be made quite homogeneous. The surprising phenomenon is that more edges (links), which make the network smaller, do not necessarily lead to stronger synchronizability. There can be situations where more edges can even suppress synchronization if they are placed improperly. We find that the synchronizability of a clustered network is largely determined by the interplay between the inter-cluster and the intra-cluster connections of the network. Strong synchronizability requires that the numbers of the inter-links and intra-links be approximately matched. In this case, increasing the number of links can indeed enhance the synchronizability. However, if the number of one type of links is fixed while the number of the other type is changed so that the matching is deteriorated, synchronization can be severely suppressed or even totally destroyed.

The oscillator models employed in Chapter 3 are discrete-time maps. In biological and technological systems, however, continuous-time oscillator models are more realistic. One aim of this contribution is to address whether synchronization can be optimized in continuous-time oscillator networks with a clustered structure [62]. Another aim is to generalize our finding by considering an alternative coupling scheme that has

not been treated previously. We shall develop a theory based on analyzing the spectral properties the network coupling matrix, which are the key to the network's ability to synchronize. Direct numerical simulations of a class of actual oscillator clustered networks provide strong support for the theory. From the viewpoint of computation, most previous works on network synchronization [47–59] are focused on the eigenvalue properties of the underlying networks. The numerical results in this Chapter are from *direct assessment* of whether or not the underlying oscillator network can achieve synchronization, which involves quite intense computations. Our results imply that, in order to achieve robust synchronization for a clustered biological or technological network, the characteristics of the links are more important than the number of links. Simply counting the number of links may not be enough to determine its synchronizability. Instead, links should be carefully distinguished and classified to predict possible synchronization-related functions of the network.

In Sec. 4.2, we show the master stability function for a typical coupled continuous-time oscillator system. In Sec. 4.3, we develop theory and present numerical results for optimization of synchronization in complex clustered networks. To be as general as possible, two types of coupling schemes have been considered. An extensive discussion of the main result and its biological implications is offered in Sec. 4.4.

4.2. Model setup and master stability function for Rössler oscillators

The approach we take to establish the result is to introduce nonlinear dynamics on each node in the network and then perform stability and eigenvalue analyses [60, 74]. The theoretical derivation yields the stability regions for synchronization in the two-dimensional parameter space defined by the probabilities of the two types of links. The analytic predictions are verified by direct numerical simulations of the dynamical network. To be specific, in this Chapter we consider the following general clustered network model: N nodes are classified into M groups, where each group has $n = N/M$ nodes. In a group, a pair of nodes is connected with probability p_s, and nodes belonging to different groups are connected with probability p_l. This forms a clustered random network. For a clustered network, the number of inter-connections is typically far less than the number of intra-connections. As a result, the parameter region of small p_l values is more relevant.

For the Rössler oscillators we used in the simulation, an example of the master stability function is shown in Fig. 8. The function $\Psi(K)$ is negative in the interval $[K_1, K_2]$, where $K_1 \approx 0.2$ and $K_2 \approx 4.62$.

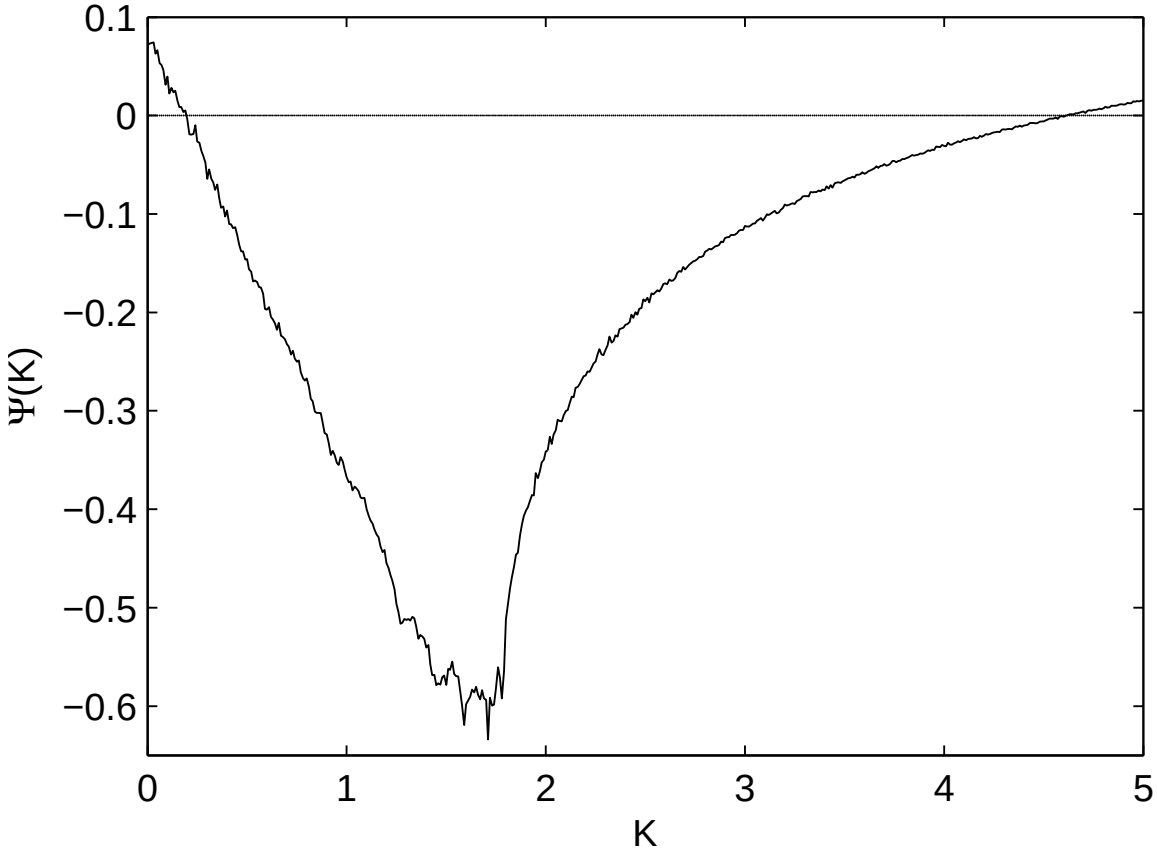

Fig. 8. For the Rössler oscillator network, an example of the master stability function $\Psi(K)$ calculated numerically from Eq. (1.14).

Thus, for $K_1 < K < K_2$, all eigenvectors (eigenmodes) are transversely stable and the network can be synchronized, which gives the condition of the boundary of synchronization region:

$$\lambda_2 \geq \frac{K_1}{\epsilon}, \tag{4.1}$$

$$\lambda_N \leq \frac{K_2}{\epsilon}. \tag{4.2}$$

The boundaries determined by these equations and the numerical simulation results are shown in Fig. 9 for type-I coupling and Fig. 14 for type-II coupling. The analysis and the numerical result agree well.

4.3. Synchronization in continuous-time oscillator clustered networks

We shall consider two types of distinct coupling schemes for complex clustered networks and develop theoretical analysis for synchronization.

4.3.1. Type-I coupling

For type-I coupling, we consider a normalized coupling matrix: for any i ($1 \leqslant i \leqslant N$), $G_{ii} = 1$, $G_{ij} = -1/k_i$ if there is a link between node i and j, and $G_{ij} = 0$ otherwise, where k_i is the degree of node i (the number of links). The coupling matrix $\mathbf{G}$ is not symmetric since $G_{ij} = -1/k_i$ while $G_{ji} = -1/k_j$. Depending on the initial conditions and the network realization, the Rössler system may have desynchronization bursts [90, 91]. It is thus necessary to characterize the network synchronizability in a statistical way. Define P_{syn} as the probability that the fluctuation width of the system $W(t)$ is smaller than a small number δ (chosen somewhat arbitrarily) at all time steps during a long observational period T_0 in the steady state, say, from T_1 to T_1+T_0, where $W(t) = \langle |x(t) - \langle x(t) \rangle| \rangle$, and $\langle \cdot \rangle$ means average over the nodes of the network. If δ is small enough, the system can be deemed as being synchronized in the period T_0, thus P_{syn} is in fact the probability of synchronization of the system in the period T_0, with $P_{syn} = 1$ if the networks for the given parameters can synchronize. Practically, P_{syn} can be calculated by the ensemble average, i.e., the ratio of the number of synchronized cases over the number of all random network realizations. In addition, the ensemble average and time average of fluctuation width $\langle \langle W \rangle_{T_0} \rangle_e$ can be a direct indicator of the degree of synchronization too. Since P_{syn} changes drastically from 0 to 1 in a small region in the parameter space, it is possible to define the boundary between synchronizable region and unsynchronizable region as follows: for a fixed p_s,

the boundary value p_{lb} is such that the quantity $\|\nabla P_{syn}(p_s, p_l)\| \equiv \sqrt{(\partial P_{syn}/\partial p_s)^2 + (\partial P_{syn}/\partial p_l)^2}|_{(p_s,p_l)}$ is maximized at (p_s, p_{lb}). Figure 9 shows the synchronization boundary in the parameter space (p_s, p_l) from both numerical calculation and theoretical prediction of Eqs. (4.1) and (4.2). It can be seen that the two results agree with each other. If the number of inter-cluster connections is fixed, say, $p_l = 0.2$ (the dashed line in Fig. 9), as the number of intra-cluster links exceeds a certain value (as p_s exceeds 0.78), the system becomes desynchronized. Figure 10 shows the synchronization probability P_{syn} on the dashed line in Fig. 9. When p_s is small, e.g. around 0.2, the number of the inter-cluster connections and the number of the intra-cluster connections are approximately matched, and the networks are synchronized. As p_s becomes larger and larger, the matching condition deteriorates, the networks lose their synchronizability, even though their average distances become smaller. That is, too many intra-cluster links tend to destroy the global synchronization. The same phenomenon persists for different parameter values. One remark concerning the physical meaning of the result, as exemplified by Figs. 9 and 10, is in order. Consider two clustered networks where (A) the two types of links are approximately matched and (B) there is a substantial mismatch. Our theory would predict that network A is more synchronizable than network B. This statement is meaningful in a probabilistic sense, as whether or not a specific system may achieve synchronization is also determined by many other factors such as the choice of the initial condition, possible existence of multiple synchronized states, and noise, etc. Our result means that, under the influence of these random factors, there is a higher probability for network A to be synchronized than network B.

Figure 11 shows the dependence of λ_N and λ_2 on the network parameters (p_l,p_s) for the 2-cluster network. The shape of the boundary in Fig. 9 depends on the coupling strength ϵ [Eqs. (4.1) and (4.2)] and on the contour lines of λ_2 and λ_N. For the clustered network of Rössler oscillators, Eq. (4.2) is always satisfied. Thus λ_2 determines the synchronizability of the system. In the following, we shall derive a theoretical formula to understand the dependence of λ_2 on p_l and p_s for small values of p_l, which is the typical parameter regime of clustered networks.

For a clustered network, the components of the eigenvector $\mathbf{e}_2$ have approximately the same value within any cluster, while they can be quite different for different clusters, as demonstrated in Fig. 12. Thus, we can

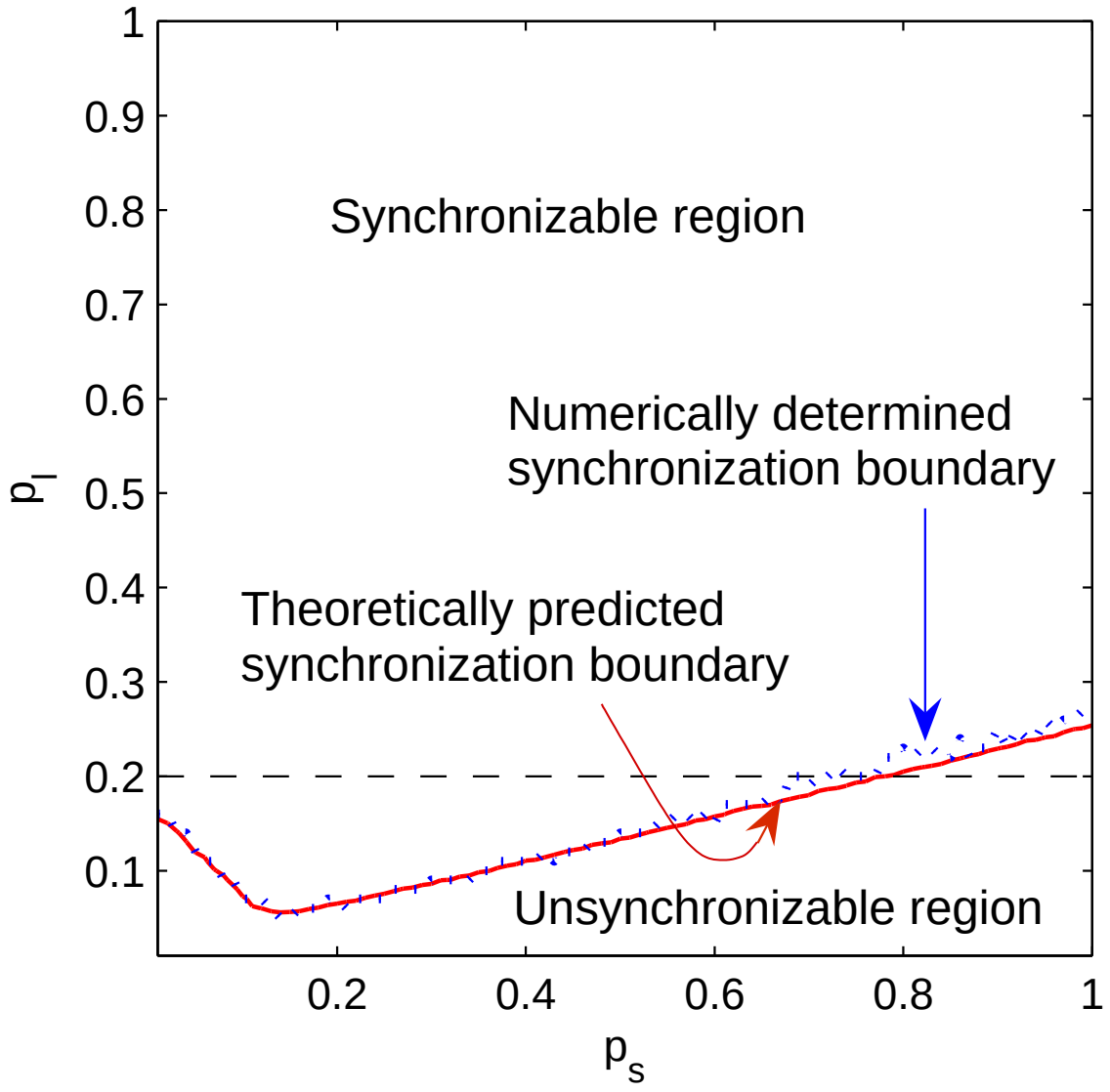

Fig. 9. Synchronization boundary of the coupled Rössler oscillators on a 2-cluster network. The dotted line is the numerically obtained boundary from the computation of P_{syn}, the solid line is from theoretical analysis [Eq. (4.1)] where λ_2 is calculated numerically. The horizontal dashed line indicates the position of the cross section of P_{syn} shown in Fig. 10. Simulation parameters are $N = 100$ and $M = 2$, $\delta = 0.01$, $T_0 = 10^4$, and $\epsilon = 0.5$. Each data is the result of averaging over 1000 network realizations. The data for this figure was obtained with 5 Pentium-IV 2.80GHz CPUs for about 2 weeks.

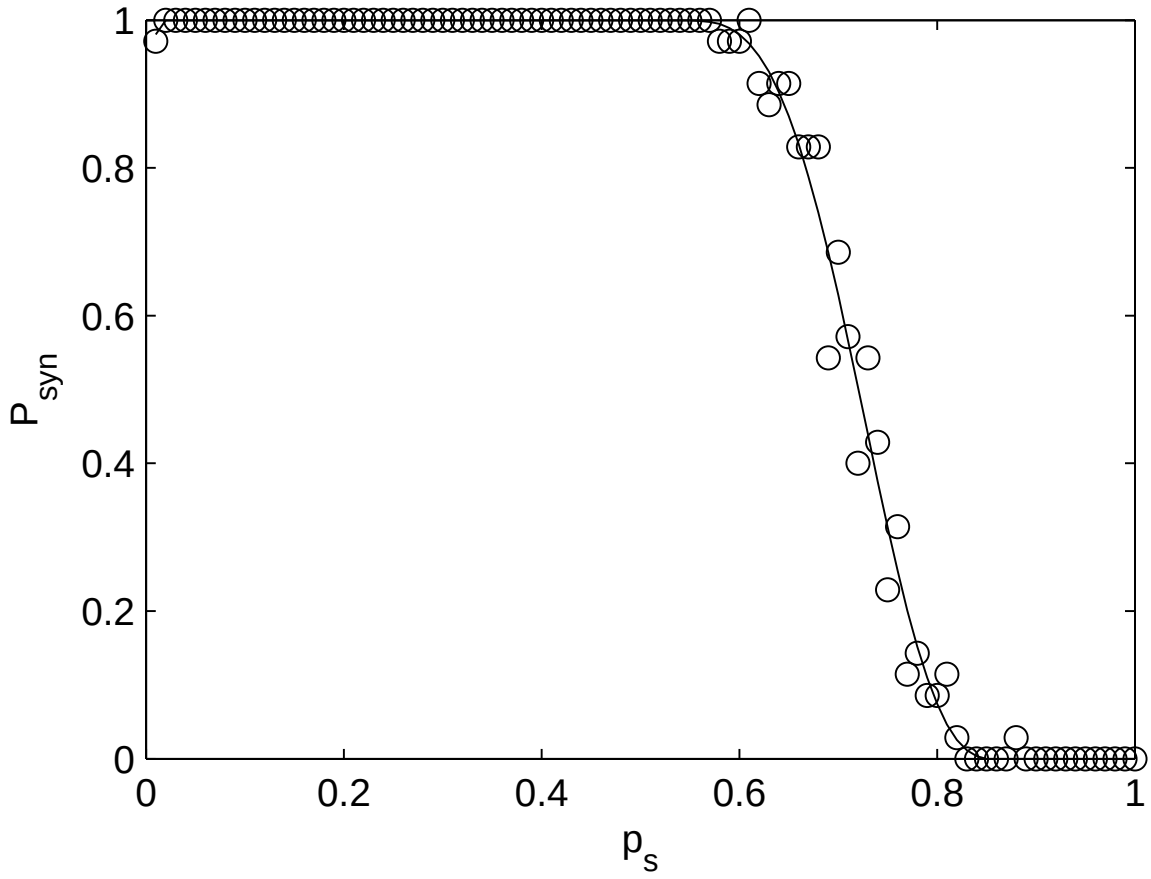

Fig. 10. Synchronization probability P_{syn} versus p_s for $p_l = 0.2$ of a clustered network of Rössler oscillators with $N = 100$ and $M = 2$. $\delta = 0.01$, $T_0 = 10^4$ and $\epsilon = 0.5$. Each data is the result of averaging over 1000 network realizations.

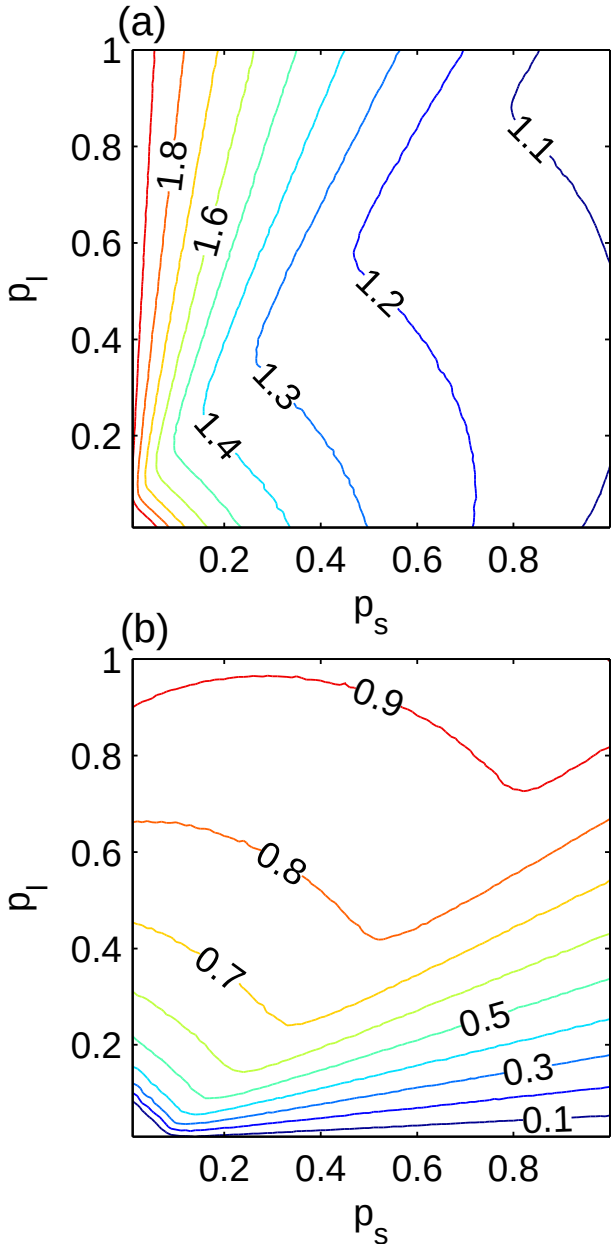

Fig. 11. Contour plots of λ_N (a) and λ_2 (b) in the (p_l, p_s) space for type-I coupling, $N = 100$ and $M = 2$. Each data is averaged over 100 realizations.

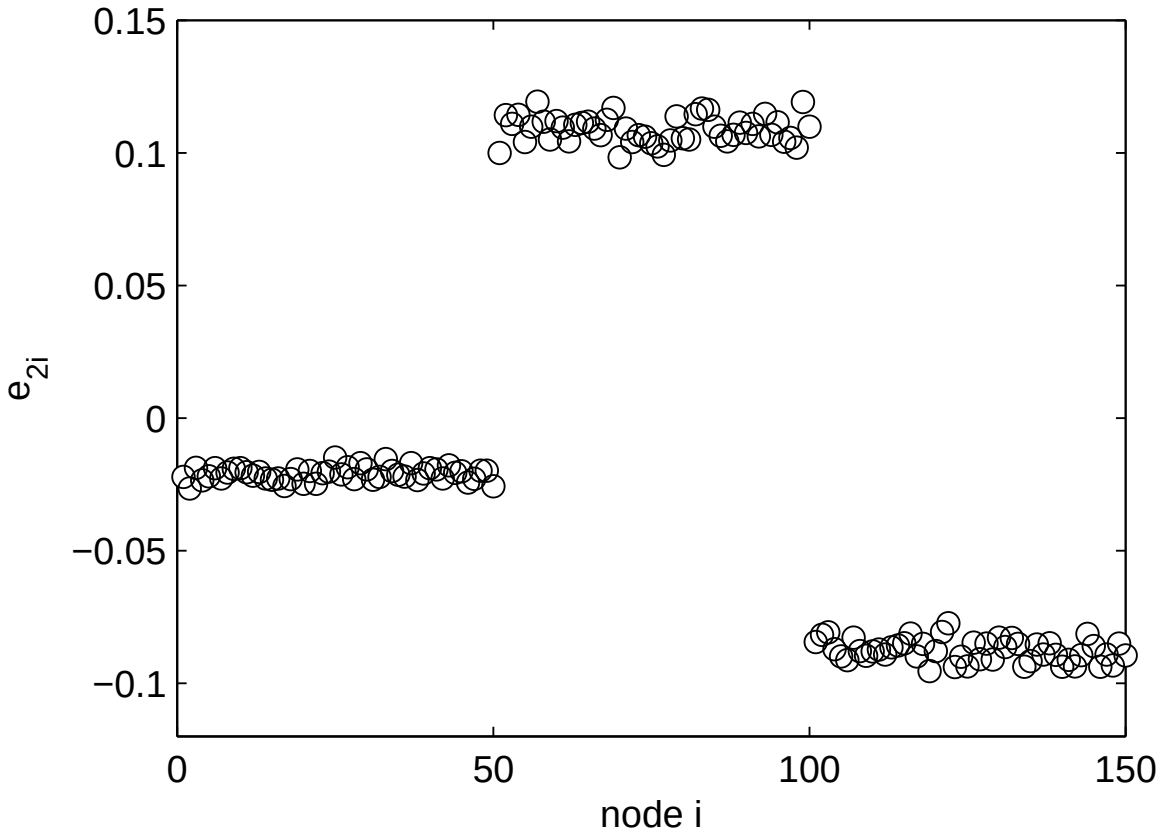

Fig. 12. A typical profile of components of the eigenvector $\mathbf{e}_2$. Parameters are $N = 150$, $M = 3$, $p_l = 0.01$, and $p_s = 0.9$.

write $\mathbf{e}_2 \approx [\widetilde{e}_1, \cdots, \widetilde{e}_1, \widetilde{e}_2, \cdots, \widetilde{e}_2, \cdots, \widetilde{e}_M, \cdots, \widetilde{e}_M]^T$, and for each I, $1 \leqslant I \leqslant M$, there are n $\widetilde{e}_I$'s in $\mathbf{e}_2$. By definition, $\mathbf{G} \cdot \mathbf{e}_2 = \lambda_2 \mathbf{e}_2$ and $\mathbf{e}_2 \cdot \mathbf{e}_2 = 1$, we have $\lambda_2 = \mathbf{e}_2^T \cdot \mathbf{G} \cdot \mathbf{e}_2 = \sum_{i,j=1}^{N} e_{2i} G_{ij} e_{2j}$, where e_{2i} is the ith component of $\mathbf{e}_2$. Expanding the summation in j yields

$$\begin{aligned} \lambda_2 &= \sum_{i=1}^{N} e_{2i}\{G_{i1}\widetilde{e}_1 + G_{i2}\widetilde{e}_1 + \cdots + G_{in}\widetilde{e}_1 \\ &\quad + G_{in+1}\widetilde{e}_2 + \cdots + G_{iN}\widetilde{e}_M\}. \end{aligned} \tag{4.3}$$

Recall that $G_{ii} = 1$; and if i and j belong to the same cluster, G_{ij} equals $-1/k_i$ with probability p_s and 0 with probability $1 - p_s$; while if i and j belong to different clusters, G_{ij} equals $-1/k_i$ with probability p_l and 0 with probability $1 - p_l$, where k_i is the degree of node i. Thus,

$$\begin{aligned} \lambda_2 &= \sum_{i=1}^{N} e_{2i}\{-n\frac{p_l}{k_i}\widetilde{e}_1 - n\frac{p_l}{k_i}\widetilde{e}_2 + \cdots \\ &\quad + \widetilde{e}_I - n\frac{p_s}{k_i}\widetilde{e}_I + \cdots - n\frac{p_l}{k_i}\widetilde{e}_M\}, \end{aligned}$$

where $\widetilde{e}_I$ is the value corresponding to the cluster that contains node i. Noting that $1 - np_s/k_i = (N-n)p_l/k_i$, we have

$$\begin{aligned} \lambda_2 &= \sum_{i=1}^{N} e_{2i}\{(N-n)\frac{p_l}{k_i}\widetilde{e}_I - n\frac{p_l}{k_i}\sum_{J\neq I}^{M}\widetilde{e}_J\} \\ &= \sum_{i=1}^{N} e_{2i}\{N\frac{p_l}{k_i}\widetilde{e}_I - n\frac{p_l}{k_i}\sum_{J=1}^{M}\widetilde{e}_J\}. \end{aligned}$$

For the clustered random network models, the degree distribution has a narrow peak centered at $k = np_s + (N-n)p_l$, thus $k_i \approx k$. The summation over i can now be carried out in a similar manner,

$$\begin{aligned} \lambda_2 &\approx \sum_{I=1}^{M} n\widetilde{e}_I\{N\frac{p_l}{k}\widetilde{e}_I - n\frac{p_l}{k}\sum_{J=1}^{M}\widetilde{e}_J\} \\ &= N\frac{p_l}{k}\sum_{I=1}^{M} n\widetilde{e}_I^2 - (n\sum_{J=1}^{M}\widetilde{e}_J)^2\frac{p_l}{k}. \end{aligned}$$

Note that $\sum_{I=1}^{M} n\widetilde{e}_I^2 \approx \sum_{i=1}^{N} e_{2i}^2 = 1$, and $n\sum_{J=1}^{M}\widetilde{e}_J = \sum_{i=1}^{N} e_{2i}$, thus we have

$$\lambda_2 = \frac{Np_l}{np_s + (N-n)p_l} - (\sum_{i=1}^{N} e_{2i})^2\frac{p_l}{k}. \tag{4.4}$$

The normalized eigenvector $\mathbf{e}_1$ of λ_1 corresponds to the synchronized state, thus its components have constant values: $\mathbf{e}_1 = [1/\sqrt{N}, \cdots, 1/\sqrt{N}]^T$. If $\mathbf{G}$ is symmetric, then eigenvectors for different eigenvalues are

orthogonal: $\mathbf{e}_i \cdot \mathbf{e}_j = \delta_{ij}$, where $\delta_{ij} = 1$ for $i = j$ and 0 else. Take $i = 1$ and $j = 2$, we have $\sum_{l=1}^{N} e_{2l} = 0$. Although the coupling matrix $\mathbf{G}$ is slightly asymmetric, $\sum_{i=1}^{N} e_{2i}$ is nonzero but small, and the second term in Eq. (4.4) can be omitted, leading to the final form:

$$\lambda_2 \approx \frac{Np_l}{np_s + (N-n)p_l}. \tag{4.5}$$

Since $n = N/M$, the above equation can be rewritten as

$$\lambda_2 \approx \frac{Mp_l}{p_s + (M-1)p_l},$$

or

$$\lambda_2 \approx \frac{Mp_l/p_s}{1 + (M-1)p_l/p_s}. \tag{4.6}$$

Figure 13(a) shows for several fixed p_l values, the dependence of λ_2 on p_s, from direct numerical calculation (symbols) and Eq. (4.5) (curves). For fixed p_l and large p_s, λ_2 decreases as p_s increases, thus the network becomes more difficult to be synchronized. This provides an analytic explanation for the numerically observed abnormal behavior in the network synchronizability. For small p_s, when $p_s \sim p_l$, the network becomes a single random network, thus λ_2 approximately follows the formula for random networks, which is an increasing function of p_s [92]. This makes clear the increasing behavior of λ_2 at small p_s cases. Furthermore, since λ_2 depends only on the ratio of p_l/p_s, this explains the straight-line patterns in Fig. 11(b) for $p_s > p_l$.

From Eq. (4.6), we can see that λ_2 is determined by the number of clusters M; it does not depend on the network size N, or the size of each cluster n, insofar as M is given. Figure 13(b) shows λ_2 versus M. The symbols are form direct numerical simulations and the curves are from theory [Eq. (4.6)] for two values of the ratio p_l/p_s: $0.05/0.8$ and $0.1/0.8$. Two cluster sizes ($n = 50$ and $n = 200$) are used. One can see that numerics agrees with the theory well for all cases. The larger cluster size case (crosses) agrees with the theory better. Since the synchronization boundaries is mainly determined by λ_2, it can be inferred that the synchronization boundary changes with the number of clusters. Even though, the straight-line pattern of λ_2 in the (p_l, p_s) plane persists, thus the synchronization boundary in the plane will have a similar straight-line pattern as for the $M = 2$ case, and our result that large p_s can deteriorate synchronization persists.

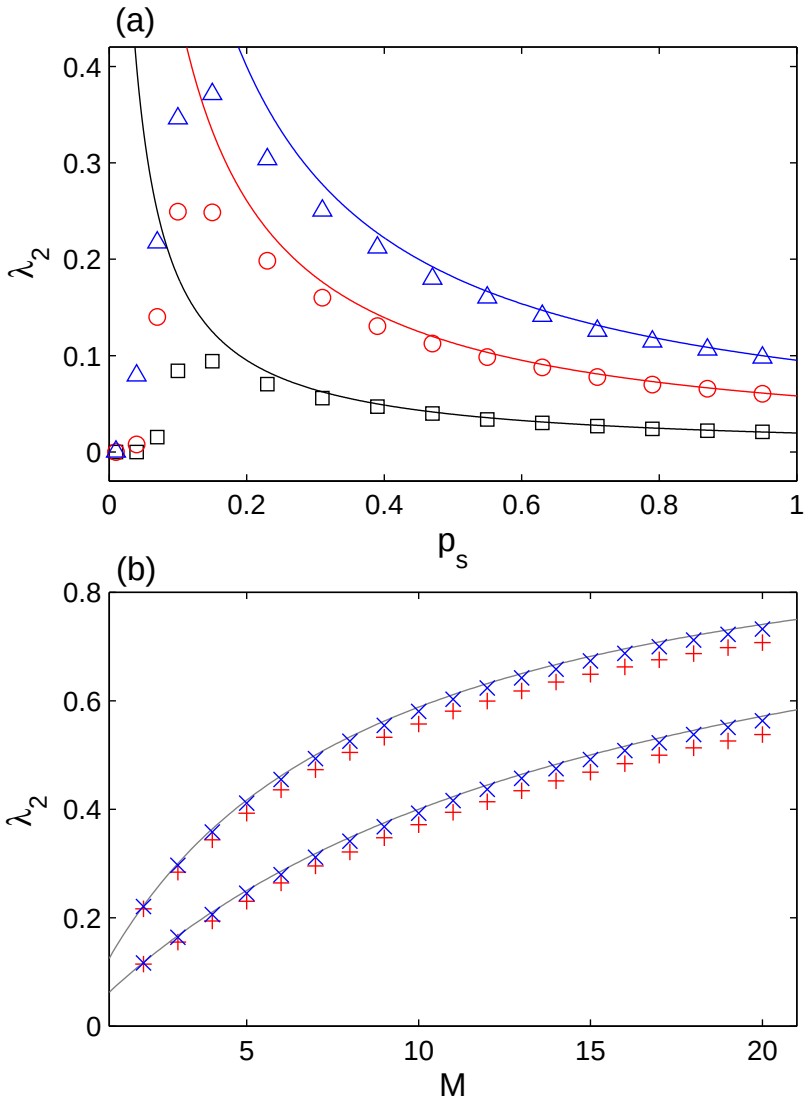

Fig. 13. (a) λ_2 vs p_s for a network with 2 clusters. From bottom to top, $p_l = 0.01$ (squares), $p_l = 0.03$ (circles), and $p_l = 0.05$ (up triangles). $N = 100$ and $n = 50$. (b) λ_2 vs the number of clusters M for $n = 50$ (pluses) and $n = 200$ (crosses). $p_s = 0.8$; $p_l = 0.05$ for the lower set of data and $p_l = 0.1$ for the upper set of data. Note that the network size $N = Mn$ is changed with M. The symbols are obtained numerically and each data point is the average of 100 network realization. The curves are from theory [Eq. (4.5)].

For large M values ($M \gg 1$), λ_2 can be approximated as $\lambda_2 \approx Mp_l/(p_s + Mp_l)$. For a given p_s value, the density of links within a cluster is fixed. Suppose the dynamical model of each node is also given, thus the critical value of λ_2 for synchronization is fixed. As a result, for networks with many clusters, the probability of inter-cluster connections p_l required for achieving synchronization decreases as $1/M$. Note that $n^2(M-1)p_l \approx n^2 M p_l$ is the average number of inter-cluster links per cluster. This means, insofar as the average number of inter-cluster links per cluster is larger than certain critical value (depending on the dynamics), the network is always synchronizable, regardless of the number of clusters (the network size). This result is consistent with that in Ref. [74], which states that for random networks, one can have chaotic synchronization for any arbitrarily large network size, if the average degree is larger than some threshold.

The above analysis can be extended to more general clustered networks, i.e., those with different cluster sizes or heterogeneous degree distributions in each cluster, by replacing n with n_I - the size of the Ith cluster - for each I, and using the degree distribution $P_I(k)$ of the Ith cluster in the summation over $1/k$. In this case, p_s and p_l can be regarded as effective parameters, and may vary for different clusters. A formula similar to Eq. (4.5) can be obtained, because even in such a case, the contribution of the second term in Eq. (4.4) to λ_2 is small. This justifies that the observed abnormal synchronization phenomenon is due to the clustered network structure, and does not depend on the details of the dynamics.

4.3.2. Type-II coupling

For type-II coupling, the coupling matrix is defined as: for any i ($1 \leqslant i \leqslant N$), $G_{ii} = k_i$, $G_{ij} = -1$ if there is a link between node i and j, and $G_{ij} = 0$ otherwise. The simulation results are shown in Fig. 14. In this case, we fix $p_l = 0.1$ (so the number of inter-cluster connections is fixed), and examine the synchronizability of the system versus p_s. When p_s is small, there are frequent desynchronization bursts [90, 91], thus the average fluctuation width $\langle\langle W\rangle_{T_0}\rangle_e$ is large and the system has a lower synchronization probability P_{syn}. As p_s increases, the system becomes more synchronizable and the intermittent desynchronization bursts become rare, and finally it stays synchronized in the whole time interval T_0 (about $p_s = 0.1$). As p_s is increased further passing through a stable range $(0.1, 0.8)$, the system becomes unstable. For even larger values of p_s, the system diverges for almost every network realization tested, which accounts for a small synchronization

probability P_{syn}. The vertical lines in Fig. 14 show the positions of the synchronization boundaries obtained from Eqs. (4.1) and (4.2). It can be seen that the theory agrees well with the numerical simulations. The eigenvalues have been obtained numerically, and contour plots of λ_N and λ_2 in the network parameter space (p_l, p_s) are shown in Fig. 15. Therefore, under the stability boundary conditions Eqs. (4.1) and (4.2), the phenomenon that the synchronizability is deteriorated and destroyed in the presence of the mismatch in the numbers of inter-cluster and intra-cluster links for type-II coupling is also originated from the clustered structure and does not depend on the details of dynamical oscillators.

For type-II coupling, both λ_N and λ_2 will affect the synchronizable region, therefore we shall provide a theoretical approach for λ_N and λ_2 in terms of p_s and p_l for the case of $p_l \ll p_s$. For $p_l \ll p_s$, the largest eigenvalue of the system λ_N is on the same order of magnitude as the largest eigenvalue of one cluster λ_n, thus it is reasonable to write $\lambda_N = \lambda_n + \delta$, where δ depends on p_l. Let us first consider λ_n. Since each cluster is a random network with size n and connecting probability p_s, λ_n is the largest eigenvalue of the coupling matrix of this random subnetwork $\mathbf{G_n}$. $\mathbf{G_n}$ can be decomposed as $\mathbf{G_n} = \mathbf{D_n} - \mathbf{A_n}$, where $\mathbf{D_n}$ is a diagonal matrix and $(D_n)_{ii} = k_i$, and $\mathbf{A_n}$ is the adjacency matrix of the random subnetwork defined as $(A_n)_{ij} = 1$ if there is a link between node i and node j and 0 otherwise. It is known that the largest eigenvalue of $\mathbf{A_n}$ approaches np_s for large n, and the spectra density of the other eigenvalues satisfies a semicircle law [93–96]:

$$\rho(\lambda) = \begin{cases} (2\pi\sigma^2)^{-1}\sqrt{4\sigma^2 - \lambda^2} & \text{if } |\lambda| < 2\sigma \\ 0 & \text{otherwise} \end{cases},$$

where $\sigma = \sqrt{np_s(1-p_s)}$. Thus the eigenvalues of $-\mathbf{A_n}$ have a minimum value of $-np_s$ and the others are approximately distributed in $(-2\sigma, 2\sigma)$. Since the degree distribution of the random network is binomial with mean value of np_s and standard variation $\sigma_k = \sigma = \sqrt{np_s(1-p_s)}$, which is much smaller than the mean value np_s, $\mathbf{D_n}$ can be approximated as $\mathbf{D_n} \approx np_s\mathbf{I_n}$, where $\mathbf{I_n}$ is the identity matrix of order n. Adding $\mathbf{D_n}$ to $-\mathbf{A_n}$ only shifts all the eigenvalues of $-\mathbf{A_n}$ by the amount np_s, and moves the minimum eigenvalue of $-\mathbf{A_n}$ to 0, which is λ_1 of $\mathbf{G_n}$. Therefore the largest eigenvalue of $\mathbf{G_n}$ is

$$\lambda_n(p_s) = np_s + 2\sigma = np_s + 2\sqrt{np_s(1-p_s)}. \tag{4.7}$$

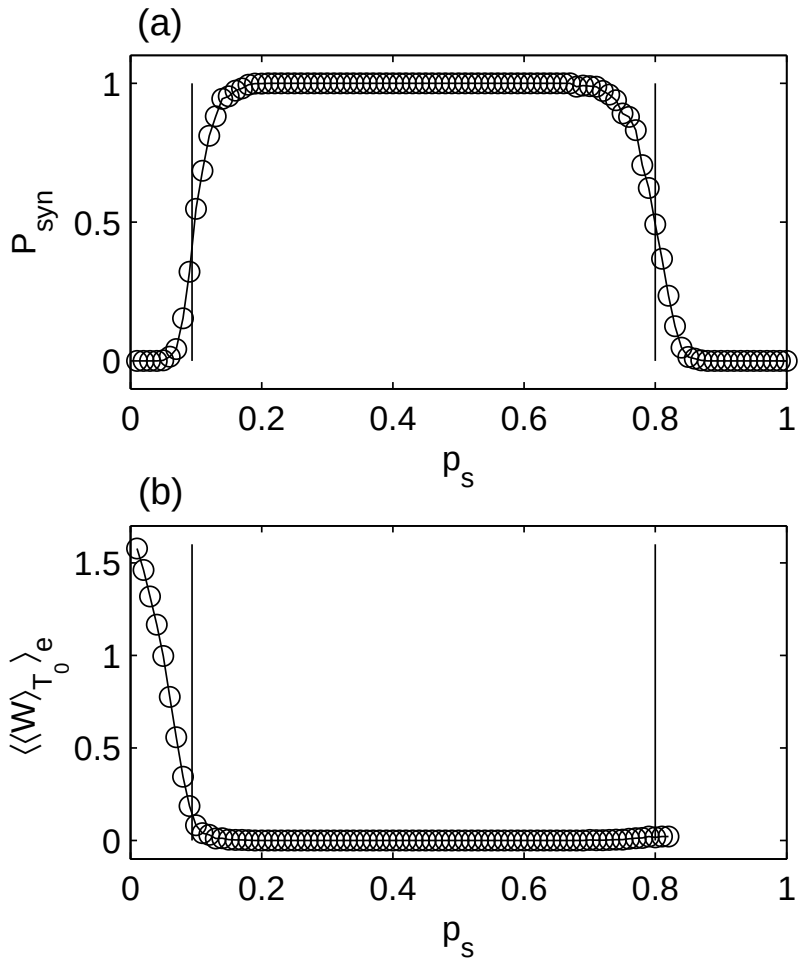

Fig. 14. Properties of the coupled Rössler system for type-II coupling. (a) the synchronization probability P_{syn} versus the intra-cluster connectivity probability p_s; (b) ensemble averaged and time averaged fluctuation width $\langle\langle W\rangle_{T_0}\rangle_e$, where $p_l = 0.1$, $T_0 = 20000$, $\delta = 0.001$, $\epsilon = 0.083$, $N = 100$, and $M = 2$. Vertical lines indicate the positions of the synchronization boundaries obtained from Eq. (4.1) and Eq. (4.2) where the eigenvalues are calculated numerically. The absence of data points for large p_s in (b) means the system variables diverge. Each data point is the result of averaging over 1000 network realizations. The data for this figure were obtained with 10 Pentium-IV 2.80GHz CPUs for about 2 weeks.

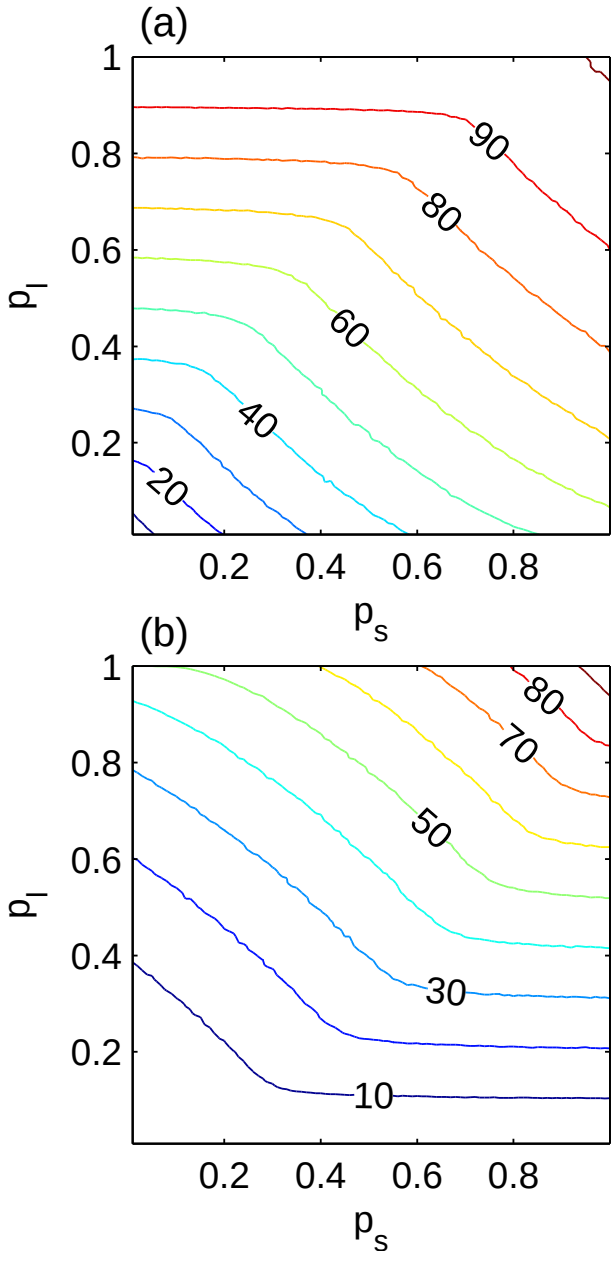

Fig. 15. Contour plots of λ_N (a) and λ_2 (b) in the (p_l, p_s) space for type-II coupling, $N = 100$ and $M = 2$. Each data is averaged over 100 realizations.

To assess δ, note that when p_l is small, δ approximately depends on p_l only, i.e., $\partial\delta/\partial p_l \gg \partial\delta/\partial p_s$. Thus $\delta(p_l, p_s) \approx \delta(p_l)$, which can be estimated at the point $p_s = p_l$:

$$\delta(p_l) = \lambda_N(p_l, p_l) - \lambda_n(p_l).$$

For $p_s = p_l$, the whole system is a homogeneous random network with connecting probability p_l, thus the largest eigenvalue can be obtained from Eq. (4.7): $\lambda_N(p_l, p_l) = Np_l + 2\sqrt{Np_l(1-p_l)}$. We have

$$\delta(p_l) = (N-n)p_l + 2(\sqrt{N} - \sqrt{n})\sqrt{p_l(1-p_l)},$$

and the largest eigenvalue of the random clustered network can be expressed as:

$$\begin{aligned} \lambda_N(p_l, p_s) &= \lambda_n(p_s) + \delta(p_l) \\ &= np_s + (N-n)p_l + 2\sqrt{np_s(1-p_s)} \\ &\quad +2(\sqrt{N} - \sqrt{n})\sqrt{p_l(1-p_l)}. \end{aligned} \tag{4.8}$$

Figure 16(a) shows the simulation results (symbols) of λ_N for different cases. The curves are from Eq. (4.8). It can be seen that the two fit well. Note that Eq. (4.8) is valid only for $p_l \ll p_s$. For $p_l > p_s$, the clustered structure vanishes and the decomposition of λ_N into λ_n is invalid.

We now turn our attention to λ_2. The corresponding eigenvector has a similar structure for type-II coupling as that for type-I coupling (see Fig. 12), therefore we have the same equation as Eq. (4.3). The coupling matrix is different from that of type-I coupling. In particular, $G_{ii} = k_i$, and if i and j belong to the same cluster, G_{ij} equals -1 with probability p_s and 0 with probability $1 - p_s$, while if i and j belong to different clusters, G_{ij} equals -1 with probability p_l and 0 with probability $1 - p_l$. We can thus write λ_2 as

$$\begin{aligned} \lambda_2 &= \sum_{i=1}^{N} e_{2i}\{-np_l\widetilde{e}_1 - np_l\widetilde{e}_2 + \cdots \\ &\quad +k_i\widetilde{e}_I - np_s\widetilde{e}_I + \cdots - np_l\widetilde{e}_M\}, \end{aligned}$$

where $\widetilde{e}_I$ is the value corresponding to the cluster that contains node i. Noting that $k_i \approx k = np_s + (N-n)p_l$,

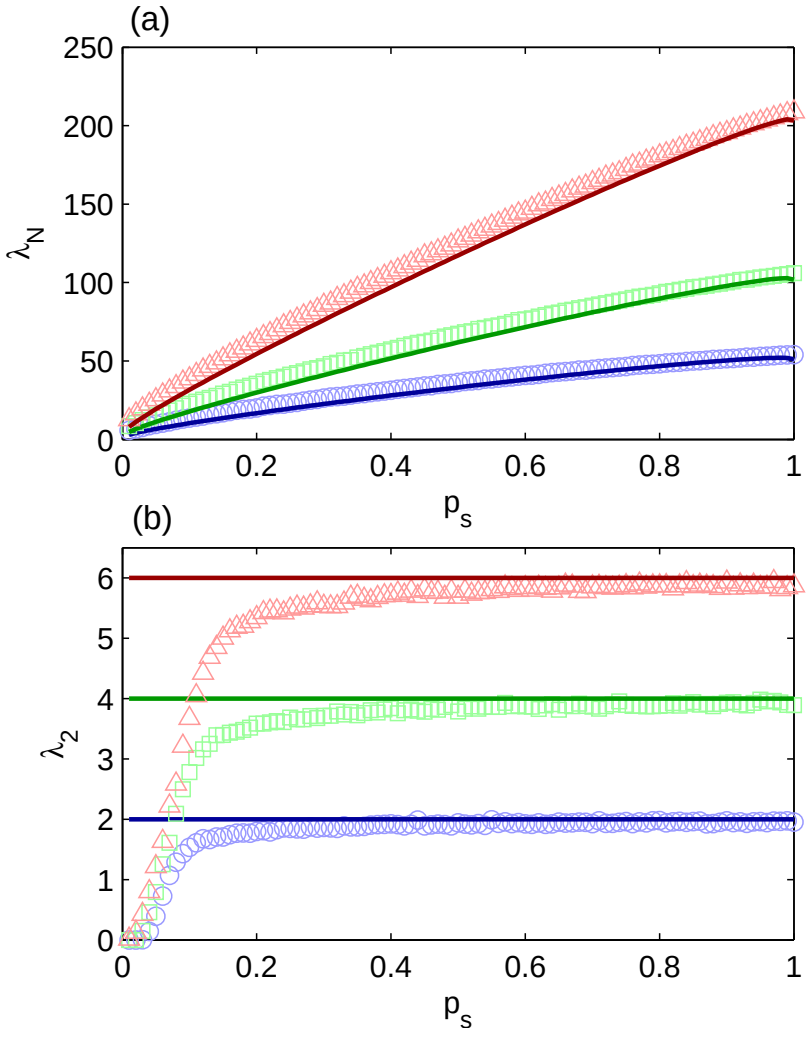

Fig. 16. For type-II coupling, (a) the largest eigenvalue λ_N versus p_s for $p_l = 0.01$ and $N = 100,\ 200,\ 400$ from bottom to top, where $M = 2$. Symbols are from direct numerical simulation, curves are from Eq. (4.8). (b) The smallest nontrivial eigenvalue λ_2 versus p_s for $N = 200$, $M = 2$ and $p_l = 0.01,\ 0.02,\ 0.03$ from bottom to top. Symbols are from direct numerical simulation, the solid lines are from Eq. (4.9). Each data is averaged over 100 realizations.

under similar manipulations to those for type-I coupling, we have

$$\begin{aligned}
\lambda_2 &= \sum_{i=1}^{N} e_{2i}\{(N-n)p_l\widetilde{e}_I - np_l\sum_{J\neq I}^{M}\widetilde{e}_J\} \\
&= \sum_{i=1}^{N} e_{2i}\{Np_l\widetilde{e}_I - np_l\sum_{J=1}^{M}\widetilde{e}_J\} \\
&\approx \sum_{I=1}^{M} n\widetilde{e}_I\{Np_l\widetilde{e}_I - np_l\sum_{J=1}^{M}\widetilde{e}_J\} \\
&= Np_l\sum_{I=1}^{M} n\widetilde{e}_I^2 - (n\sum_{J=1}^{M}\widetilde{e}_J)^2 p_l.
\end{aligned}$$

Note that $\sum_{I=1}^{M} n\widetilde{e}_I^2 \approx \sum_{i=1}^{N} e_{2i}^2 = 1$, and $n\sum_{J=1}^{M}\widetilde{e}_J = \sum_{i=1}^{N} e_{2i} = 0$ ($\mathbf{G}$ is symmetric for type-II coupling), finally we have

$$\lambda_2 \approx Np_l. \tag{4.9}$$

Figure 16(b) shows the dependence of λ_2 on p_s. The theory [Eq. (4.9), curves] agrees well with the numerical simulations (symbols). The analytical results about λ_N and λ_2 [Eqs. (4.8) and (4.9)] explain the patterns in Fig. 15 for the $p_l < p_s$ region. Since λ_N increases with p_s, for large p_s, λ_N could be too large, leading to an instability in the corresponding eigenmode of the system. This explains that too many intra-cluster links can depress the synchronizability of the system.

4.4. Discussions

In conclusion, we have presented theory and numerical evidence that optimal synchronization of continuous-time oscillator clustered networks can be achieved by matching the probabilities of inter-cluster and intra-cluster links. That is, at a global level, the network has the strongest synchronizability when these probabilities are approximately equal. Overwhelmingly strong intra-cluster connection can counterintuitively weaken the network synchronizability. This can be better understood by the following considerations. Network synchronizability is usually characterized by the spread of the nontrivial eigenvalues. What our analytical formulae suggest is that spread becomes minimal when the two probabilities are approximately matched. For instance, when the inter-cluster linking probability p_l is fixed, increasing the intra-cluster connection probability p_s could result in desynchronization. On the other hand, for realistic clustered networks, p_l is always smaller than p_s, and is usually much smaller. Our analysis indicates that, insofar as the network is

clustered ($p_s > p_l$), a larger p_l will lead to better synchronizability. To give another example, consider a particular set of (p_l, p_s) values for which the network cannot be synchronized. Then, increasing p_l while decreasing p_s (so as to keep the average degree fixed) can lead to synchronization (Figs. 11 and 15). While our theory gives a general picture for the network synchronizability in the two-dimensional parameter plane (p_l, p_s), the optimal cases where the two probabilities match approximately do not seem to occur in realistic situations, where p_l is usually much smaller than p_s.

While our network model is somewhat idealized, we have argued that similar phenomena should persist in more general clustered networks. In real biological or technological systems with a clustered structure, if global synchronization is the best performance of the system, special attention needs to be paid to distinguishing the inter-connections and intra-connections as in this case, a proper distribution of the links is more efficient than adding links blindly. For biological networks, such as the metabolic network and the protein-protein interaction network, certain nodes may have many more links than the others, which forms a hierarchical clustered structure [11]. This indicates a power-law distribution of the degree k: $P(k) \sim k^{-\gamma}$. Therefore it is interesting to study clustered scale-free networks, networks where each cluster contains a scale-free subnetwork. We have studied the synchronizability of such clustered networks. In particular, for each cluster, the subnetwork was generated via the preferential attachment rule [43]. Initially, there is a fully connected small subset of size m_0, then a new node is added with m links, and the probability that a previous node i is connected to this new node is proportional to its current degree k_i. New nodes are continuously added until a prescribed network size n is reached. In our simulation, we take $m_0 = 2m + 1$ so that the average degree of this network is $2m$. M such scale-free subnetworks are generated. Then we connect each pair of nodes in different clusters with probability p_l. For this model, p_l controls the number of inter-cluster links, and m controls the number of intra-cluster links. We have carried out numerical simulations, and found that the patterns for the eigenvalues λ_N and λ_2 are essentially the same as that for the clustered network where each cluster contains a random subnetwork (Figs. 11 and 15). In fact, we have compared the simulation results to Eq. (4.5) for the type-I coupling, where we took $p_s = 2m/n$. The mean field theory Eq. (4.5) fits

reasonably well with the simulation results. This indicates that optimization of synchronization by matching different types of links is a general rule.

The general observation is that the synchronizability of the clustered networks is mainly determined by the underlying clustered structure. Insofar as there is a clustered structure, details such as how nodes within a cluster connect to each other, what kind of dynamics are carried by the network and what the parameters are, do not appear to have a significant influence on the synchronization in the coupled oscillator networks supported by the clustered backbone. A practical usage is that, even if the details about the dynamics of a realistic system are not available, insofar as the underlying network has a clustered structure, we can expect similar synchronization behaviors as presented in this Chapter.

An interesting issue about the synchronization dynamics on a clustered network is how it desynchronizes. As discussed in Ref. [90, 91], when desynchronization occurs, the deviation from the synchronization state, $x_i - \langle x_i \rangle$, will have the same form as the unstable eigenmodes (eigenvectors). As a result, if the desynchronization is caused by λ_2's being too small [violation of condition (4.1)], the desynchronized dynamics will have a clustered structure, due to a clustered structure in the corresponding eigenvector $\mathbf{e}_2$: nodes within a cluster have approximately the same dynamical variables, while they can be quite different among clusters. That is, desynchronization occurs among clusters. However, if the desynchronization is caused by λ_N's being too large [violation of condition (4.2)], the deviation $x_i - \langle x_i \rangle$ will not have a clustered structure, since $\mathbf{e}_N$ typically does not exhibit any clustered features. In this case, desynchronization occurs both among and within clusters.

The clustered topology has also been identified in technological networks such as computer networks and certain electronic circuit networks [97–99]. For a computer network, the main functions include executing sophisticated codes to carry out extensive computations. Suppose a large-scale, parallel computational task is to be accomplished by the network, for which synchronous timing is of paramount importance. Our result can provide useful clues as to how to design the network to achieve the best possible synchronization and consequently optimal computational efficiency.

5 . ALTERNATING SYNCHRONIZABILITY OF COMPLEX CLUSTERED NETWORK WITH REGULAR LOCAL STRUCTURE

5.1. Background

Synchronization in complex networks has attracted much attention recently [6,54,61,85,100–102]. Earlier works have found that random [103], small-world [42], and scale-free [43] networks, due to their small network distances, are generally more synchronizable than regular networks [100]. However, small network distance alone is not a guarantee for strong synchronizability. For example, for a scale-free network, the existence of hubs contributes to a small network distance but the underlying heterogeneous degree distribution can cause a wide spread in the eigenvalues of the coupling matrix, which can actually inhibit network synchronization [54]. More recent works have found that, by assigning larger weights to the hubs or introducing a gradient field from hub nodes to small degree nodes, scale-free networks can be more synchronizable than random networks [101]. Modifying local connecting structure, if done properly, can also change the synchronizability significantly [102]. Synchronizability of complex clustered networks has begun to be investigated only recently [6, 61, 85].

In this Chapter, we investigate the synchronizability of locally regular, complex clustered networks [63] (see Sec. 5.2 for motivations from systems biology). A clustered network consists of a number of groups, where nodes within each group are densely connected, but the linkages among the groups are sparse. In fact, the tendency to form a clustered network structure appears to be a key organizational feature in biological systems, such as protein-protein interaction networks [3,5,16] and metabolic graphs [2]. Previous works have also revealed that the clustered topology is fundamental to many types of social and technological networks [104]. Our recent work [61] on the synchronizability of clustered networks with *random* subnetworks has revealed an interesting phenomenon, namely, more links, which make the network smaller, do not necessarily lead to a stronger synchronizability. There can be situations where extra links, if placed improperly, can suppress synchronization. Realistic considerations stipulate that the globally random connections among clusters be sparse. Thus a key question is what can happen to network synchronizability when the density of intra-cluster links is varied. We find that, for a typical locally regular clustered network, its synchronizability exhibits an alternating, highly non-monotonic behavior as a function of the intra-cluster link density. In fact,

there are distinct regions of the density for which the network synchronizability is maximized, but there are also parameter regions in between for which the synchronizability diminishes. We show that, while surprising, this phenomenon of *alternating synchronizability* can be fully explained theoretically based on analyzing the behavior of the eigenvalues and eigenvectors of the coupling matrix. A feature that makes our theoretical analysis feasible is that, due to the locally regular topology of the network, some key eigenvectors within each individual cluster exhibit periodic wave patterns. Both numerical eigenvalue calculations and direct simulation of the actual synchronization dynamics of the underlying oscillator network provide firm support for the theory. One implication is that, in order to achieve robust synchronization, the density of the local connections within a cluster needs to be appropriately tuned since both high density and low density can hinder synchronization.

Considerations from systems biology that motivate our work are described in Sec. 5.2. A detailed theoretical treatment of the synchronizabilities of clustered networks with regular subnetworks is provided in Sec. 9.2. In particular, we begin with relatively simple networks of two clusters and then extend the analysis to networks with multiple clusters. The issue of robustness of the alternating-synchronization behavior will also be addressed. Direct numerical support from actual simulations of synchronous dynamics is provided in Sec. 5.4. Discussions are presented in Sec. 9.4.

5.2. Biological motivations

Complex multicellular organisms such as the human body require multi-scale organizational structures, including formation of organs from large numbers of cells and integration of many organs into the systemic structure necessary for individual survival and proliferation. The organs typically consist of large numbers of multicellular functional units such as crypt in the colon, nephron in the kidney, lobule in the liver, and alveolus in the lung, etc. While extensive recent work has focused on the structure and dynamics of intracellular molecular networks [17–21], there has been little effort to extend this kind of analysis to the interactions among cells within functioning multicellular organs which allow, for example, the human liver to synchronize as many as 10^{12} individual cells into a single functioning unit. There are two general methods by which cells can communicate with each other. Locally, cells usually establish their mutual communication chan-

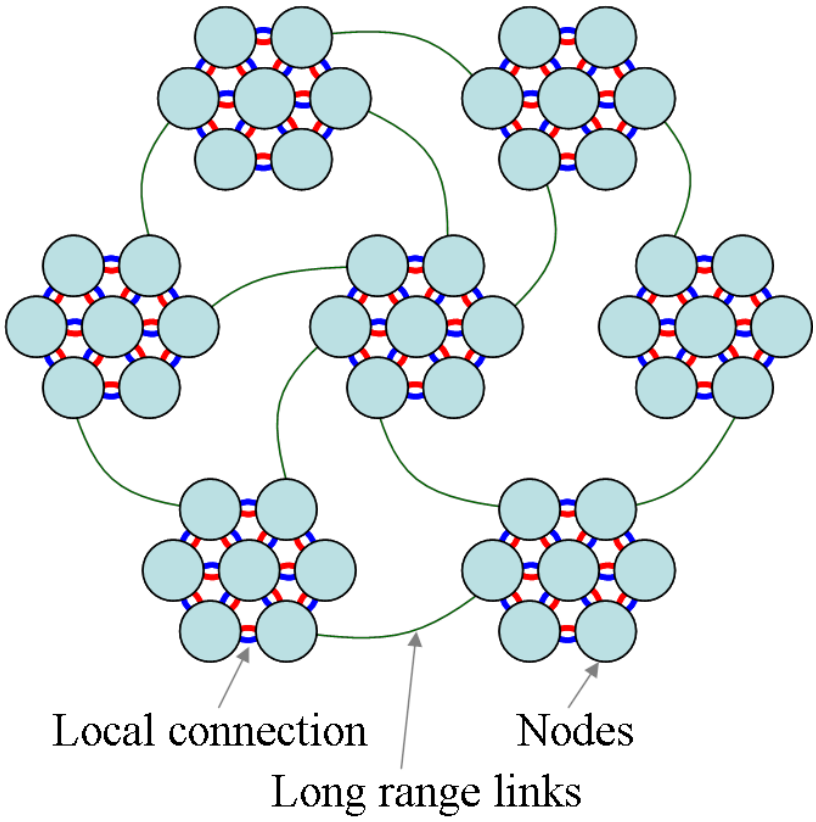

Fig. 17. Schematic illustration of our clustered network model with regular subnetworks.

nels through transmembrane pathways such as gap junctions that allow small molecules to pass between two cells in both directions. At a larger scale, cells communicate with each other through diffusing signals with cell-specific receptors. The interaction is usually directed in the sense that signals such as growth factors are produced by some, but not all cells, and can be received only by other cells that express the appropriate receptors. Despite the fact that many of the specific pathways by which cells communicate have been reasonably well characterized, remarkably little is known about the organizational principles that govern communications among large numbers of cells and permit synchronized function over substantial distances [22, 23].

Since cells communicate with each other using the two general methods described above, an intercellular-information network contains two essential features: a *locally regular* topology based on local communication with neighbors via membrane structures such as gap-junction and integrins [24] and *globally*

random, directional couplings based on long-range diffusing signals and the corresponding cell membrane receptors. To better distinguish between local and global interactions, it is useful to assume that local interactions are confined within clusters, and global interactions occur among the clusters, as shown in Fig. 17. The result is a class of complex clustered networks with a regular subnetwork in each cluster but with random, sparse couplings among clusters. We shall address the issue of synchronization on this class of networks. This is reasonable because there are two basic biological requirements for such a network: (1) there must be a sufficient degree of synchronization to permit the entire organ to function as a single unit, so as new cells are "added" during growth and repair, their precise locations and differentiated phenotypes are specified with nearly perfect accuracy; and (2) the synchronization must be robust so that lost cells (due, for example, to a wound) can be replaced and the system is resistant to cascading failure, enabling isolation of infections such as viruses to prevent rapid, global spread.

5.3. Synchronizability via spectral analysis

We consider the following network structure: N nodes are grouped into M clusters, where each cluster contains $n = N/M$ nodes. In each cluster, the nodes are ordered on a ring so that the subnetwork is regular. Each node connects to m nearest neighbors. Each pair of nodes in different clusters is connected with probability p. While biological considerations stipulate that the long-range links, i.e. links between clusters, be directional, to be as general as possible we shall treat both bi-directional and directional coupling cases. To facilitate analytic derivation and understanding, we first consider a network consisting of two clusters with bi-directional inter-cluster links and then generalize the theory to M-cluster networks for $M > 2$.

The standard approach to addressing the synchronizability of a complex network is to consider a corresponding coupled oscillator network [100], where one nonlinear oscillator is placed on each node of the network. The dynamical system can be described by

$$\frac{d\mathbf{x}_i}{dt} = \mathbf{F}(\mathbf{x}_i) - \epsilon \sum_{j=1}^{N} G_{ij}\mathbf{H}(\mathbf{x}_j), \;\; i = 1,\, 2, \cdots,\, N, \tag{5.1}$$

where ϵ is a global coupling parameter, $\mathbf{G}$ is the coupling matrix determined by the network topology, and $\mathbf{H}(\mathbf{x})$ is a coupling function. The coupling matrix $\mathbf{G}$ is defined as $G_{ij} = -1/k_i$ if there is a link between

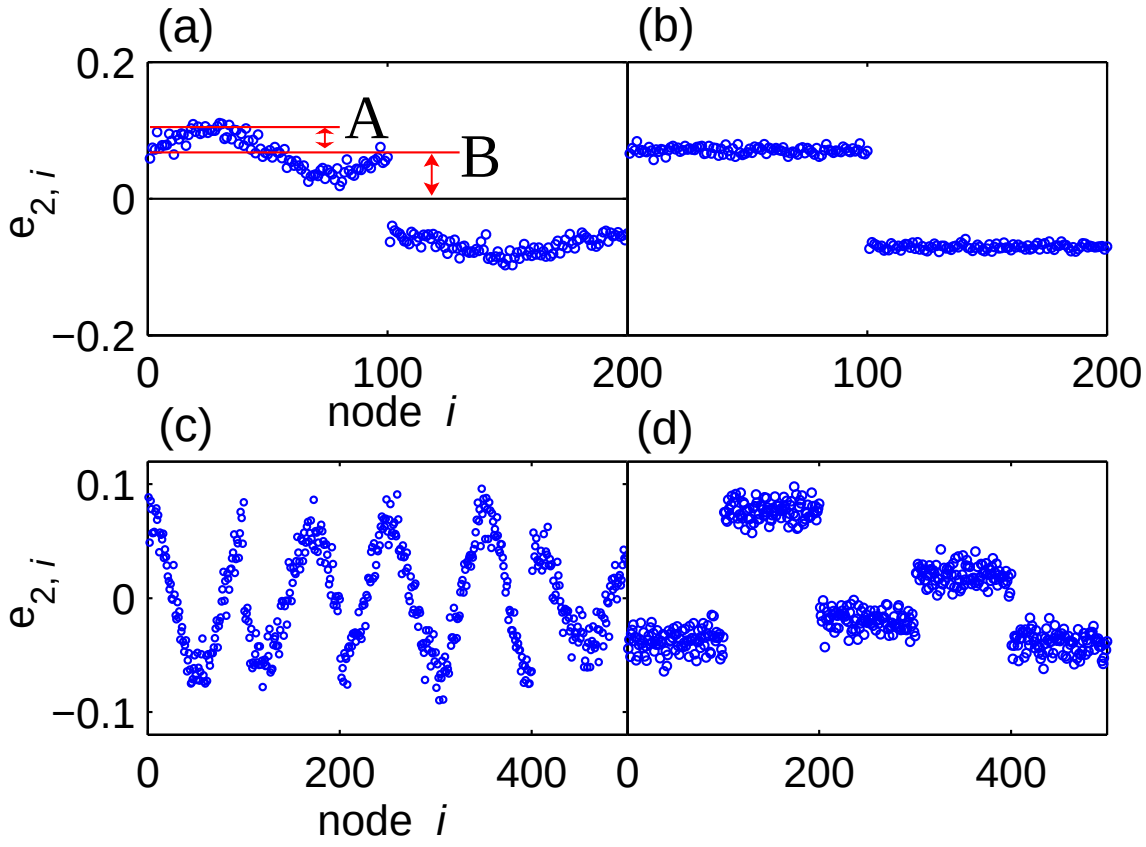

Fig. 18. Typical configurations of $\mathbf{e}_2$ for a two-cluster network of parameters $N = 200$ and $p = 0.2$ [(a) $m = 52$ and (b) $m = 80$] and for a five-cluster network with $N = 500$ and $p = 0.3$ [(c) $m = 40$ and (d) $m = 80$].

node i and j, where k_i is the degree (the number of links) of node i, $G_{ii} = 1$, and $G_{ij} = 0$ otherwise. For a bi-directional network, the eigenvalues of $\mathbf{G}$ are real and non-negative, and can be sorted as $0 = \lambda_1 < \lambda_2 \leq \cdots \leq \lambda_N$ [74]. The coupled system is synchronizable only if the effective coupling strength $K = \epsilon\lambda_i$ $(i > 1)$ falls into a certain interval $(K_1,\ K_2)$, or $K_1 < \epsilon\lambda_2$ and $K_2 > \epsilon\lambda_N$, where K_1 and K_2 depend only on the dynamics of a single oscillator [60]. For typical oscillators the second condition can be easily satisfied, so the synchronization condition is $\lambda_2 > K_1/\epsilon$ [61]. The goal of our analysis is to derive a formula for λ_2 for clustered networks with a regular local structure.

5.3.1. Networks with two clusters

The transpose of a matrix and the matrix itself have the same set of eigenvalues. Let $\mathbf{e}_i$ be the normalized eigenvector such that $\mathbf{G}^T \cdot \mathbf{e}_i = \lambda_i \mathbf{e}_i$, where $[*]^T$ denotes the transpose. Since $\sum_j G_{ij} = 0$, we have $\sum_j e_{i,j} = 0$ if $\lambda_i \neq 0$ [105]. It is known that for a one-dimensional ring network, the eigenvector $\mathbf{e}_2$ associated with λ_2 has a sinusoidal wave form: $e_{2,i} \sim \sin(2\pi i/n)$, where n is the total number of nodes on the ring. For two coupled ring subnetworks, we find numerically that, when the inter- and intra-connections are not too dense, components in $\mathbf{e}_2$ have a similar wave pattern for each subnetwork, although the mean values can be different, as shown in Fig. 18. Since the two subnetworks are identical, the amplitudes of the periodic waves are the same. The zero-sum property of $\mathbf{e}_2$ requires that the mean values of the two sinusoidal waves have opposite signs. To characterize such a wave pattern, we define A to be the amplitude of the sinusoidal waves, and B as the positive mean value, as indicated in Fig. 18(a). Thus $\mathbf{e}_2$ can be written approximately as

$$\begin{aligned} \mathbf{e}_2 = \quad & [\{B + A\sin(2\pi i_1/n + \phi_1)\}_{i_1}, \\ & \{-B + A\sin(2\pi i_2/n + \phi_2)\}_{i_2}]^T, \end{aligned}$$

where $i_1, i_2 = 1, 2, \cdots, n$, and ϕ_1 and ϕ_2 are the phases of the first node in each cluster. We can relabel the nodes so that $\phi_1 = \phi_2 = 0$, thus have

$$\mathbf{e}_2 = [\{B + A\sin(2\pi i_1/n)\}_{i_1}, \{-B + A\sin(2\pi i_2/n)\}_{i_2}]^T.$$

The normalization condition $\mathbf{e}_2^T \mathbf{e}_2 = 1$ gives

$$\sum_{i_1=1}^{n} [B + A\sin(\frac{2\pi i_1}{n})]^2 + \sum_{i_2=1}^{n} [-B + A\sin(\frac{2\pi i_2}{n})]^2 = 1,$$

which yields

$$2nB^2 + nA^2 = 1. \tag{5.2}$$

For a network whose $\mathbf{e}_2$ has a periodic wave pattern in each cluster, the corresponding eigenvalue λ_2 can be calculated *analytically*. Likewise, if $\mathbf{e}_2$ is constant within each cluster, λ_2 can be obtained analytically

as well [61]. The key observation is that, as the intra-cluster link density is increased, there is a transition from the former to the latter. That is, there exists a critical value m_t, where for $m < m_t$, the eigenvector $\mathbf{e}_2$ possesses a periodic wave pattern in each cluster but, for $m > m_t$, $\mathbf{e}_2$ is approximately constant in each cluster. Our effort below will then be to obtain m_t, based on which the eigenvalue λ_2 can be calculated.

To proceed, we note that, from the definition $\mathbf{G}^T \cdot \mathbf{e}_2 = \lambda_2 \mathbf{e}_2$, we have

$$\lambda_2 = \mathbf{e}_2^T \cdot \mathbf{G}^T \cdot \mathbf{e}_2 = \sum_{i,j=1}^{N} G_{ij} e_{2,i} e_{2,j}.$$

The coupling matrix $\mathbf{G}$ has the structure that, for $i - m/2 \le j < i$ and $i < j \le i + m/2$, $G_{ij} = -1/k_i$, and for j belonging to different clusters, $G_{ij} = -1/k_i$ with probability p. The degree k_i follows approximately a Gaussian distribution: $P(k) \sim N(m+pn,\ \sqrt{pn})$, thus we can use the mean value $k \equiv m+pn$ to approximate k_i. As a result, λ_2 can be expanded as

$$\begin{aligned}
\lambda_2 \quad = \quad & \sum_{i_1=1}^{n} [B + A\sin(\frac{2\pi i_1}{n})] \Big\{ [B + A\sin(\frac{2\pi i_1}{n})] \\
& -\frac{1}{k} \sum_{l=-m/2, l\neq 0}^{m/2} [B + A\sin(\frac{2\pi (i_1+l)}{n})] \\
& + \sum_{i_2=1}^{n} G_{i_1(n+i_2)} [-B + A\sin(\frac{2\pi i_2}{n})] \Big\} + \text{cc},
\end{aligned}$$

where cc stands for the summation for the second cluster, i.e. with i_1 and $n + i_2$ interchanged. Since the clusters are identical, the two summations are the same. The first term in the summation for the first cluster, which is $\mathbf{e}_2^T \cdot \mathbf{e}_2/2$, gives $1/2$. For the third term, note that $G_{i_1(n+i_2)}$ equals $-1/k$ with probability p. Because of this randomness, the summation over $A\sin(2\pi i_2/n)$ vanishes, and

$$\sum_{i_1=1}^{n} [B + A\sin(2\pi i_1/n)] = nB.$$

Thus the third term equals $nB(-1/k)np(-B) = n^2 pB^2/k$. The second term, when expanded, gives

$$\begin{aligned}
-\frac{1}{k} \quad & \Big\{ \sum_{i_1=1}^{n} [B + A\sin(\frac{2\pi i_1}{n})] \sum_{l=-m/2}^{m/2} [B \\
& + A\sin(\frac{2\pi (i_1+l)}{n})] - \sum_{i_1=1}^{n} [B + A\sin(\frac{2\pi i_1}{n})]^2 \Big\}.
\end{aligned}$$

Since

$$\sum_{i_1=1}^{n}\sum_{l=-m/2}^{m/2}\sin\frac{2\pi(i_1+l)}{n}=\sum_{l=-m/2}^{m/2}\sum_{i_1=1}^{n}\sin\frac{2\pi(i_1+l)}{n}=0,$$

the second term can be simplified as

$$\begin{aligned}
& -\frac{1}{k}\Big\{n(m+1)B^2 \\
& \qquad +A^2\sum_{i_1=1}^{n}\sin(\frac{2\pi i_1}{n})\sum_{l=-m/2}^{m/2}\sin[\frac{2\pi(i_1+l)}{n}]-\frac{1}{2}\Big\} \\
\approx\ & -\frac{1}{k}\Big\{n(m+1)B^2-\frac{1}{2} \\
& \qquad +A^2\int_0^n\sin(\frac{2\pi x}{n})dx\int_{-m/2}^{m/2}\sin[\frac{2\pi(x+y)}{n}]dy\Big\} \\
=\ & -\frac{1}{k}\Big\{n(m+1)B^2-\frac{1}{2}+\frac{n^2A^2}{2\pi}\sin\frac{\pi m}{n}\Big\} \\
=\ & -\frac{1}{k}\Big\{nmB^2+\frac{nA^2}{2}\big[\frac{n}{\pi}\sin\frac{\pi m}{n}-1\big]\Big\},
\end{aligned}$$

where the last equality is due to Eq. (5.2). Adding all the three terms, we have

$$\begin{aligned}
\lambda_2 &= 2\Big\{\frac{1}{2}+\frac{n^2pB^2}{k}-\frac{nmB^2}{k}-\frac{nA^2}{2k}\big[\frac{n}{\pi}\sin\frac{\pi m}{n}-1\big]\Big\} \\
&= 1+\frac{2nB^2(np-m)}{k}-\frac{NA^2}{2k}\big[\frac{n}{\pi}\sin\frac{\pi m}{n}-1\big]. \qquad (5.3)
\end{aligned}$$

While the parameter A represents the magnitude of the waveform, B can be regarded as the strength of the clustering of the network. Figure 19 shows the value of B versus m/n. There is a sudden transition of B from 0 to $1/\sqrt{N}$ (or correspondingly, A from $\sqrt{2/N}$ to 0). Thus we can approximate B (or A) by a step function of m/n. The transition point m_t where the wave patterns vanish (A becomes 0) can be calculated, as follows. For $B=0$, we have $A=\sqrt{2/N}$ and Eq. (5.3) becomes

$$\lambda_2=1-\frac{1}{k}(\frac{n}{\pi}\sin\frac{\pi m}{n}-1). \qquad (5.4)$$

For $B=1/\sqrt{N}$, we have $A=0$. Noting that $k=(N-n)p+m$, we can simplify Eq. (5.3) as

$$\lambda_2=1+\frac{np-m}{k}=\frac{Np}{k}. \qquad (5.5)$$

Since λ_2 is continuous, at the transition point m_t, the values of λ_2 obtained from Eq. (5.4) and from (5.5)

must be equal. This yields

$$p = \frac{m_t}{n} - \frac{1}{\pi}\sin\frac{\pi m_t}{n} + \frac{1}{n}. \tag{5.6}$$

For the parameters used in Fig. 19, the transition point is $m_t \approx 0.508$, as indicated by the vertical line. The analytical value agrees well with the simulation result. Thus, for a two-cluster network, λ_2 can be approximated by Eq. (5.4) for $m < m_t$ and by Eq. (5.5) for $m \geq m_t$. Figure 20(a) shows simulation results and the theoretical prediction for λ_2 for both the bi-directional (circles) and directional (triangles) inter-cluster coupling case. There is an alternating behavior in λ_2 as the intra-cluster link density m/n is increased and the theory captures the behavior of λ_2 reasonably well.

5.3.2. Multi-cluster networks

For a multi-cluster network, periodic wave patterns can arise in each cluster as well [Fig. 18(c)]. We have observed numerically that the amplitudes of the wave patterns for different clusters are approximately equal, so the average amplitude A can again be used to characterize the wave patterns. Similar to the two-cluster case, there is a sharp transition of A from a constant value to zero as m/n increases. For $A = 0$, the wave pattern diminishes, and $\mathbf{e}_2$ has the structure that its components within one cluster have approximately the same value but they can vary significantly in different clusters [Fig. 18(d)]. In this case, it can be shown that λ_2 is given by Eq. (5.5) [61]. To treat the case where $A \neq 0$, we assume the network has M clusters. The eigenvector $\mathbf{e}_2$ has the form of (after relabelling)

$$[\{A\sin(2\pi i_1/n)\}_{i_1},\ \cdots,\ \{A\sin(2\pi i_M/n)\}_{i_M}]^T,$$

for $i_1,\ \cdots,\ i_M = 1,\ 2,\ \cdots,\ n$. The normalization condition of $\mathbf{e}_2$ gives $(n/2)A^2M = NA^2/2 = 1$, which yields

$$A = \sqrt{\frac{2}{N}}. \tag{5.7}$$

Again we have $\lambda_2 = \sum_{i,j=1}^{N} G_{ij}e_{2,i}e_{2,j}$. Note that the index $i_1,\ \cdots,\ i_M$ are interchangeable, thus we can focus the summation over i on a single cluster and carry out summation over j. Doing so, we find that λ_2 is

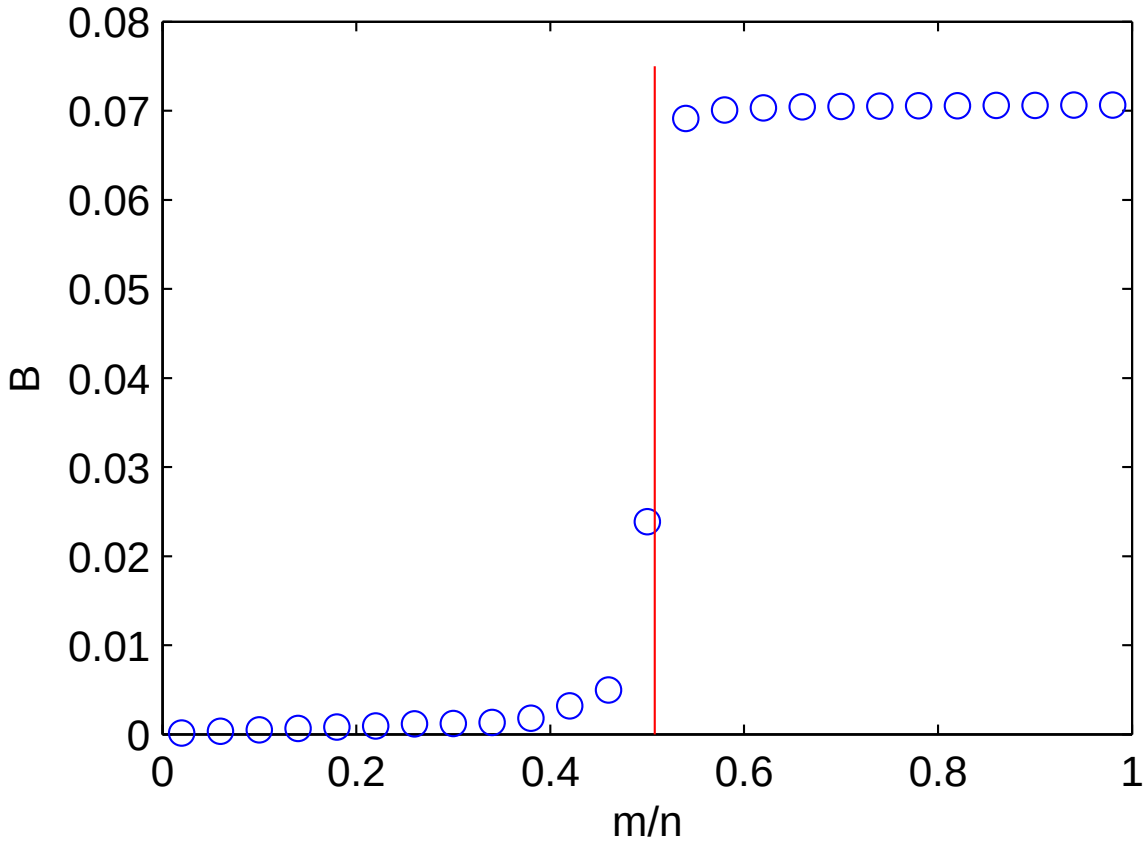

Fig. 19. For a two-cluster network with $N = 200$, and $p = 0.2$, quantity B versus m/n from simulation, where each point is the average of 100 runs. For $m/n > 0.5$, B approaches $1/\sqrt{N} \simeq 0.071$. The vertical line indicating the transition point of B is predicted by theory.

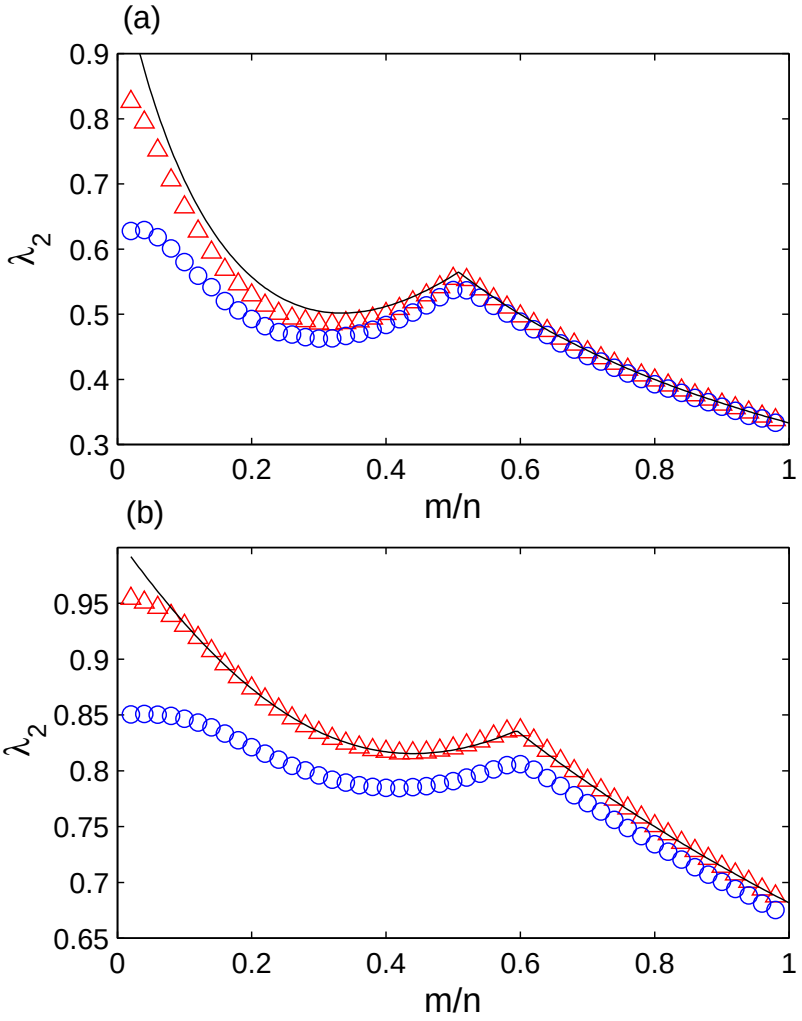

Fig. 20. (a) For a two-cluster network with $N = 200$ and $p = 0.2$ and (b) a five-cluster network with $N = 500$ and $p = 0.3$, λ_2 versus m/n. The data points are obtained from simulation for both bi-directional (circles) and directional (triangles) inter-cluster connections. For the directional case, only the real part of λ_2 is presented ($\mathrm{Im}\lambda_2 \sim 10^{-3}\mathrm{Re}\lambda_2$). Each point is the average of 100 realizations. Solid curves are from theory.

M times such summations:

$$\begin{aligned}\lambda_2 &= M\sum_{i=1}^{n} A\sin\frac{2\pi i}{n}\Big[A\sin\frac{2\pi i}{n} \\ &\quad -\frac{1}{k_i}\sum_{l=-m/2,l\neq 0}^{m/2} A\sin(\frac{2\pi(i+l)}{n}) \\ &\quad +\sum_{j\notin V_i} G_{ij}A\sin(\frac{2\pi j}{n})\Big], \end{aligned} \tag{5.8}$$

where V_i is the set of nodes in the cluster containing i. Since G_{ij} equals $1/k_i$ with probability p and 0 otherwise, the third term leads to 0. Using the mean value $k \equiv m + p(M-1)n$ to approximate k_i, we have

$$\begin{aligned}\lambda_2 &= M\sum_{i=1}^{n} A\sin\frac{2\pi i}{n}\{\frac{k+1}{k}A\sin\frac{2\pi i}{n} \\ &\quad -\frac{1}{k}\sum_{l=-m/2}^{m/2} A\sin[\frac{2\pi(i+l)}{n}]\} \\ &= \frac{k+1}{k} - M\sum_{i=1}^{n}\frac{1}{k}A\sin\frac{2\pi i}{n}\sum_{l=-m/2}^{m/2} A\sin[\frac{2\pi(i+l)}{n}]. \end{aligned}$$

The second term can be approximated by integration, which yields

$$\begin{aligned}\lambda_2 &= \frac{k+1}{k} - \frac{MA^2}{k}\frac{n^2}{2\pi}\sin\frac{\pi m}{n}, \\ &= 1-\frac{1}{k}\left(\frac{n}{\pi}\sin\frac{\pi m}{n}-1\right), \end{aligned} \tag{5.9}$$

where the second equality results from using Eq. (5.7). This expression is the same as Eq. (5.4) for the two-cluster network case. Since the expressions for λ_2 for both nonzero A and zero A cases are the same as those in the 2-cluster case, the transition point m_t can again be determined by Eq. (5.6), which is independent of M. Thus λ_2 can be approximated by Eq. (5.4) [or Eq. (5.9)] for $m < m_t$ and by Eq. (5.5) for $m \geq m_t$. Figure 20(b) shows the theoretical prediction of λ_2 together with simulation results for a five-cluster network. It can be seen that the alternating behavior in λ_2 persists and is reasonably well predicted by theory.

5.3.3. Robustness of alternating synchronization behavior

An immediate question is whether the predicted alternating behavior in λ_2 is robust. To address this, we need to determine the value of m_c for which λ_2 in Eq. (5.4) has a minimum value, or, $d\lambda_2/dm|_{m_c} = 0$. We

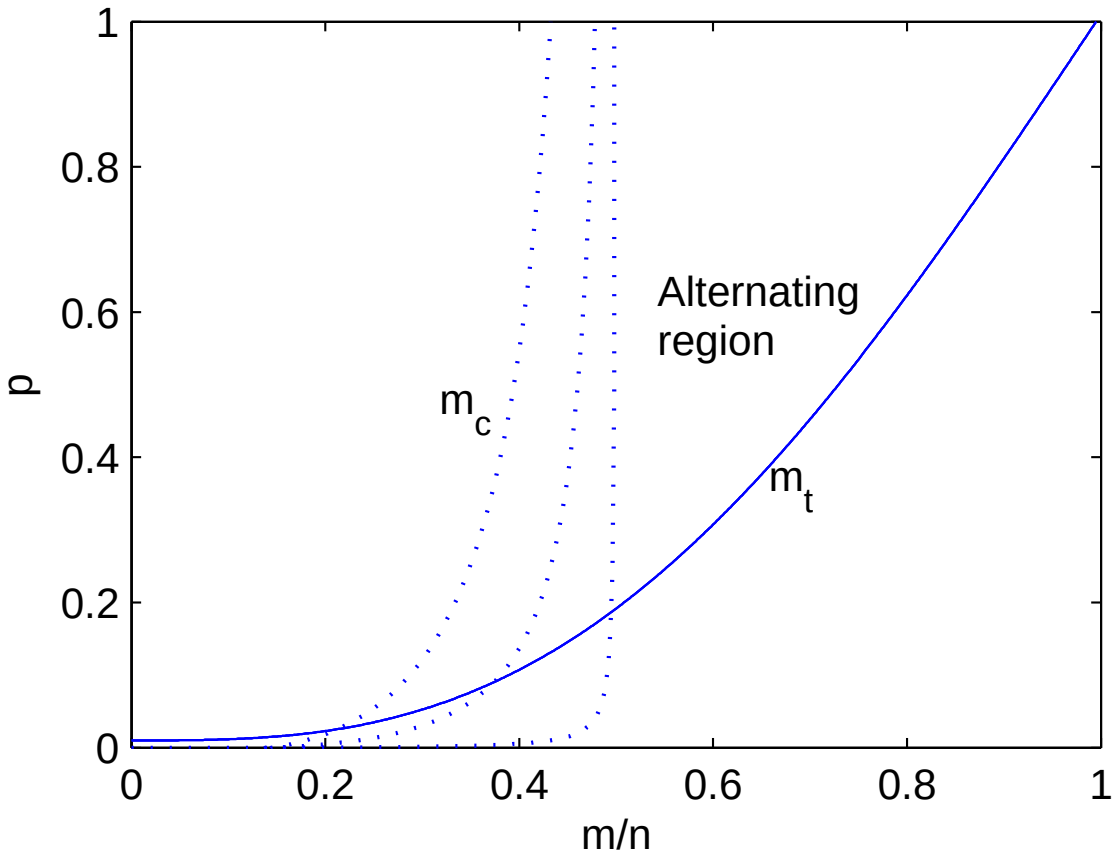

Fig. 21. For clustered networks with parameters $M = 2,\ 5,\ 100$ and $n = 100$, p versus m_t/n (solid lines) and versus m_c/n (dotted lines), where three dotted cases from left to right correspond to $M = 2,\ 5,\ 100$, respectively. The region between the m_c line and the m_t line, i.e. $m_c < m < m_t$, is the region that λ_2 and therefore the synchronizability exhibit an alternating behavior.

obtain

$$p = \left(\frac{\frac{1}{\pi} \sin \frac{\pi m_c}{n} - \frac{1}{n}}{\cos \frac{\pi m_c}{n}} - \frac{m_c}{n} \right) \Big/ (M-1). \tag{5.10}$$

For a given set of parameters ($M,\ n,\ p$), λ_2 is maximized at m_t and reaches minimum at m_c. Thus the system can be synchronized at m_t and desynchronized at m_c. As a result, the alternating behavior exists if $m_c < m_t$. Neglecting the term $1/n$, m_t/n only depends on p [Eq. (5.6)], while m_c/n depends on both p and M [Eq. (5.10)]. Figure 21 shows m_c and m_t for different M values. For clarity only one n value is used since the curves for $n = 100$ and $n = 1000$ are almost identical. For large values of M, for any p, m_c approaches $n/2$. Thus for the particular parameter setting in Fig. 21, insofar as $p > 0.2$, networks with arbitrary number of clusters exhibit the alternating behavior. When M is smaller, the critical value for p for the alternating behavior decreases and the parameter region for the alternating behavior broadens. The conclusion is that the alternating behavior in synchronization is a quite robust feature in locally regular, complex clustered networks.

5.4. Numerical simulations of actual synchronous dynamics

While the alternating-synchronizability behavior is predicted and verified using eigenvalue analysis, direct numerical simulations of coupled oscillator networks give strong evidence for the existence of this behavior. For instance, we have chosen for each oscillator, when isolated, the Rössler dynamics $d\mathbf{x}/dt = \mathbf{F}(\mathbf{x})$, where $\mathbf{x} = [x, y, z]^T$, $\mathbf{F}(\mathbf{x}) = [-(y+z), x + 0.2y, 0.2 + z(x-9)]^T$, $\epsilon = 0.4$, and $\mathbf{H}(\mathbf{x}) = [x, 0, 0]^T$. Numerically we find $K_1 = 0.2$, $K_2 = 4.62$. Since the Rössler system can have desynchronization bursts, it is necessary to characterize the synchronization in a statistical way. In particular, we define

$$W(t) = \langle |x(t) - \langle x(t) \rangle| \rangle$$

as the fluctuation width of the system at time t, where $\langle \cdot \rangle$ denotes average over all nodes in the network. The ensemble and time averages of the fluctuation width $\langle \langle W \rangle_{T_0} \rangle_e$ can be an indicator of the degree of synchronization, i.e., if the system is synchronized, $\langle \langle W \rangle_{T_0} \rangle_e \approx 0$, and if not, $\langle \langle W \rangle_{T_0} \rangle_e$ may assume some large value. Figure 22(a) shows $\langle \langle W \rangle_{T_0} \rangle_e$ versus m/n for both the bi-directional and directional inter-cluster coupling cases. When m is small ($m/n < 0.2$), $\langle \langle W \rangle_{T_0} \rangle_e$ is small and the system is synchronized. As m

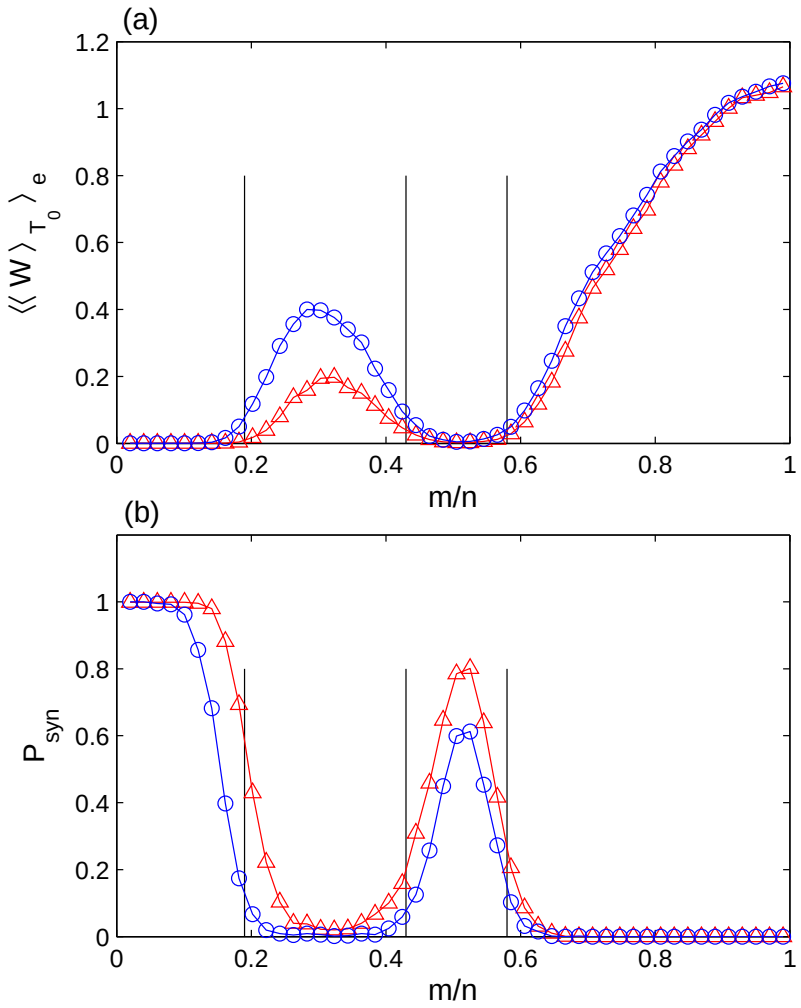

Fig. 22. For a cluster oscillator network with parameters $N = 200$, $M = 2$, $p = 0.2$, (a) $\langle\langle W\rangle_{T_0}\rangle_e$ versus m/n and (b) P_{syn} versus m/n. Circles and triangles indicate cases with bi-directional and directional inter-cluster connections, respectively. Simulation parameters are $T_0 = 10^4$ and $\delta = 0.005$. The vertical lines indicating the boundaries are determined by $\lambda_2 = K_1/\epsilon = 0.5$. Each data point is the average of 700 realizations. The data for this figure were obtained with 15 Pentium-IV 2.80GHz CPUs for about 2 months.

is increased ($m/n = 0.3$), $\langle\langle W\rangle_{T_0}\rangle_e$ becomes large and desynchronization occurs. As m increases further ($m/n = 0.5$), the fluctuation width reduces and the system becomes synchronized again, and for $m/n > 0.6$, the network loses its synchronizability. The probability of synchronization, P_{syn}, defined as the probability that $W(t)$ is smaller than a small number δ at all time steps during a time interval T_0 in the steady state, can also be used to characterize the synchronizability. Practically, P_{syn} can be calculated by the ensemble average, i.e., the ratio of the number of synchronized cases over the total number of network realizations. Figure 22(b) shows P_{syn} versus m/n. The alternating synchronization phenomena is apparent, as predicted.

5.5. Discussions

In this Chapter, motivated by the problem of tissue organization and intercellular communication in biology, we have studied the synchronizability of a class of clustered networks where each cluster contains a regular subnetwork. Our finding is that the network synchronizability exhibits an alternating, highly non-monotonic behavior as the number of intra-cluster links (gap junctions in a biological network) changes. Although speculative, the results may suggest that the synchronized function of organs in the face of perturbation may be controlled by the ability of individual cells to vary the number of gap junctions expressed on the membrane, which has been observed in variations in gap junctional intercellular communication and connexion expression in fibroblasts derived from keloid and hypertrophic scars [106–108].

Using more biophysically detailed dynamical models for simulation of synchronous dynamics is an interesting problem. However, a detailed model that can satisfactorily treats the actual dynamical interactions in intercellular communication is beyond the scope of present research. Our goal in this Chapter has thus been to understand the synchronizability of the network, as synchronization is an important factor determining intercellular communications. The main advantage of the synchronizability analysis is that it allows us to draw quite general conclusions about the ability for nodes in the network to be synchronized. The key theoretical tool required for the analysis is spectral properties of the coupling matrix of the underlying network. We wish to emphasize that, although the synchronizability analysis can yield qualitative information about the likelihood for the network to achieve synchronization, it is not able to yield information about the detailed dynamical process that leads to synchronization. Because of this limitation, making the individual-node

dynamics more "biological" is not very helpful from the standpoint of spectral analysis. In fact, insofar as the dynamics are oscillatory and somewhat random, we expect them to produce synchronization phenomena consistent with the predictions from the synchronizability analysis. That is why we have chosen the chaotic Rössler oscillator as a proper model for actual simulation of the synchronization dynamics. Indeed, the results from such numerical computations agree, qualitatively, with the theoretical predictions based on spectral analysis.

Time delays of the interaction along the long-range links are important and relevant to the biological system. However, as discussed above, our synchronizability analysis is not designed to deal with time delays. This should be an interesting topic for future explorations.

6 . SYNCHRONIZATION IN GRADIENT CLUSTERED NETWORKS

6.1. Background

It has been recognized in biological physics that at the cellular level, information vital to the functioning of the cell is often processed on various networks with complex topologies [109]. At a systems level, organizing information using the network idea has also become fundamental to understanding various biological functions. A key organizational feature in many biological systems is the *clustered* structure where biophysical and biochemical interactions occur at a hierarchy of levels. Examples include various protein-protein interaction networks [3, 110] and metabolic networks [2]. In biology and network science, a fundamental issue is synchronization [73, 111]. The aim of this Chapter is to study synchronization in clustered complex networks with uneven cluster-size distribution and asymmetrical coupling. Since this type of network structure is also important to physical and technological systems such as electronic-circuit networks and computer networks [98, 112, 113], understanding synchronization in such networks will be of broad interest.

There has been recent effort to study synchronization in complex clustered networks [85,114]. A general assumption in these works is that all clusters in a network are on the equal footing in the sense that their sizes are identical and the interactions between any pair of clusters are symmetrical. In realistic applications the distribution of the cluster size can be highly uneven. For example, in a clustered network with a hierarchical structure, the size of a cluster can in general depend on the particular hierarchy to which it belong. More importantly, the interactions between clusters in different hierarchies can be highly asymmetrical. For instance, the coupling from a cluster at a top hierarchy to a cluster in a lower hierarchy can be much stronger than the other way around. An asymmetrically interacting network can in general be regarded as the superposition of a symmetrically coupled network and a directed network, both being weighted. A weighted, directed network is a *gradient network* [25, 26], a class of networks for which the interactions or couplings among nodes are governed by a gradient field. Our interest is then the synchronizability and the actual synchronous dynamics on complex clustered networks with a gradient structure [64].

For a complex gradient clustered network, a key parameter is the strength of the gradient field between the clusters, denoted by g. A central issue is how the network synchronizability depends on g. As g is increased, the interactions among various clusters in the network become more directed. From a dynamical-

system point of view, uni-directionally coupled systems often possess strong synchronizability [115, 116]. Thus, intuitively, we expect to observe enhancement of the network synchronizability with the increase of g. The question is whether there exists an optimal value of g for which the network synchronizability can be maximized. This is in fact the problem of optimizing synchronization in clustered gradient networks, and our findings suggest an affirmative answer to the question. In particular, we are able to obtain solid analytic insights into a key quantity that determines the network synchronizability. The theoretical formulas are verified by both numerical eigenvalue analysis and direct simulation of oscillatory dynamics on the network. The existence of an optimal state for gradient clustered networks to achieve synchronization may have broad implications for evolution of biological networks and for practical applications such as the design of efficient computer networks.

6.2. Model setup

Our general setting is network with N nodes and M clusters, where n_m is the size of cluster m and V_m denotes the set of nodes it contains ($m = 1, ..., M$). Each pair of nodes is connected with probability p_s in the same cluster and with probability p_l in different clusters, where $p_s > p_l$ [85]. For a coupled oscillator network with arbitrary connecting topology, its synchronizability is determined [49] by the interplay between the transverse stability of the local-node dynamics $\mathbf{F}(\mathbf{x})$ and the eigenvalue spectrum of the coupling matrix C, which can be sorted conveniently as $\lambda_1 = 0 < \lambda_2 \leqslant \cdots \leqslant \lambda_N$, where $\lambda_1 = 0$ underlies the synchronization solution. A typical nonlinear oscillator in the synchronization manifold is transversely stable only when some generalized coupling parameter σ falls in a finite range: $\sigma \in [\sigma_1, \sigma_2]$, which is determined by the single-oscillator dynamics. The network is synchronizable if all the normalized eigenvalues except λ_1 can be contained within this range: $\sigma_1 < \varepsilon\lambda_2 \leqslant \cdots \leqslant \varepsilon\lambda_N < \sigma_2$, where ε is a specific coupling parameter. For convenience, we consider the following class of coupled-map networks: $\mathbf{x}^i_{t+1} = \mathbf{f}(\mathbf{x}^i_t) - \varepsilon \sum_j C_{ij}\mathbf{H}\left[\mathbf{f}(\mathbf{x}^j_t)\right]$, where $\mathbf{x}^i_{t+1} = \mathbf{f}(\mathbf{x}^i_t)$ is a d-dimensional map representing the local dynamics of node i, ε is a global coupling parameter, and $\mathbf{H}$ is a coupling function. The rows of the coupling matrix C have zero sum to guarantee an exact synchronized solution: $\mathbf{x}^1_t = \mathbf{x}^2_t = ... = \mathbf{x}^N_t = \mathbf{s}_t$. For certain types of oscillator dynamics and coupling functions, say, for example, the linearly coupled logistic oscillators we are going to study in the

following, σ_N is sufficiently large [117]. In such cases the condition $\varepsilon\lambda_N < \sigma_2$ is naturally satisfied and the synchronizability of network is only determined by λ_2. For simplicity, we will restrict our study to such types of oscillator dynamics and coupling functions.

6.3. Eigenvalue analysis for gradient two-cluster networks

We first develop a theory for networks consisting of two clusters (the theory can be generalized to multiple-cluster networks). Without a gradient field, the adjacent matrix A is such that $A_{ij} = 1$ if there is a link between node i and node j, and $A_{ij} = 0$ otherwise. To introduce a coupling gradient field from cluster 1 to cluster 2, for each inter-cluster link (i, j), $i \in V_1$ and $j \in V_2$, we deduce an amount g from A_{ij} (corresponding to the coupling from node j to node i) and add it to A_{ji} so that the total coupling strength is conserved. In this sense the gradient field can be said to point from cluster 1 to cluster 2. The coupling matrix C is defined as $C_{ij} = -A_{ij}/k_i$, where $k_i = \sum_{j=1}^{N} A_{ij}$ is the weighted degree of node i, and $C_{ii} = 1$.

The eigenvalue spectra of C and of its transpose C^T are identical. Let

$$\hat{e}_2 = (e_1, e_2, ..., e_{n_1}, e_{n_1+1}, ..., e_N)^T$$

be the normalized eigenvector associated with λ_2 of C^T. Since $\sum_{j=1}^{N} C^T_{j,i} = \sum_{j=1}^{N} C_{ij} = 0$, the eigenvectors associated with non-zero eigenvalues of C^T have zero sum: $\sum_{j=1}^{N} \hat{e}_{2,j} = 0$ [118]. From $C^T\hat{e}_2 = \lambda_2\hat{e}_2$ we have $\lambda_2 = \hat{e}_2^T C^T \hat{e}_2 = \sum_{i,j=1}^{N} e_i C_{ij} e_j$. For a clustered network, the elements in $\hat{e}_2$ have a special distribution: $e_i \approx E_1$ for $i \in V_1$ and $e_j \approx E_2$ for $j \in V_2$ [85], where the two constant values E_1 and E_2 can be obtained from the normalization condition $\hat{e}_2^T\hat{e}_2 = 1$ and the zero-sum property. We obtain $E_1 = -\sqrt{n_2/(n_1n_2 + n_1^2)}$ and $E_2 = \sqrt{n_1/(n_1n_2 + n_2^2)}$ (the signs of E_1 and E_2 are interchangeable since $E_1E_2 < 0$). This can greatly simplify the calculation of λ_2, which now can be written as $\lambda_2 \approx \sum_{i=1}^{N} e_i\{(C_{i1} + C_{i2} + ... + C_{in_1})E_1 + (C_{in_1+1} + C_{in_1+2} + ... + C_{iN})E_2\}$. The non-zero elements in C can be calculated as follows. For $i \in V_1$, $k_i \approx n_1p_s + n_2p_l(1-g)$, if $j \in V_1$, $C_{ij} = -1/k_i \equiv g_{11}$, and there are approximately n_1p_s non-zero elements for each i. If $j \in V_2$, we have $C_{ij} = -(1-g)/k_i \equiv g_{12}$. For $i \in V_2$, $k_i \approx n_2p_s + n_1p_l(1+g)$, if $j \in V_1$, $C_{ij} = -(1+g)/k_i \equiv g_{21}$ and, if $j \in V_2$, $C_{ij} = -1/k_i \equiv g_{22}$. Since $C_{ii} = 1$, the calculation can be further simplified as $\lambda_2 \approx \sum_{i=1}^{n_1} e_i\{E_1 + g_{11}E_1n_1p_s + g_{12}E_2n_2p_l\} + \sum_{i=n_1+1}^{N} e_i\{g_{21}E_1n_1p_l + E_2 + g_{22}E_2n_2p_s\}$.

Using $\sum_{i=1}^{n_1} e_i \approx n_1 E_1$, $\sum_{i=n_1+1}^{N} e_i \approx n_2 E_2$ and $n_1 E_1^2 + n_2 E_2^2 = 1$ (the normalization condition), we obtain

$$\lambda_2 = 1 + (E_1^2 n_1^2 g_{11} + E_2^2 n_2^2 g_{22}) p_s + E_1 E_2 n_1 n_2 p_l (g_{12} + g_{21}). \tag{6.1}$$

In Eq. (6.1), the unity comes from the diagonal elements in C, it defines the upper limit for λ_2 (this special case is associated with one-way coupled tree-structure networks [115, 116]). The second term is contributed by the intra-connection of cluster 1 and cluster 2. The last term corresponds to the inter-connection between the clusters. The parameter g is contained in these terms via g_{ij}. For a given 2-cluster network, the optimal gradient strength g_0 that maximizes λ_2 can be determined by setting $\partial\lambda_2/\partial g = 0$, which gives

$$g_o = \frac{2n_1 - N}{N p_l}(p_s - p_l). \tag{6.2}$$

(Please note that in deriving g_0 we actually get two such values: g_0 and $g_0^{'} = N(p_s + p_l)/[(N - 2n_1)p_l] < -1$. Since in our network model $|g|$ is defined within range $[0, 1]$, the value $g_o^{'}$ is therefore discarded.)

Equation (6.1) reveals some interesting features about the dependence of λ_2 on key parameters of the clustered network. To give an example, we show in Fig. 23 a contour plot of λ_2, calculated using the theoretical formula Eq. (6.1), in the parameter plane spanned by n_1 and g, where $n_1 + n_2 = 300$. It gives, for fixed value of n_1, the dependence of λ_2 on gradient strength. Since, by our construction, the gradient field points from cluster 1 to cluster 2, the upper half region ($n_1 > 150$) in Fig. 23 represents gradient clustered networks for which the gradient field points from the large to the small cluster. For any network defined in this region, for any fixed value of g, λ_2 increases monotonically with n_1, indicating enhanced network synchronizability with the size of the large cluster. However, for a fixed value of n_1, λ_2 first increases, reaches maximum for some optimal value of $g \equiv g_0$, and then decreases with g. The dependence of g_0 on n_1 is revealed by the dashed line in the figure [Eq. (6.2)]. We see that, when the gradient field is set to point from the large to the smaller cluster, in order to optimize the network synchronizability, larger gradient strength is needed for larger difference in the cluster sizes. In contrast, in the lower-half of Fig. 23 where $n_1 < n_2$, λ_2 tend to decrease as g is increased (for fixed n_1) or when the difference between the sizes of the two clusters

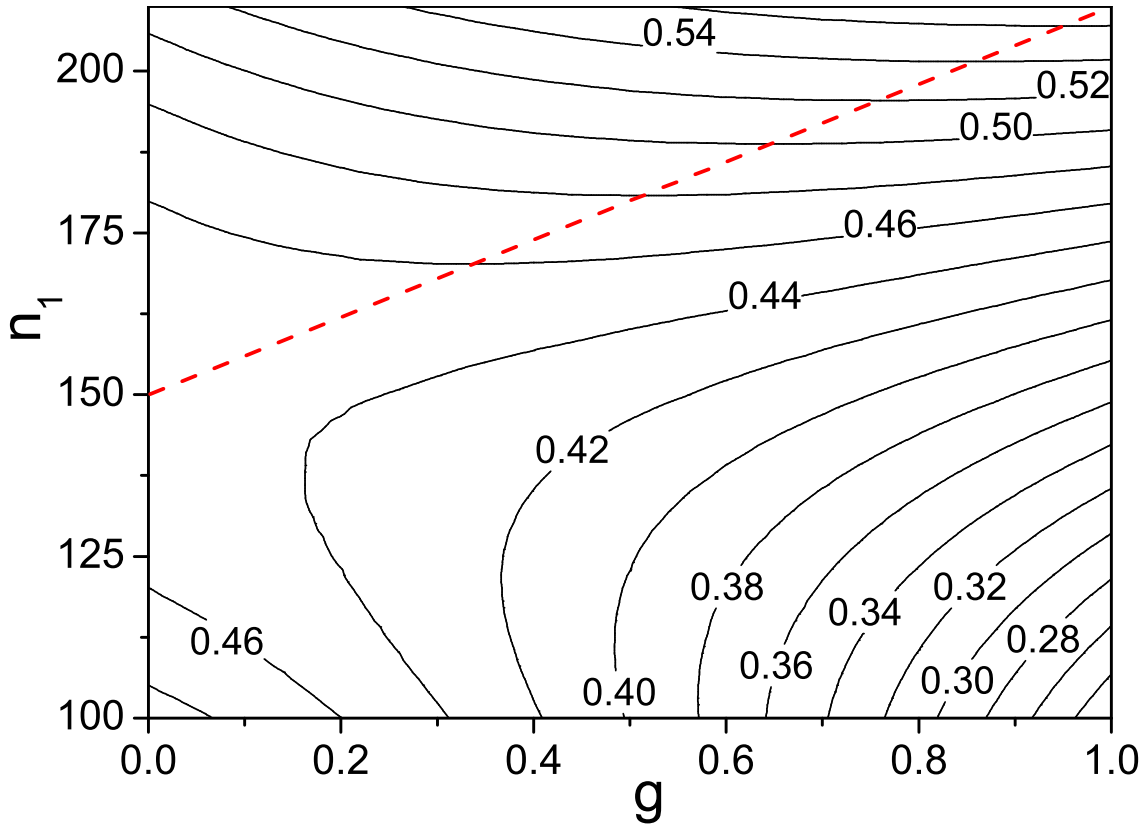

Fig. 23. Theoretical contour plot of λ_2 in the (g, n_1) plane, for a 2-cluster network of $n_1 + n_2 = 300$ nodes. Other parameters are $p_l = 0.2$ and $p_s = 0.7$. The dashed line is given by Eq. (6.2), which determines, for fixed value of n_1, the optimal gradient strength g_0.

enlarges. This indicates that, when the gradient points from the smaller to the larger cluster, the network synchronizability continuously weakens as the the gradient field is strengthened.

To provide support for our theoretical formula Eq. (6.1), we consider the same network in Fig. 24 and directly calculate the eigenvalue spectrum for a systematically varying set of values of g. Figure 24(a) shows λ_2 versus g (open circles) for the case where the gradient field points from the large to the small cluster ($n_1 = 190 > N/2$) and Fig. 24(b) is for an opposite case ($n_1 = 110 < N/2$). The solid curves are theoretical predictions. We observe a good agreement. To gain insight into the actual dynamics of synchronization on the network, we use the logistic map $f(x) = 4x(1-x)$ as the local dynamics, $\varepsilon = 1$, and choose $\mathbf{H}(\mathbf{x}) = x$ as the coupling function. For the logistic map, we have $\sigma_1 = 0.5$, $\sigma_2 = 1.5$ [74]. We find numerically $\lambda_N \approx 1.1 < \sigma_2$. Thus the synchronization condition becomes $\lambda_2 > \sigma_1 = 0.5$. We have calculated the average synchronization time T as a function of g, where T is the time needed to reach $\sum_{i=1}^{N} \left|(x^i - \langle x \rangle)\right| /N < \delta = 10^{-5}$ and $\langle x \rangle \equiv \sum_{i=1}^{N} x^i/N$ (the system is considered as unsynchronizable when $T > 10^4$). As g approaches the optimal value g_0, we observe a sharp decrease in T, as shown in Fig. 24(c), indicating a significant enhancement of the network synchronizability. After reaching the minimum at g_0, the time increases as g is increased further, as predicted by theory.

6.4. Eigenvalue analysis for gradient multi-cluster networks

The theory we have developed for two-cluster networks can be extended to multiple-cluster networks. Consider a M-cluster network, where each cluster contains a random subnetwork. Assume the size of the clusters satisfy $n_1 > n_2 > n_3 \geqslant \cdots \geqslant n_M$, a coupling gradient field can be defined as for the two-cluster case. For a random clustered network, the weighted degree can be written as $k_i \approx \sum_{j=1}^{N} A_{ij} = n_m p_s + (N - n_m)p_l + p_l g(\sum_{l,n_m<n_l} n_l - \sum_{l',n_m>n_{l'}} n_{l'}) \equiv K_m$. Define g_{ml} as the average value of the non-diagonal, non-zero elements C_{ij}. For $i \in V_m$ and $j \in V_l$, we have $g_{mm} = -1/K_m$, $g_{ml} = -(1-g)/K_m$ for $n_m > n_l$, $g_{ml} = -(1+g)/K_m$ for $n_m < n_l$, and $g_{ml} = -1/K_m$ for $n_m = n_l$. For the second eigenvector of C^T, e.g. $C^T \hat{e}_2 = \lambda_2 \hat{e}_2$, its components have a clustered structure, i.e., for all $i \in V_m$, $\hat{e}_{2,i} \approx E_m$ while they may vary significantly for different clusters. The eigenvalue λ_2 can then be expressed as $\lambda_2 = \hat{e}_2^T C^T \hat{e}_2 = \sum_{i,j=1}^{N} e_i C_{ij} e_j = \sum_{i=1}^{N} e_i \{E_m + E_m n_m p_s g_{mm} + \sum_{l \neq m} E_l n_l p_l g_{ml}\} =$

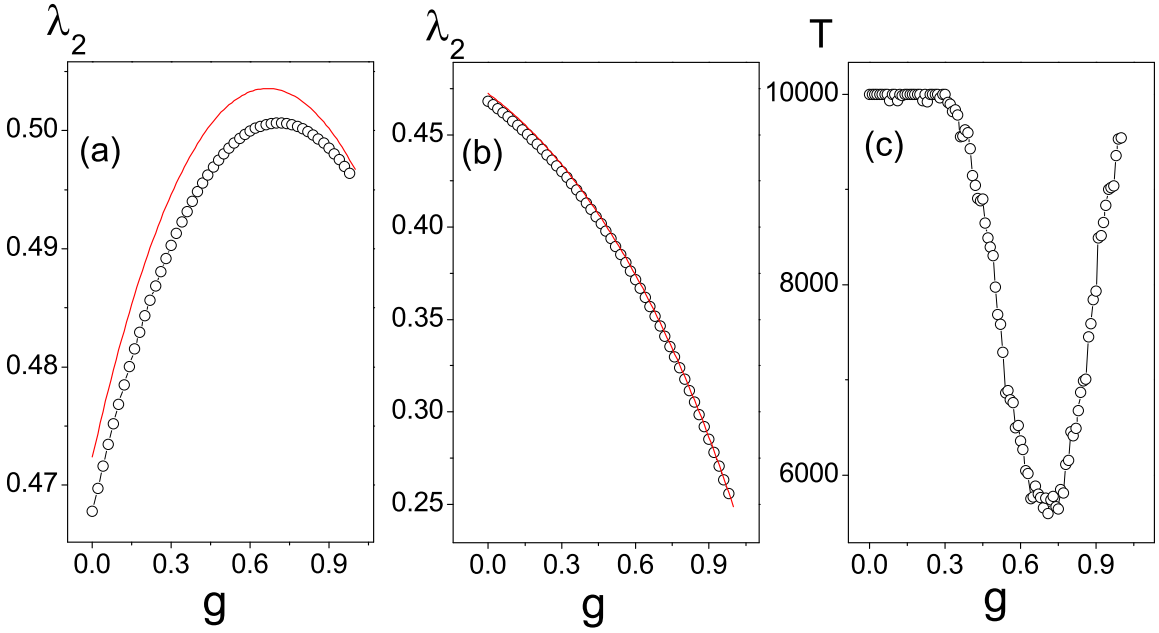

Fig. 24. For a gradient network of two clusters with $N = 300$ nodes, numerically obtained (circles) dependence of λ_2 on the strength g of the gradient field for the two cases where (a) the gradient field points from the larger to the small cluster ($n_1 = 190 > N/2$) and (b) the opposite ($n_1 = 110 < N/2$). The solid curves are from theory. (c) For $n_1 = 190$, actual synchronization time versus g for a clustered network of chaotic logistic maps. We observe a sharp reduction in the time as g approaches its optimal value, indicating a stronger synchronizability. Other parameters are $p_l = 0.2$, $p_s = 0.7$. Each point is the average of 100 random realizations.

$\sum_{m=1}^{M} n_m E_m^2 + \sum_{m=1}^{M} E_m^2 n_m^2 p_s g_{mm} + \sum_{l \neq m} E_m E_l n_m n_l p_l g_{ml}$. Taking into consideration the normalization condition $\hat{e}_2^T \hat{e}_2 = 1$, we get $\lambda_2 = 1 + \sum_{m=1}^{M} E_m^2 n_m^2 p_s g_{mm} + \sum_{m,l=1;l\neq m}^{N} E_m E_l n_m n_l p_l g_{ml}$.

For a general multiple-clustered network, it is mathematically difficult to obtain an analytic formula for the quantity E_m. However, E_m can be determined numerically. Once this is done, the general dependence of λ_2 on g and subsequently the optimal gradient strength g_0 can be obtained. In some particular cases, explicit formulas for E_m and λ_2 can be obtained. Focusing on the role of the gradient in determining the synchronizability, we consider the extreme gradient case: $g = 1$. Numerically, we find that for this case, with respect to the second eigenvector $\hat{e}_2$, only E_1 and E_2 (corresponding to the largest and the second largest clusters) have non-zero values, while for all $m > 2$, $E_m = 0$. From the normalization condition $\hat{e}_2^T \hat{e}_2 = 1$ and the zero-sum property $\sum_{j=1}^{N} \hat{e}_{2,j} = 0$ (since $\sum_{j=1}^{N} C_{ij} = 0$), we can solve for E_1 and E_2 as $E_1 = -\sqrt{n_2/(n_1 n_2 + n_1^2)}$ and $E_2 = \sqrt{n_1/(n_1 n_2 + n_2^2)}$. Noticing $g_{12} = 0$, we finally obtain

$$\begin{aligned} \lambda_2 &= 1 + \sum_{m=1}^{2} E_m^2 n_m^2 p_s g_{mm} + \sum_{m,l,l\neq m}^{2} E_m E_l n_m n_l p_l g_{ml} \\ &= 1 + (E_1^2 n_1^2 g_{11} + E_2^2 n_2^2 g_{22}) p_s + E_1 E_2 n_1 n_2 p_l g_{21}. \end{aligned} \tag{6.3}$$

A numerical verification of Eq. (6.3) is provided in Fig. 3(a). An observation is that, except for the difference in g_{ij}, Eq. (6.3) has the same form as Eq. (6.1), indicating that λ_2 is mainly determined by the first two largest clusters and it has little dependence on the details of size distributions of the remaining clusters. The remarkable implication is that, for different gradient clustered networks, regardless of the detailed form of the cluster size distribution, insofar as the two dominant clusters have similar properties, all networks possess nearly identical synchronizability.

6.5. Discussion

The model of gradient clustered network we have investigated here is different to the asymmetrical network models in literature. In Ref. [111, 115, 116], asymmetrical couplings have been employed to improve network synchronization and it is found that, for *non-clustered networks*, synchronization is optimized when all nodes are one-way coupled and the network has a tree-structure [115]. Different to this, in our model asymmetrical couplings are only introduced to inter-cluster links, while couplings on intra-cluster links are

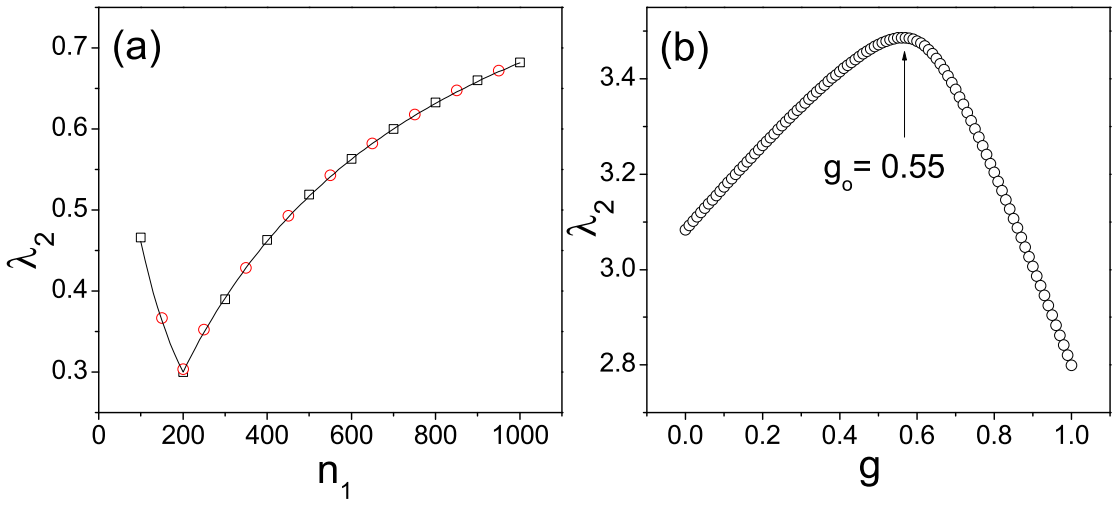

Fig. 25. (a) For a 5-cluster network (circles) and a 10-cluster network (squares), λ_2 versus n_1, the size of the largest cluster. The solid curve is from theory [Eq. (6.3)]. For the 5-cluster network, the size of the remaining clusters are $n_2 = 200$, $n_3 = 50$, $n_4 = 30$, $n_5 = 20$. For the 10-cluster network, we have $n_2 = 200$, n_3 to n_{10} are 90, 80, 70, 60, 50, 40, 30, 20, respectively. Other parameters are $p_l = 0.15$ and $p_s = 0.7$. For $n_1 < n_2$, the gradient is actually from cluster 2 to cluster 1. Each point is the average result of 100 network realizations. (b) For a "cortico-cortical network" of the cat brain, numerical results of the dependence of λ_2 on gradient strength g. Synchronization is optimized for $g_0 \approx 0.55$

still symmetrical. This special coupling scheme induces some new properties to the functions of the gradient. Firstly, increase of gradient will not monotonically enhance synchronization. That is, directed coupling between clusters, i.e. $g = 1$, is not always the best choice for synchronization. In many cases the optimal gradient stregth g_0 is some value between 0 and 1, while the exact value is determined by the other network parameters [Eqs. (6.1,6.3)]. Secondly, the direction of gradient can not be arranged randomly, it should be always pointing from large to small clusters. Finally, in the case of $g = 1$, network synchronizability is still related to the network topology, i.e. by the topology of the first two largest clusters; while for non-clustered network, synchronizability is only determined by the local dynamics [115].

Can synchronization optimization be expected in realistic networks? To address this question, we have tested the synchronizability of a "cortico-cortical network" of cat brain, which comprises 53 cortex areas and about 830 fiber connections of different axon densities [119]. The random and small-world properties of this network, as well as its hierarchical structure, have been established in several previous papers [120]. According to their functions, the cortex areas are grouped into 4 divisions of variant size: 16 areas in the visual division, 7 areas in the auditory division, 16 areas in the somato-motor division, and 14 areas in the frontolimbic division. Also, by the order of size, these divisions are hierarchically organized [119]. With the same gradient strategy as for the theoretical model, we plot in Fig. 3(b) the variation of λ_2 as a function of the gradient strength. Synchronization is optimized at gradient strength about $g_o \approx 0.55$. An interesting finding is that the actual average gradient of the real network, $g_{ave} \approx 0.37$ [121], is deviating from the optimal gradient g_o, indicating a strong but non-optimized synchronization in healthy cat brain.

While our theory predicts the existence of a gradient field for optimizing the synchronizability of a complex clustered network, we emphasize that the actual value of the optimal gradient field may or may not be achieved for realistic networked systems. Due to the sophisticated procedure involved to determine the optimal gradient strength and the actual value for a given network, their numerical values can contain substantial uncertainties. A reasonable test should involve a large scale comparison across many networks of relatively similar type (say, many different animals), hopefully demonstrating some kind of correlation between the optimum gradient and the observed values. Furthermore, such a test would include a sense of

how large the difference between the optimum and observed is. Due to the current unavailability of any reasonable number of realistic complex, gradient, and clustered networks, it is not feasible to conduct a systematic test of our theory. (As a matter of fact, we are able to find only one real-world example of gradient clustered network, the cat-brain network that we have utilized here.) It is our hope that, as network science develops and more realistic network examples are available, our theory and its actual relevance can be tested on a more solid ground.

In short, we have uncovered a phenomenon in the synchronization of gradient clustered networks with uneven distribution of cluster sizes: the network synchronizability can be enhanced by strengthening the gradient field, but the enhancement can be achieved only when the gradient field points from large to small clusters. We have obtained a full analytic theory for gradient networks with two clusters, and have extended the theory to networks with arbitrary number of clusters in some special but meaningful cases. For a multiple-cluster network, a remarkable phenomenon is that, if the gradient field is sufficiently strong, the network synchronizability is determined by the largest two clusters, regardless of details such as the actual number of clusters in the network. These results can provide insights into biological systems in terms of their organization and dynamics, where complex clustered networks arise at both the cellular and systems levels. Our findings can also be useful for optimizing the performance of technological networks such as large-scale computer networks for parallel processing.

7 . UNDERSTANDING AND PREVENTING CASCADING BREAKDOWN IN COMPLEX CLUSTERED NETWORKS

7.1. Background

Recently, cascading breakdown [65–67] in complex networks has received considerable attention [68–71]. The phenomenon is referred to as an avalanching type of process, where the failure of a single or of a few nodes can result in a large-scale breakdown of the network. In particular, in a physical network nodes carry and process certain loads, such as electrical power, and their load-bearing capacities are finite. When a node fails, the load that it carries will be redistributed to other nodes, potentially triggering more failures in the network as a result of overloading. This process can propagate through the entire network, leading to its breakdown. Indeed, cascading breakdown appears to be particularly relevant for large-scale failures of electrical power grids, and efforts have been made to understand the dynamical origin of such failures [72]. From the standpoint of network security, scale-free networks [43], where a small subset of nodes (hubs) possess substantially more links than those of an average node and therefore carry disproportionally more loads, are especially vulnerable to cascading breakdown, as attack on one of the hub nodes can cause a significant load redistribution [66, 69]. In this regard, a strategy for protecting scale-free networks against cascading breakdown has been proposed [70], where a selective set of "unimportant" nodes that process little but contribute relatively large loads to the network are pre-emptively removed so as to reduce the overall load in the network.

Networks with a community structure, or clustered networks, are relevant to a plethora of biological, social, and technological systems [122]. A clustered network consists of a number of groups, where nodes within each group are densely connected but the linkage among the groups is sparse. A clustered network can be heterogeneous in the sense that its degrees obey a power-law distribution, which can be realized, for example, by incorporating the scale-free topology in each cluster. Recently various dynamics on complex clustered networks have been studied [61].

In this Chapter, we address the dynamical origin of cascading processes on complex clustered networks and, more importantly, investigate how such a network can be made secure in response to attacks. In view of the particular vulnerability of scale-free networks to cascading breakdown, we focus on networks where each

individual cluster contains a scale-free subnetwork. To motivate our work and illustrate the challenges, we consider the problem of virus spread starting from one of the clusters, such as a remote village in a human epidemic network. A common practice to prevent a global spread is to isolate this particular cluster from the network. Now, consider the network-security problem by assuming that an attack has occurred in one of the clusters. A naive strategy to prevent breakdown of the network on a global scale is to isolate this cluster by cutting all the links that connect this cluster with other clusters so that failures would be restricted to the original cluster. This intuitive thinking, however, cannot be correct for a load-distributed network, because cutting off a cluster would transfer the load originally processed by this cluster to other clusters of the network, increasing the likelihood of overloading and possibly resulting in a more disastrous situation. Indeed, this is what we have found in simulations: a clustered network is particularly vulnerable to cascading breakdown in the sense that the general prevention strategy in [70], which is quite effective for scale-free networks, would increase significantly the probability of a global avalanche if not properly implemented.

Our main idea is to classify and understand the roles played by various nodes in the network and devise a control strategy accordingly that can effectively prevent global cascades. Our achievement is illustrated in Fig. 26, plots of the relative size G of the largest connected component of the network versus some generic network capacity parameter λ in response to an attack on a hub node, where $G = 1$ represents a fully connected network and $G \ll 1$ indicates that the network has disintegrated effectively. The data points represented by open squares correspond to the situation where no control is taken to protect the network, and those represented by open circles are the result of cutting off the particular cluster within which the attack occurs. We observe that, as λ is reduced, G decreases rapidly but strikingly, there is essentially no difference in the values of G between these two cases, indicating the ineffectiveness of an straightforward implementation of the prevention strategy which tries to localize the destruction within one community. In contrast, implementing our control strategy results in much higher values of G (data points represented by open triangles). In what follows, we present a sequence of reasonings, supported by numerical computations, that lead to a relatively complete understanding of the cascading phenomenon in complex clustered networks, and consequently, to an effective control strategy.

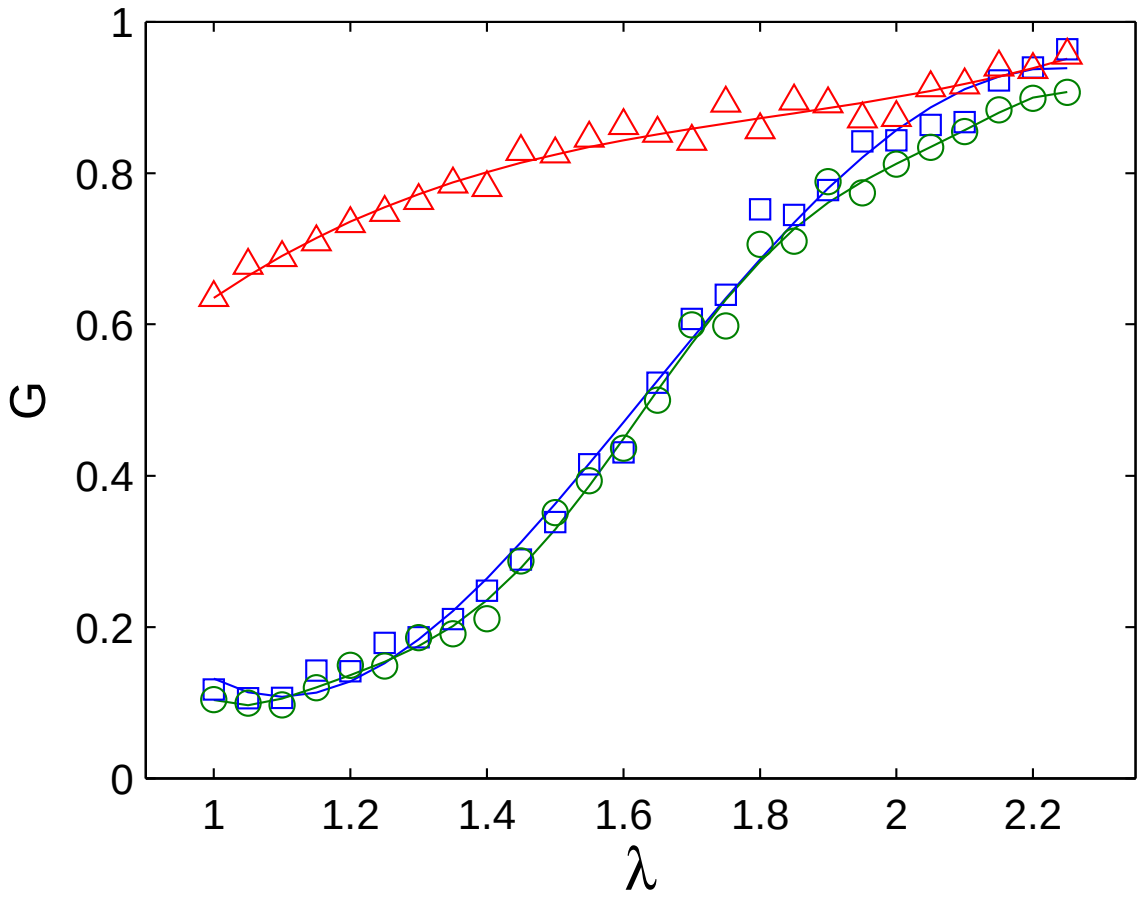

Fig. 26. For a representative clustered network of $N = 5600$ nodes, average degree $\langle k \rangle = 4$, $M = 50$ clusters, and average inter-cluster number of links $k_M = 2$, the relative size G of the largest connected component in the network versus the network capacity parameter λ in response to a targeted attack. Each data point is the result of averaging 100 network realizations (see text for details of the meanings of the three different data curves). The attack disables a single node in a cluster that has the largest load. For a non-clustered scale-free network, the value of G can be about zero for $\lambda \simeq 1$ [66]. However, for a clustered network, failures propagate from one cluster to another, during which a few connected clusters may be separated from the rest but still remain connected. As a result, the value of G for small values of λ is small but not zero; it is of the order of $1/M$.

We consider an ensemble of clustered networks, each of N nodes and M clusters, where $N \gg M$. Any cluster within the network is a scale-free subnetwork of $n = N/M \gg 1$ nodes [43]. The number of inter-cluster links is $k_M M$, and they are placed randomly among the clusters. To conserve the average degree of the entire network, we cut off $k_M M$ intra-cluster links randomly while keeping the network fully connected. Since the number of inter-cluster links is much smaller than that of intra-cluster links, removing a small number of intra-cluster links has little effect on the dynamics of the network. To investigate cascading breakdown, we use the prototypical model of load dynamics [66]. In particular, the load L_i at node i is defined as the total number of directed shortest paths passing through this node. Paths that end at or start from the node are also counted. The total load of the network is given by $S = \sum L_i = N(N-1)(D+1)$, where D is the average network distance. The capacity of a node is the maximum load that the node can handle, which is assumed to be proportional to its initial load L_{i0}: $C_i = \lambda L_{i0}$, where the constant $\lambda \geqslant 1$ is a uniform capacity parameter. An attack at a particular node is defined as an event that disables or removes this node from the network. If the load that this node handles is relatively large, a load redistribution over the network can occur. Any node in the network is considered to have failed and is removed from the network if the load imposed on it is larger than its capacity. The damage after the network reaches a new steady state can be conveniently quantified by the relative size $G = N'/N$, where N' is the number of nodes in the largest connected component remaining after the attack. For $G \lesssim 1$, the network remains mostly connected, so the effect of attack on the network is not severe. For $G \gtrsim 0$, breakdown of the network occurs at a global scale.

7.2. Traffic flow pattern and cascading

To understand the dynamical origin of cascading failures in a clustered network, we note that nodes connecting different clusters, or *bridge nodes*, transmit inter-cluster load flows and they are critical to maintaining the connections of the network. For the ensemble of networks used in Fig. 26, we find that the fraction of the bridge nodes is about 3.5%, but they carry about 41% of the total load of the network. An intuition is, then, that assigning relatively large capacities to the bridge nodes may mitigate cascades. To test this hypothesis, we conduct the following numerical experiments. First, we randomly select a set of nodes, which has the same number as that of the bridge nodes, and assign them with different capacities as characterized by the

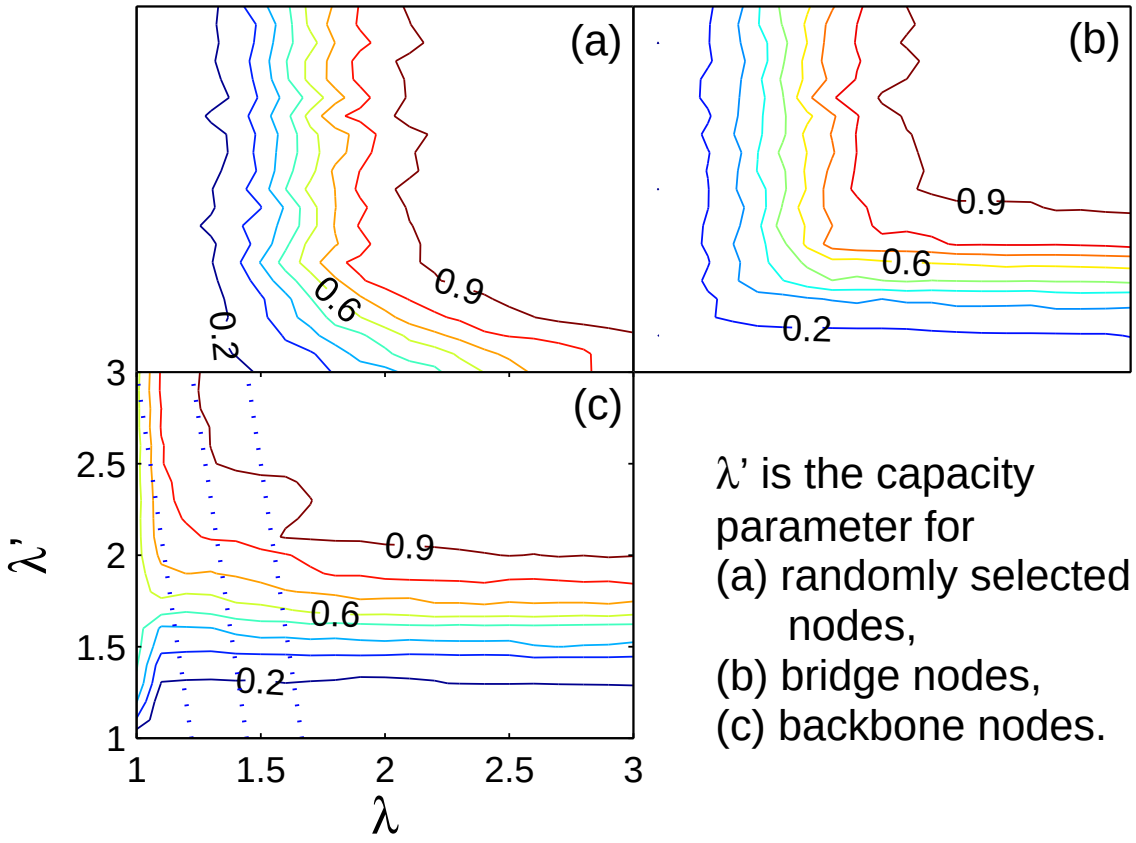

Fig. 27. Contour plots of G versus λ and λ'. The dotted lines in (c) correspond to effective total capacity parameter of 1.2, 1.4, and 1.6 (from left to right). Network and simulation parameters are the same as for Fig. 26.

parameter λ' (the remaining nodes in the network have the capacity parameter λ). We then examine, in the two-dimensional parameter plane (λ, λ'), contours of various values of G. The result is shown in Fig. 27(a), where the contours are mostly vertical, indicating little dependence of G on λ'. Thus, having a random set of nodes with high capacities cannot help prevent cascading failures, as expected. Next, we assign λ' but only to the set of bridge nodes. As shown in Fig. 27(b), in this case, the contour lines are approximately symmetric with respect to $\lambda' = \lambda$, indicating that G depends mainly on λ' but only in the region where $\lambda' < \lambda$. For $\lambda' > \lambda$, G has little dependence on λ', revealing the ineffectiveness of having high-capacity bridge nodes in limiting cascading failures. There is in fact a bottleneck effect at the bridge nodes: if their capacities are small, they will hinder the load-transferring capability of the network, but increasing their capacities in general can only facilitate load transfers among the clusters via inter-cluster links. Since the majority of links in the network are intra-cluster links, load transfers within individual clusters are prevalent. As a result, having large-capacity bridge nodes cannot enhance the network's load-transferring ability in general.

The results in Figs. 27(a) and 27(b) suggest the need to identify a different set of nodes that are more important to the load dynamics than the bridge nodes. Our key idea is to examine, within any given cluster, the set of nodes that are on the shortest paths connecting the bridge nodes. We call such nodes *skeleton nodes*, as the shortest paths through them are the main avenues for load transfers within the cluster. The bridge and the skeleton nodes thus form the *backbone* of load traffic on the network. Indeed, for the model network in Fig. 26, the fraction of these two types of backbone nodes is 13% but they carry 79% of the total load. A typical scenario for traffic flow on the network is then as follows. Say node A in one cluster wishes to transfer a certain amount of load to node B in a different cluster. Node A first sends the load to a closest skeleton node in the same cluster, which will then be sent to a bridge node along the shortest path. Such shortest paths can be regarded as "highways" for load traffic. The load is then transported to the destination cluster along a series of "highways" connecting various backbone nodes. Upon arrival at the destination cluster, the load is finally sent to node B via some "local" connections in that cluster. This picture is analogous to the surface transportation system in a modern infrastructure. We may expect that increasing the capacities of the backbone nodes can reduce the likelihood of overloading in the network, thereby making the network more

tolerant to cascading breakdown. Figure 27(c) shows the contours of a number of values of G in the (λ, λ') plane, where λ' now is the capacity parameter for both types of backbone nodes. Indeed, for a fixed value of λ, as λ' is increased, G can be increased significantly. Setting a high value of λ' is practical, as the number of backbone nodes is small (typically about 10% of the total number of nodes in the network). To give a concrete example, assume first all nodes have the same capacity: $\lambda' = \lambda = 1.4$. After the attack, G is about 0.3, indicating that only 30% of the nodes are still connected. However, if we set $\lambda' = 2.3$ and $\lambda = 1.3$ so that the total capacity of the network is the same as for the case of $\lambda' = \lambda = 1.4$, we find that G can be maintained at about 0.9, a three-fold increase over the previous case!

7.3. Preventing cascading on complex clustered networks

The above analysis suggests an effective way to implement the strategy of removing "unimportant" nodes in the network to prevent cascading breakdown [70], i.e., to remove a certain fraction of *non-essential* nodes that are neither skeleton nor bridge nodes. These non-essential nodes contribute loads to the network but they process or transfer little loads, so a controlled removal can reduce the total load while keeping intact the overall traffic flow of the network. A key issue is the optimal fraction of the non-essential nodes that should be removed to maximize the network's robustness against cascading breakdown. In the following, we develop a physical analysis and numerical computations to address this issue.

We order the clusters by their average distances to the cluster under attack. In particular, we denote the cluster where a cascading process is originated as $I_M = 1$ and calculate the average distances between nodes in this cluster and nodes in other clusters: $l_{1J} = 1/n^2 \sum d_{ij}$, $J = 2,\ 3,\ \ldots,\ M$, where the sum is over all nodes i in cluster 1 and all nodes j in cluster J. The average distances l_{1J} are arranged in an ascending order, i.e. the cluster that has the smallest distance l_{1J} is denoted by $I_M = 2$, and so on. The order thus characterizes the closeness of an arbitrary cluster to the cluster under attack. We find that removing non-essential nodes from clusters that are close to the original cluster can lead to higher values of G, as shown in Fig. 28(a). This can be understood as follows. By removing some non-essential nodes in a cluster, the load decrease in the skeleton and bridge nodes in this cluster is $n_n(N-n)d$, where $n_n \sim n$ is the number of non-essential nodes, and d is the average path length for load at a non-essential node to travel through the backbone nodes

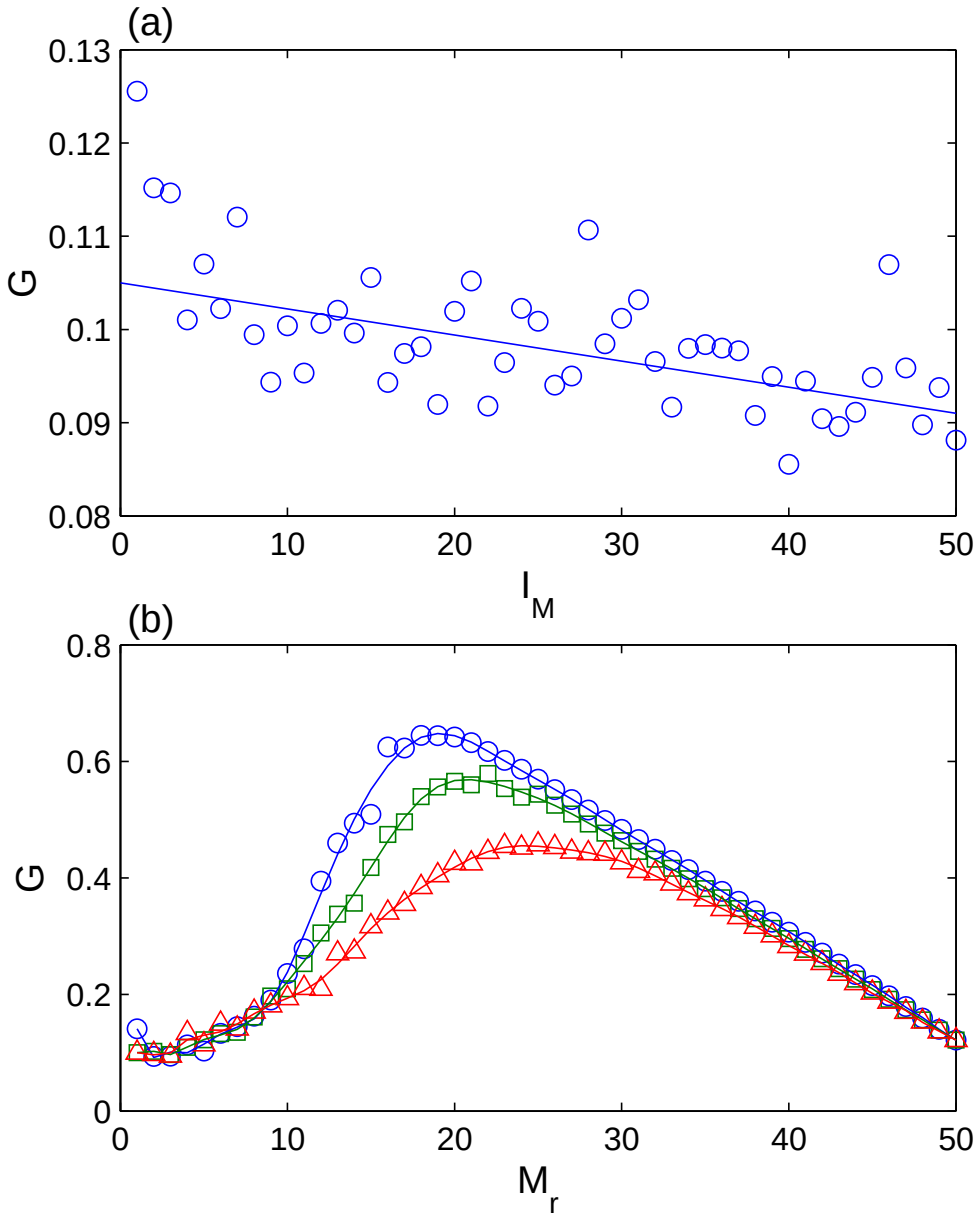

Fig. 28. For $\lambda = 1$, (a) G versus the index I_M of the cluster from which non-essential nodes are removed. (b) G versus the number of clusters M_r where controlled removal occurs. Circles: from clusters with small index to large index; squares: from randomly selected clusters; triangles: from clusters with large index to small index.

in this cluster. The load decrease over all backbone nodes is approximately $n(N-n)(D-d)$. Because of the clustered topology of the network, D is much larger than d. For example, for the parameters used in Fig. 27, $D \simeq 14$ and $d \simeq 2$. The average load decrease associated with the backbone nodes in each cluster is then $n(N-n)(D-d)/(M-1)$, which is much less than the load decrease in the original cluster. In general, the closer a cluster is to the original cluster, the more load decrease occurs. Thus, to significantly increase the network's ability to resist cascading breakdown while at the same time to minimize its impact on the network, non-essential nodes in clusters that are closer to the original cluster should be targeted for removal. Figure 28(b) shows this effect by comparing the consequence of removing non-essential nodes from randomly selected clusters and from clusters that are more distant from the original cluster. We see that removing non-essential nodes from close clusters results in about 20% of improvement in G as compared with node removal from randomly chosen clusters, and the improvement is about 50% when comparing with removal from some more distant clusters.

For controlled node removal from some randomly chosen clusters, the optimal removing size M_{rc} that maximizes G can be estimated, as follows. Before removal, the total load is $S = N(N-1)(D+1)$. After removing int$[fN]$ non-essential nodes, the total load becomes $S' = N'(N'-1)(D'+1)$, where $N' = \text{int}[(1-f)N]$ and D' is the new network distance. Since the backbone nodes play a dominant role in load processing, $D' \approx D$ and $S'/S \approx (1-f)^2$. That is, the load of an average backbone node i decreases by a factor of $(1-f)^2$ as the result of controlled removal. After the attack, the load of node i will in general increase from L_i to $L_i' = \beta L_i$, where β is a constant depending on the network structures. The new load can thus be written as $(1-f)^2\beta L_i$. If the capacity λL_i of node i is larger than the new load, i.e., $\lambda L_i > (1-f)^2\beta L_i$, cascading failures will not occur. In this sense, the quantity β characterizes the network's ability to resist cascading breakdown.

Generally, the value of the parameter β depends on nodes, thus it is more accurate to write $L_i' = \beta_i L_i$. Most of the nodes in the network have β values close to 1, with a small set of nodes having larger β values. The probability distribution of $\beta_i - 1$ is shown in Fig. 29. We observe that for scale-free networks without clustered structure, the distribution decays exponentially for large β_i (inset of Fig. 29). This is consistent with previous

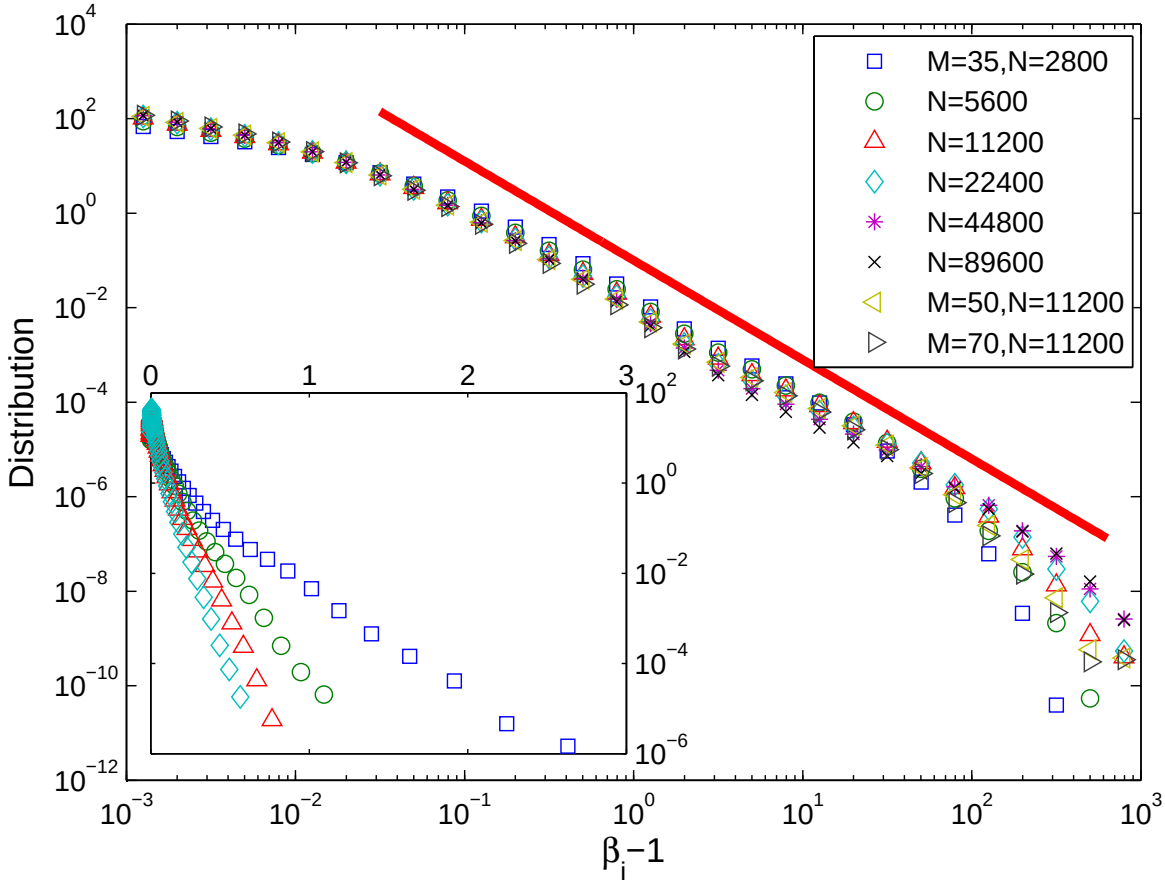

Fig. 29. The distribution of the shifted load ratio $\beta_i - 1$. For clustered networks, the distribution has a long tail and is independent to network details such as the number of clusters and network size, indicating the existence of large load fluctuations before and after attack. The straight line has a slope of -2.1. Inset: the same quantity for a single scale-free network (by setting $M = 1$). $N = 5600$, $\langle k \rangle = 4, 6, 8, 10$ from right to left. The distribution for the shifted ratio is exponential. Each data is the result of averaging at least 100 random realizations.

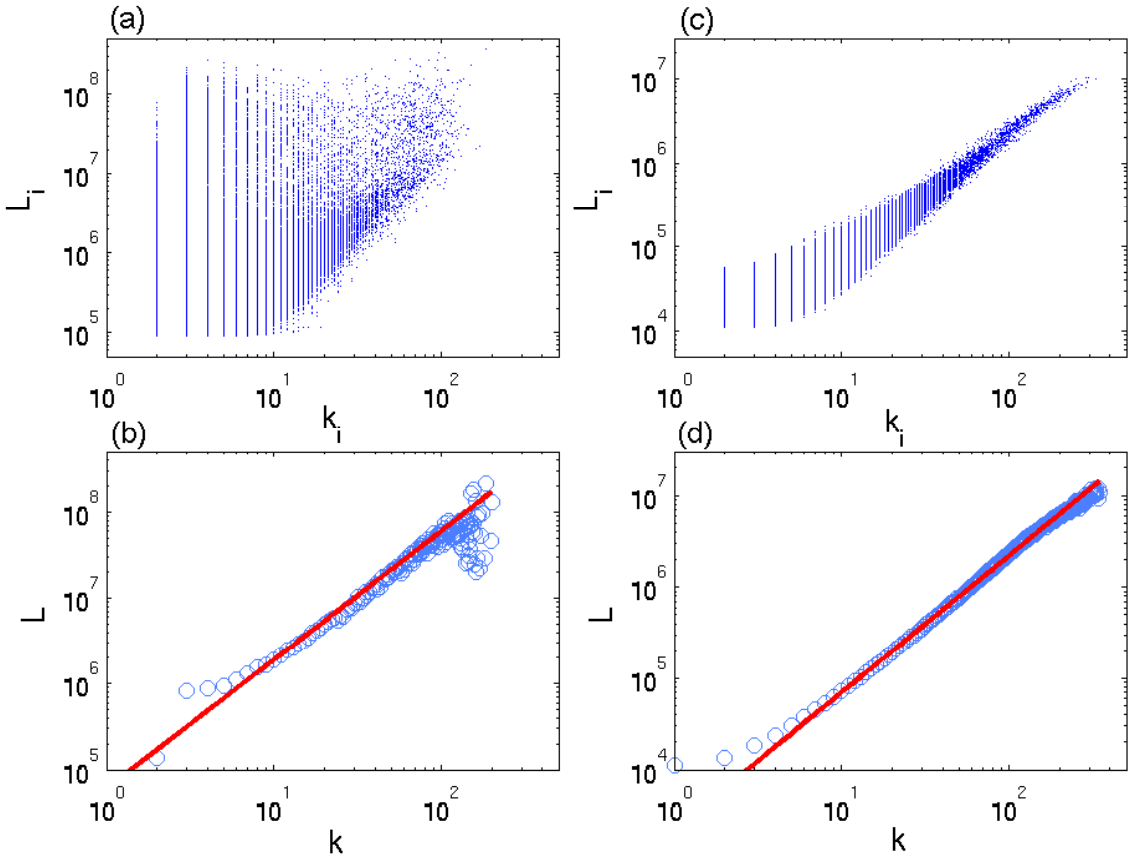

Fig. 30. Load versus degree for clustered networks with $M = 35$, $N = 44800$ (a)(b), and for scale-free networks with $N = 5600$, $\langle k \rangle = 4$ (c)(d). (a)(c) Scattered plots for all (k_i,L_i) pairs. (b)(d) The averaged load L over all the nodes with the same degree versus node degree k. The straight line has a slop of 1.5. The data are obtained from more than 100 random realizations.

results that for networks without a clustered structure, $\beta - 1 \approx 0$ [69]. However, for a clustered network, the distribution of β_i has a long tail compared with exponential decay, indicating large load fluctuations after the initial attack. Heuristically, this could be understood, as follows. A single network is compact and its structure is homogeneous, i.e., removing some nodes results in a smaller network but with similar properties. For example, for a scale-free network the load L_i and the degree k_i satisfy the scaling relation $L_i \sim k_i^{\alpha}$, where $\alpha \approx 1.5$. After removing a few nodes, it is still a scale-free network, thus the relation $L_i' \sim k_i'^{\alpha}$ still holds, where prime means the corresponding network quantities after the removal. Since the number of nodes removed is small, one expects the change in the degree to be small as well, thus $k_i' \approx k_i$, and $L_i' \approx L_i$ [69]. However, for a clustered network, although the averaged load $L(k)$ over the nodes with the same degree k scales as $L \sim k^{\alpha}$ [Fig. 30(b)], the relation does not hold for individual nodes [Fig. 30(a)], contrasting with that of scale-free networks [Fig. 30(c)]. Indeed, the load for such a network is determined by the type of the nodes. Generally, the bridge nodes have the largest loads, followed by the skeleton nodes, and then by the *non-essential* nodes. Since the links between clusters are established among randomly selected nodes, the backbone nodes can have both large and small degrees [Fig. 30(a)]. Furthermore, when the network is attacked, the backbone structure is altered. On one hand, some new nodes may become backbone nodes, and their loads will increase drastically. For example, for the case where backbone nodes (13% of all nodes) carry 79% of the total load S, the average load carried by them is about $6S/N$, while the non-essential nodes carry an average load of $0.2S/N$. Thus, when a non-essential node becomes a backbone node, the ratio β is of the order of 30, and due to heterogeneity of the nodes (each cluster is a scale-free network), the ratio can be as high as several hundred. On the other hand, the load flow in the backbone may be redistributed after the attack, leading to huge load changes as well. This accounts for the long tail in the distribution of the shifted ratio $\beta - 1$. Although the ratio for a single node can be as high as several hundred, the number of such nodes can be several orders of magnitude smaller, as indicated by Fig. 29. We find, numerically, the effective value of $\beta \approx 2$ for a clustered network.

Thus, for a given value of λ, the optimal fraction of controlledly removed nodes is $f_c = 1 - \sqrt{\lambda/\beta}$. Noting that f can be written as $f = \eta M_r/M$, where η is the fraction of non-essential nodes, we have

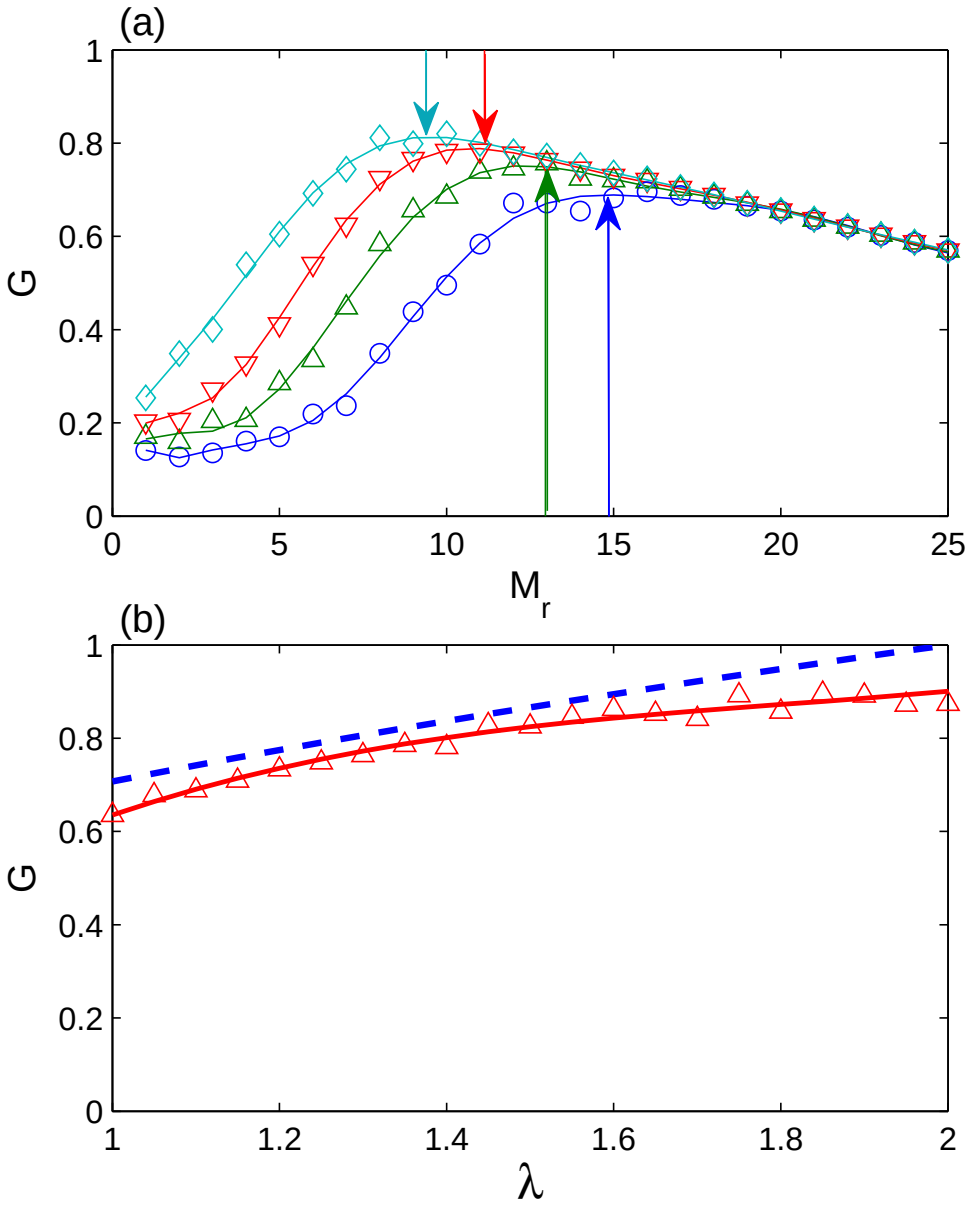

Fig. 31. (a) G versus M_r for $\lambda = 1.1$ (circles), 1.2 (upward triangles), 1.3 (downward triangles), and 1.4 (diamonds). The arrows indicate the predicted value of M_{rc}. (b) G versus λ for our strategy. The dashed line represents our theoretical prediction.

$M_{rc} = Mf_c/\eta$. Since M_{rc}, the optimal number of clusters where controlled removal occurs, assumes approximately the same value for different ways of selecting the clusters [Fig. 28(b)], our estimate for M_{rc} should practically hold for all three cases and it can thus be considered as a general theoretical prediction. For parameters used in Fig. 31(a), we have $\eta = 0.87$. The predicted M_{rc} values are indicated by arrows in the figure for several λ values. They agree with the simulation results reasonably well.

We now summarize the steps of executing our strategy for preventing cascading breakdown in a complex clustered network. Assume that the network parameters λ, β, and η are available (either they are pre-assigned or they can be calculated when the network structure is known) and the backbone nodes in various clusters have been identified. The immediate response to an attack on some hub nodes in a particular cluster should be to calculate the distances between all other clusters to this cluster and assign indices I_M to these clusters. The critical cluster index $M_{rc} = \mathrm{int}[M(1 - \sqrt{\lambda/\beta})/\eta]$ is then calculated. Non-essential nodes in clusters whose indices satisfy $I_M \leq M_{rc}$ are removed. Cascading breakdown can then be avoided, where the resultant maximum value of G is given by $G_{\max} = 1 - f_c = \sqrt{\lambda/\beta}$. Numerical verification of our strategy is shown in Fig. 31(b), where the value of G versus λ is displayed. The result of executing our optimal strategy of controlled node removal is represented by the solid curve, while the dashed curve is predicted by the above physical analysis. We observe that, even when the node capacity parameter assumes the minimum value $\lambda = 1$, our method can result in a connected component that contains more than 60% of the original nodes after an attack. In this sense, cascading breakdown has been effectively prevented. We emphasize that, given the structure of the network to be protected, the required computations in response to an attack can be done extremely efficiently, and the results of which can then be used for quick, controlled node removal so as to prevent possible cascading breakdown.

8 . DYNAMICS-BASED SCALABILITY OF COMPLEX NETWORKS

8.1. Background

Scalability is an important issue in many branches of science and engineering. For example, in biology, synchronization can occur in systems of different sizes, ranging from neuronal and cellular networks to population dynamics in natural habitats of vast distances. In computer science, whether a particular program can work in systems containing orders-of-magnitude different numbers of components is always a pressing issue. Similar scalability issues arise in large-scale circuit designs. Our interest here is in *dynamics-based scalability* of complex networks. In particular, we ask, if a dynamical phenomenon of interest occurs in networks of size N_1, can the same phenomenon be anticipated in networks of size N_2, where N_2 is substantially larger than N_1? More importantly, does the scalability so defined depend on the network topology? Addressing these questions can provide insights into fundamental issues such as the ubiquity of certain types of networks in nature with respect to specific dynamical functions. A good understanding of the scalabilities of networks of different topologies can also be important for practical design of various technological networks. Despite extensive research on complex networks in recent years, the issue of network scalability has not been considered.

To address the issue of network scalability, we focus on synchronization, a fundamental type of collective dynamics in biological systems [73], and investigate the interplay between synchronization-based scalability and network topology. The distinct type of network topologies included in our pursuit are globally connected, locally coupled regular, random [42, 103], and scale-free [43]. We assume an identical nonlinear dynamical process on every node. The associated master-stability function (MSF) [60, 123, 124] $\Psi(K)$ can then be determined, where K is a generalized coupling parameter. Let $0 = \lambda_1 < \lambda_2 \leq \ldots \leq \lambda_N$ be the eigenvalue spectrum of the coupling (Laplacian) matrix $\mathbf{L}$ for a given network. The system allows a stable synchronization state if for all $i = 2, \ldots, N$, $\Psi(K_i)$ is negative [123], where $K_i = \varepsilon\lambda_i$ and ε is the actual coupling strength. There are three typical classes of node dynamics under which synchronization can occur [see Appendix A]: (class-I) $\Psi(K) < 0$ in a finite interval (K_a, K_b); (class-II) $K_b \to \infty$; (class-III) $\Psi(K) < 0$ in several distinct intervals (K_{a1}, K_{b1}), (K_{a2}, K_{b2}), ... , (K_{af}, K_{bf}), where K_{bf} can be either finite or infinite. Consider, for example, class-I node dynamics. The stability condition becomes $K_a < \varepsilon\lambda_2 \leq \varepsilon\lambda_N < K_b$.

As a result, we shall analyze the dependence of λ_2 and λ_N on parameters N and ε so that regions in the two-dimensional parameter plane (N, ε), where the underlying network is synchronizable, can be determined analytically. Since the scalability results for class-III node dynamics can be inferred from those from class-I and class-II dynamics, and class-II is actually a special case of class-I (a synchronizable system under class-I node dynamics is also synchronizable under class-II dynamics), it is convenient to focus on class-I dynamics and discuss situations of class-II dynamics where the network is unsynchronizable for class-I dynamics.

The main results of this Chapter are as follows. For globally connected and random networks, for any system size N, there exists a non-zero coupling-parameter interval $(\varepsilon_a, \varepsilon_b)$ for which the network is synchronizable [123]. However, for locally coupled regular and scale-free networks, no such interval exists for sufficiently large system size if K_b is finite. That is, these networks cannot be synchronized if their sizes are too large when the node dynamics belong to class-I. For class-II node dynamics, scale-free networks can be synchronized, but locally coupled regular networks require arbitrarily large coupling to be synchronized so that they are practically not scalable. Our findings can provide insights into some fundamental issues in sciences and engineering. For example, in biology, synchronization can occur on networks of various sizes [73]. However, large scale-free networks can be unsynchronizable and, hence, the scale-free topology may not be important, or less ubiquitous, in situations where synchronization is key to system functions. From the standpoint of network design to achieve some desired synchronization-dependent performance, random networks are advantageous.

8.2. Globally coupled networks

For such a network, every node is coupled to all other nodes in the network ($L_{ii} = N - 1$, $L_{ij} = -1$ if $i \neq j$) and we have $\lambda_1 = 0$ and $\lambda_2 = \ldots = \lambda_N = N$. The network is synchronizable if $K_2 = \lambda_2 \varepsilon > K_a$ and $K_N = \lambda_N \varepsilon < K_b$. Synchronization is stable if $K_a/\lambda_2 < \varepsilon < K_b/\lambda_N$, and we thus have $\varepsilon_a = K_a/N$ and $\varepsilon_b = K_b/N$ and, hence, $\Delta\varepsilon = (K_b - K_a)/N \sim N^{-1}$. That is, for any physical network whose size is finite, there exists a finite interval of the coupling parameter for which synchronization can be achieved. The behavior is shown in Fig. 32(a), where the shaded strip in the parameter plane (N, ε) (on a logarithmic scale) indicates the synchronizable region. For any fixed system size, as the coupling parameter is increased, the

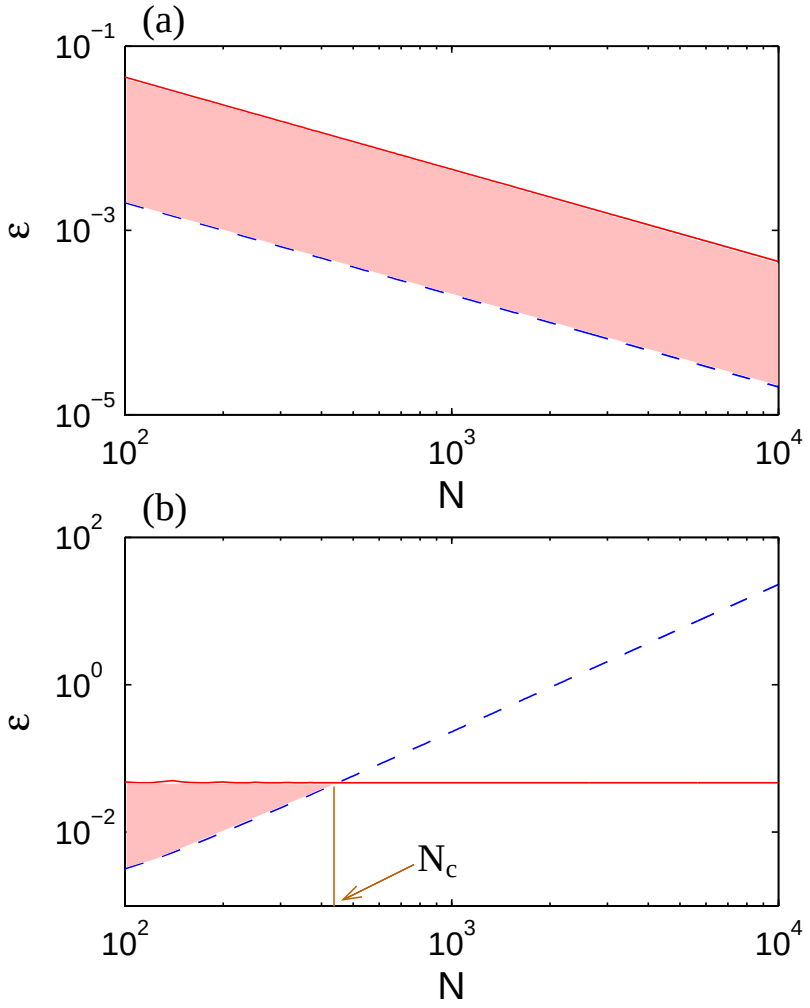

Fig. 32. Synchronizable region (shaded) in the parameter plane (N, ε) for (a) globally coupled networks, and (b) locally coupled regular networks with fixed average degree $\langle k \rangle = 80$. The node dynamics is described by the chaotic Rössler oscillator: $d\mathbf{x}/dt = \mathbf{F}(\mathbf{x}) \equiv [-(y+z), x + 0.2y, 0.2 + z(x-9)]^T$, for which we find $K_a \approx 0.2$ and $K_b \approx 4.6$.

network can undergo transitions from desynchronization to synchronization, and to desynchronization again. A remarkable feature is that, for a reasonably fixed coupling parameter, as its size is increased, a network can go from being desynchronized to being synchronized and then to being desynchronized again. This means that, a globally coupled network can be synchronized if its size is neither too small nor too large. There exists an optimal range of the system size for which synchronization can be achieved. This is basically a system-size resonance phenomenon [125].

8.3. Locally coupled regular networks

In such a network, every node is connected to m nearest neighbors, i.e., $\langle k\rangle = m$. We assume periodic boundary conditions. The elements of the Laplacian matrix $\mathbf{L}$ are then $L_{ii} = m$, $L_{ij} = -1$ for $j = i \pm 1, \ldots, i \pm m/2$ and $L_{ij} = 0$ otherwise. The eigenvector associated with λ_2 is $\mathbf{e}_2 = \sqrt{2/N}[\sin(2\pi/N), \sin(4\pi/N), \ldots, \sin(2\pi)]^T$, where $(\cdot)^T$ denotes transpose. The key eigenvalue λ_2 can then be expressed as $\lambda_2 = \mathbf{e}_2^{\mathrm{T}} \cdot \mathbf{L} \cdot \mathbf{e}_2 = \sum_{i,j=1}^{N} L_{ij} e_{2i} e_{2j}$, where $e_{2i} = \sqrt{2/N} \sin(2\pi i/N)$. After a lengthy algebra, we obtain

$$\lambda_2 = m + 2 - 2\cos(\frac{m\pi}{2N}) \frac{\sin(\frac{\pi}{N} + \frac{m\pi}{2N})}{\sin(\frac{\pi}{N})}.$$

The largest eigenvalue can be obtained by manipulating $\lambda_N = \mathbf{e}_N^{\mathrm{T}} \cdot \mathbf{L} \cdot \mathbf{e}_N = \sum_{i,j=1}^{N} L_{ij} e_{Ni} e_{Nj}$, where $e_{Ni} = \sqrt{2/N} \sin[(2\pi j/(N/f)]$ and f is the basic spatial Fourier frequency, an integer between 1 and $N/2$. A similar calculation gives

$$\lambda_N = m + 2 - 2\cos(\frac{m\pi}{2N/f}) \frac{\sin(\frac{\pi}{N/f} + \frac{m\pi}{2N/f})}{\sin(\frac{\pi}{N/f})}.$$

Because of the frequency dependence of λ_N, the upper bound of the synchronizable parameter interval is given by $\varepsilon_b = K_b/\lambda_{N,max}$, where $\lambda_{N,max} = \lambda_N(f_c)$ and f_c is given by $f_c = \min\{f | d\lambda_N(f)/df = 0\}$. For a sparse network, we have $\langle k\rangle = m \ll N$. In this case, the expression for $\lambda_2(N)$ and $\lambda_{N,max}(N)$ can be further simplified by proper Taylor expansions. We obtain $\lambda_2 \approx \pi^2(m+2)(m^2+m+1)/6N^2$ and $\lambda_N \approx m$. That is, $\varepsilon_a = \alpha N^2$ and $\varepsilon_b = K_b/m$ (independent of N), where $\alpha \equiv 6K_a/[\pi^2(m+2)(m^2+m+1)]$. We then have $\Delta\varepsilon = K_b/m - \alpha N^2$. The key feature that distinguishes a locally coupled network from a globally coupled network is the existence of a critical system size, above which the network is unsynchronizable, regardless of

the coupling. Our analysis gives the following formula for the critical system size: $N_c = \sqrt{K_b/(m\alpha)}$. In principle, knowing the specific node dynamics (which gives specific values of K_a and K_b), we can predict N_c. A typical behavior of the network synchronizability in the parameter plane (N, ε) is shown in Fig. 32(b). We see that locally coupled regular networks are unscalable for class-I node dynamics. Physically, this could be understood that for globally coupled network, the number of links per node increases with network size. While for locally coupled regular network the number of links per node is a constant. Thus as network size increases, the network distance becomes larger and it is more difficult for a node to communicate with its diametrical counterparts, leading to degraded synchronizability. For class-II dynamics, $K_b \to \infty$, the stability condition becomes $\varepsilon > K_a/\lambda_2$, which can be satisfied in principle. A practical issue is that, since λ_2 can be small for large N, the coupling parameter needs to be unreasonably large, e.g. $\varepsilon > \alpha N^2$, for synchronization to occur. If there exists a limit of the coupling parameter, say ε_u, the critical network size is given by $N_c = \sqrt{\varepsilon_u/\alpha}$. In this sense, locally coupled regular networks are not scalable.

8.4. Random networks

Let p be the probability for a pair of nodes to be connected. The average degree of the network is $\langle k \rangle = pN$. For the adjacency matrix $\mathbf{A}$ ($A_{ij} = -1$ if nodes i and j are connected, $A_{ij} = 0$ otherwise and $A_{ii} = 0$), the distribution of the eigenvalues $\lambda_i^{(A)}$ follows the Wigner semicircle law [126], where the center of the semicircle is at zero. In particular, we have $\lambda_1^{(A)} \approx -Np$, $\lambda_2^{(A)} \approx -2\sqrt{Np(1-p)}$, $\lambda_N^{(A)} \approx 2\sqrt{Np(1-p)}$, and $\sum_i \lambda_i^{(A)} = 0$. For the Laplacian matrix $\mathbf{L}$, where $L_{ij} = A_{ij}$ for $i \neq j$ and $L_{ii} = k_i$, we have $\lambda_1 = 0$ and $\mathrm{Tr}(\mathbf{L}) = \sum_i k_i = N^2 p$. The nontrivial eigenvalues are still distributed according to the semicircle law except that the center of the semicircle is now at Np. We thus have $\lambda_2 \approx Np - 2\sqrt{Np(1-p)}$ and $\lambda_N \approx Np + 2\sqrt{Np(1-p)}$, which give $\varepsilon_a = K_a/[Np - 2\sqrt{Np(1-p)}]$ and $\varepsilon_b = K_b/[Np + 2\sqrt{Np(1-p)}]$.

Random networks arising in nature are typically sparse [42]. For a sparse random network, the average degree satisfies $\langle k \rangle \ll N$ or $p \ll 1$. We thus obtain $\varepsilon_a \approx K_a/(\langle k \rangle - 2\sqrt{\langle k \rangle})$ and $\varepsilon_b \approx K_b/(\langle k \rangle + 2\sqrt{\langle k \rangle})$. A remarkable consequence is that, if $\langle k \rangle$ is fixed, both ε_a and ε_b are independent of the network size! As a result, arbitrarily large networks can be synchronized, insofar as the network becomes increasingly sparse and the coupling strength falls in a constant interval [127]. The size of this interval does not decrease

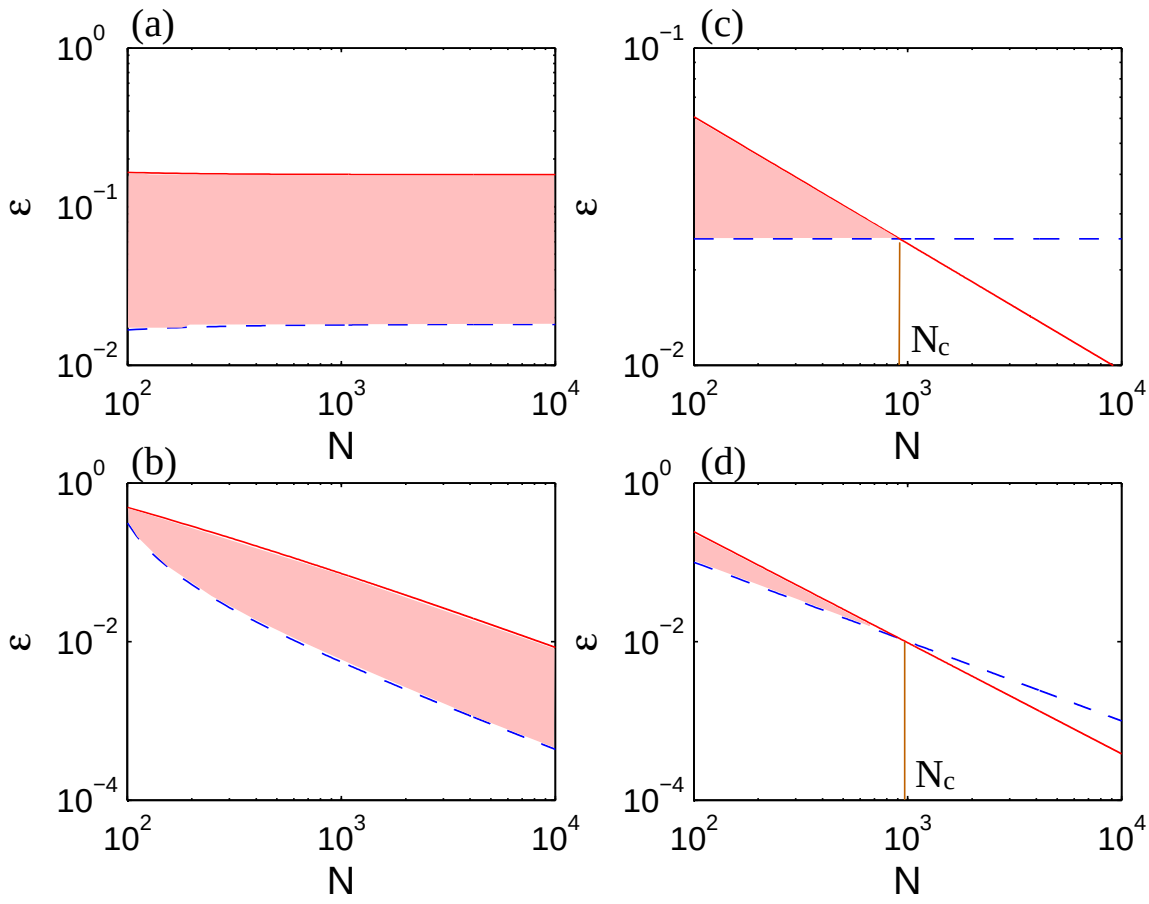

Fig. 33. For the same node dynamics as in Fig. 32, synchronizable region (shaded) in the parameter plane (N, ε) for (a) random networks with fixed average degree $\langle k \rangle = 20$, (b) random networks with $\langle k \rangle = 0.05N$, (c) scale-free networks with degree exponent $\gamma = 3.5$ and fixed average degree $\langle k \rangle = 20$, and (d) scale-free networks with $\langle k \rangle = 0.05N$.

as N is increased, as exemplified in Fig. 33(a) for $\langle k\rangle = 20$. In this sense, random networks are more synchronizable than globally connected networks, as for the latter, the synchronizable parameter interval $\Delta\varepsilon$ decreases inversely with the increase of the system size [Fig. 32(a)]. Note, however, if $\langle k\rangle$ increases with N (e.g., $\langle k\rangle = pN$ and p is fixed), then for large N, we have $\langle k\rangle \gg \sqrt{\langle k\rangle}$ and, hence, $\Delta\varepsilon \approx (K_b - K_a)/\langle k\rangle \sim 1/N$, as shown in Fig. 33(b). This is similar to the synchronization behavior of a globally connected network. Thus random networks are scalable for all three classes of node dynamics.

8.5. Scale-free networks

For a scale-free network, the degree distribution follows a power law [43]: $P(k) = ak^{-\gamma}$ for $k \geq m_0$, where $\gamma > 0$ is the degree exponent and a is a constant. The minimum degree is $k_{min} = m_0$. The constant a can be determined by $\int_{m_0}^{\infty} P(k)dk = 1$. For a scale-free network of infinite size, the maximum degree k_{max} diverges. However, for any physical network, its size is finite. One can consider the average number of nodes that have degrees larger than k_{max}, which is $N\int_{k_{max}}^{\infty} P(k)dk$. If this number is less than one, k_{max} is the largest degree. This condition yields $\int_{k_{max}}^{\infty} P(k)dk \approx 1/N$, which gives $k_{max} \approx m_0 N^{1/(\gamma-1)}$. For scale-free networks, we have $\lambda_2 \approx Ck_{min}$, where the constant C is of the order of unity, and $\lambda_N \approx k_{max}$ [128]. Thus λ_2 is independent of the system size but λ_N increases with N as a power law. We then have $\varepsilon_a \approx K_a/(Cm_0)$ and $\varepsilon_b \approx (K_b/m_0)N^{-1/(\gamma-1)}$ and, consequently, $\Delta\varepsilon \approx (K_b/m_0)N^{-1/(\gamma-1)} - K_a/(Cm_0)$. The point is that there exists a critical system size $N_c \approx [K_a/(CK_b)]^{-(\gamma-1)}$, above which synchronization is impossible. The synchronizable region in the (N, ε)-plane is shown in Fig. 33(c) for scale-free networks of fixed average degree. A qualitatively similar behavior occurs when the average degree increases with the system size, as shown in Fig. 33(d) for $\langle k\rangle = 0.05N$. Thus large scale-free networks are not synchronizable if the node dynamics belong to class-I. For class-II dynamics, since λ_2 does not decrease with network size N, synchronization can occur when the coupling parameter is in a proper range, regardless of the system size. Therefore, scale-free networks are not scalable for class-I node dynamics but scalable for class-II dynamics. An implication is that, if synchronization is important for the functions of some complex networked systems, the scale-free topology should not be the choice if the node dynamics has a finite K_b. Likewise, in biological

situations where synchronization can occur in systems of all kinds of sizes, we expect the random-network topology to be more pervasive since it is scalable for all cases.

8.6. Direct numerical verification

We now provide direct numerical support for our analysis. To compare with eigenvalue analysis we again use class-I node dynamics. The oscillatory networked system is described by $d\mathbf{x}_i/dt = \mathbf{F}(\mathbf{x}_i) - \varepsilon \sum_{j=1}^{N} L_{ij}\mathbf{H}(\mathbf{x}_j)$, where $\mathbf{F}(\mathbf{x}) = [-(y+z), x+0.2y, 0.2+z(x-9)]^T$, $\mathbf{H}(\mathbf{x}) = [x,0,0]^T$ is a coupling function. Because of the complexity of the system dynamics, the degree of synchronization can be characterized only statistically. In particular, we define the synchronization probability P_{syn} as the probability that the fluctuation width $W(t)$ of the system is smaller than a small number δ (chosen somewhat arbitrarily) at all time steps during an interval T_0 in the steady state, where $W(t) = \langle |x(t) - \langle x(t)\rangle|\rangle$, and $\langle\cdot\rangle$ denotes average over nodes of the network. In computation, P_{syn} can be calculated by the ensemble average, i.e., the ratio of the number of synchronized cases over the number of all random network realizations. Figure 34 shows P_{syn} versus the system size for both random and scale-free networks, where panel (a) corresponds to the situation where $\langle k\rangle = 20$ and panel (b) is for $\langle k\rangle = 0.05N$. Indeed, for random networks of fixed average degree, synchronization can occur for all system sizes tested [open circles, panel (a)]. However, a scale-free network with fixed average degree cannot be synchronized if its size becomes too large [open triangles, panel (a)]. When the average degree of the network is proportional to its size, for both random and scale-free networks, for a fixed coupling parameter, there exists a range of system size with which synchronization can occur [panel (b)]. These results agree with those from our spectral analysis.

In summary, we have addressed the fundamental issue of scalability in both complex and regular networks, by focusing on their synchronizabilities. Our analysis indicates that random networks are scalable in the sense that they are synchronizable, regardless of their sizes, insofar as the coupling parameter is chosen properly. However, scale-free networks are scalable only for certain types of node dynamics. For the regular topology, globally coupled networks are scalable but locally coupled networks are not. Investigating network scalability not only can provide a better understanding of the workings of networks in nature, but also is important for designing technological networks, notably computer networks in information infrastructure.

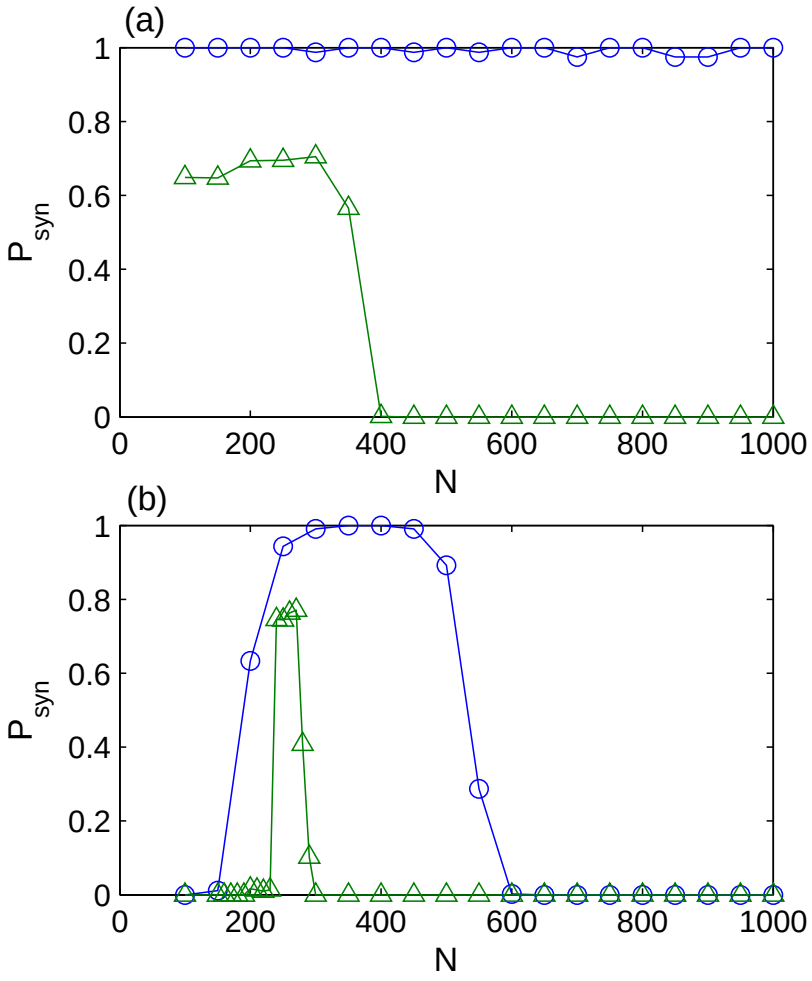

Fig. 34. Synchronization probability versus network size. (a) Fixed average degree $\langle k \rangle = 20$ for random (circles, $\varepsilon = 0.05$) and scale-free (triangles, $\varepsilon = 0.035$, $\gamma = 3.5$) networks. (b) Average degree proportional to network size: $\langle k \rangle = 0.05N$, for random (circles, $\varepsilon = 0.1$) and scale-free (triangles, $\varepsilon = 0.06$, $\gamma = 3.5$) networks. Simulation parameters are $T_0 = 3000$ and $\delta = 0.01$. Each data point is from 1000 network realizations.

9 . SYNCHRONIZATION-BASED SCALABILITY IN COMPLEX CLUSTERED NETWORKS

9.1. Background

Recently, synchronization in complex networks has received considerable attention [49,50,54,55,59,61, 115, 116, 129, 130]. There are two main motivations: (1) synchronization is fundamental to many phenomena in nature, especially in biology [73], and (2) many natural and technological systems exhibit traits of complex networks [12,42,43,131,132]. Most existing studies have focused on the synchronizability, addressing the role played by different network topologies [55, 59, 115, 130]. Various coupling schemes have been proposed to enhance the network synchronizability. The issue of scalability, i.e., the dependence of dynamical properties of the network on its size, has also begun to be considered [62, 133]. The focus of this chapter is on the scalability of synchronization of complex clustered networks, networks whose characteristics have been found in various biological, social, and technological systems [1–6].

A clustered network consists of a number of subnetworks (clusters), where nodes within each cluster are densely connected but the linkage among the clusters is sparse. A clustered network can be complex in the sense that, not only the inter-cluster linkage can be random, but the connections within each individual cluster can also be random [75], small-world [42], or scale-free [43]. Recently synchronization in complex clustered networks has been studied [61], but the issue of size-dependence has not been systematically explored. The main question addressed in this chapter is then: if a clustered network of small size is synchronizable, under what conditions will networks of the same topology but of much larger size be still synchronizable? Answer to this question can reveal the interplay between synchronization and the clustered topology and help provide insights into whether *large* complex clustered networks can be pervasive in natural systems with respect to synchronization.

We will use the standard approach of network spectral analysis, namely the master-stability-function (MSF) approach [60] to explore the size-dependence issue. In particular, previous works have established that the synchronizability of a network can be characterized by the spread of the eigenvalue spectrum of the underlying coupling matrix [49, 50, 54]. Given a clustered network, we shall obtain analytic estimates for both the smallest and the largest nontrivial eigenvalues as a function of the network size, based on which the range of the coupling parameter, say ε, for which synchronization is possible can be obtained. A network is

regarded as scalable with respect to synchronization if there exists a finite range of ε in which synchronization can occur, insofar as the network size is finite. Likewise, a network is not scalable if the synchronizable parameter range becomes zero as the network size exceeds a critical value. To state our main result, it is necessary to define parameters to characterize a complex clustered network. In this regard the probabilities of inter-cluster and intra-cluster links, denoted by p_l and p_s, respectively, are most relevant. For the clustered topology to be distinct, it is required by definition that $p_l \ll p_s$. Our analysis indicates that, for fixed values of p_l and p_s, the network is scalable with respect to synchronization. However, as we will see, when p_l and p_s are fixed, the densities of the inter-cluster and intra-cluster linkages increase in a different manner as the network size is increased. If the size is sufficiently large, the inter-cluster link density can surpass the intra-cluster link density (unless the number of clusters is small). When this occurs, the characteristics of the clustered topology is completely lost, reducing the network to one with the standard complex topology determined by the specific topology of the individual subnetwork. On the other hand, if the inter-cluster link density is fixed so that the clustered topology is maintained, the network synchronizability is lost when its size becomes sufficiently large. The general phenomenon is then that complex clustered networks are not scalable with respect to synchronization. An implication is that, if synchronization is important to the functions of a large networked system, the complex clustered topology is not desirable. For large networks in biology, if synchronization is fundamental, they are most likely to be non-clustered. Our result also provides a dynamics-based explanation to the difficulty to achieve synchronization in many social networks that are typically large and clustered.

The aim of our study is to address network scalability by focusing on the network's ability to synchronize, not on actual synchronization. This approach would allow general conclusions to be drawn, in spite of the complexity of the problem. If actual synchronization were to be considered, general insights would be difficult to obtain as the synchronization would depend on many specific details such as initial conditions. Thus, in this chapter, when we say that certain networks are scalable with respect to synchronization, we mean only that the networks can be synchronized, regardless of its size, if the coupling parameter and initial conditions are chosen properly. In contrast, if a class of networks is not scalable, they absolutely cannot be

synchronized if their sizes exceed a critical value, regardless of how coupling or initial conditions are adjusted. It is in this sense of scalability which makes the MSF formalism [60] a powerful theoretical tool. In what follows we shall briefly describe the MSF framework and argue for its applicability when different types of node dynamics are taken into account.

We consider the following network of N coupled oscillators:

$$\frac{d\mathbf{x}_i}{dt} = \mathbf{F}(\mathbf{x}_i) - \varepsilon \sum_{j=1}^{N} G_{ij}\mathbf{H}(\mathbf{x}_j), \tag{9.1}$$

where $i = 1, \ldots, N$, $d\mathbf{x}/dt = \mathbf{F}(\mathbf{x})$ describes the dynamics of each individual oscillator, **H(x)** is the coupling function to each oscillator, $\mathbf{G} = (G_{ij})$ is the coupling matrix determined by the network topology, and ε is a coupling parameter. The matrix $\mathbf{G}$ satisfies the condition $\sum_{j=1}^{N} G_{ij} = 0$ for any i, ensuring the existence of a synchronized state $\mathbf{x}_i(t) = \mathbf{s}(t), \forall i$, where $d\mathbf{s}/dt = \mathbf{F}(\mathbf{s})$ is a solution to Eq. (9.1).

Linearizing Eq. (9.1) about the synchronized state yields the master stability functions (MSF). For different types of node dynamics, the MSF shows some different behaviors. What has often been assumed in the network-synchronization literature [49, 50, 54] is that the MSF is negative in a single, finite interval. However, to encompass all possible situations, we shall also address the cases where the interval tends to infinity and where the MSF has several distinct stable regions.

Class-I node dynamics. To be concrete, we assume chaotic dynamics on any single node so that $\Psi(0) > 0$. For synchronization to be possible, $\Psi(K)$ must be negative in some region of K. There is thus a cross point of $\Psi(K)$ with K-axis at which $\Psi(K)$ becomes negative, say K_1. As K is increased, $\Psi(K)$ becomes positive again at K_2 and remains positive thereafter. In this case, $\Psi(K)$ is negative in a finite interval $[K_1, K_2]$, and the stability condition for synchronization becomes

$$\lambda_2 \geq \frac{K_1}{\varepsilon} \quad \text{and} \quad \lambda_N \leq \frac{K_2}{\varepsilon},$$

or

$$\frac{K_1}{\lambda_2} \leq \varepsilon \leq \frac{K_2}{\lambda_N}.$$

Let $\varepsilon_1 = K_1/\lambda_2$ and $\varepsilon_2 = K_2/\lambda_N$. For a given network ($\lambda_2$ and λ_N fixed) and given node dynamics (K_1

and K_2 fixed), the interval of coupling strength that permits a stable synchronization of the system is

$$\Delta\varepsilon = \varepsilon_2 - \varepsilon_1 = \frac{K_2}{\lambda_N} - \frac{K_1}{\lambda_2}. \tag{9.2}$$

If $\Delta\varepsilon > 0$, the system can be made synchronizable for proper choices of the coupling parameter ε and of the initial conditions. For given K_1 and K_2, this leads to the condition for synchronization:

$$Q \equiv \frac{\lambda_N}{\lambda_2} < \frac{K_2}{K_1}, \tag{9.3}$$

where Q is the eigenratio. If $\Delta\varepsilon < 0$ or $Q > K_2/K_1$, synchronization will not occur no matter how the coupling parameter ε may be adjusted. The eigenratio Q can thus be used as an indicator of the synchronizability of the network [49]: the smaller the value of Q, the higher the probability that the system can synchronize. For a network with given node dynamics, K_2/K_1 is constant. For the network to be scalable with respect to synchronization, $\Delta\varepsilon$ should be positive for any size N of the network. Or equivalently, the eigenratio Q should not exceed K_2/K_1 as the size of the network is increased.

Class-II node dynamics. In this case, $K_2 \to \infty$, i.e., the MSF $\Psi(K)$ is negative for $K \in [K_1, \infty)$. With respect to scalability, this is a special case of *Class-I node dynamics*, in the following sense: a synchronizable or scalable system for class-I dynamics is also synchronizable or scalable for class-II dynamics.

Class-III node dynamics. In this case, $\Psi(K)$ is negative in several distinct regions, say $[K_{a1}, K_{b1}], [K_{a2}, K_{b2}], \ldots, [K_{af}, K_{bf}]$ where $K_{a1} < K_{b1} < K_{a2} < K_{b2} < ... < K_{af} < K_{bf}$ and K_{bf} can be either finite or infinite. When K_{bf} is finite, if each interval $[K_{ai}, K_{bi}]$ is regarded as the synchronizable interval $[K_1, K_2]$ for class-I node dynamics, results on the scalability for class-I dynamics can be applied. Note that it is possible that K_i may reside in different stable intervals where the system is still synchronizable. For $K_{bf} \to \infty$, if a particular finite interval is of interest, results from class-I node dynamics are pertinent; otherwise results for class-II dynamics are applicable.

The above discussion suggests that, in order to address the issue of scalability, focusing on class-I node dynamics suffices.

In Sec. 9.2, we provide a spectral analysis for complex clustered networks under two coupling schemes.

In Sec. 9.3, we apply the results in Sec. 9.2 to obtain analytic results concerning the scalability of such networks and provide numerical support. Conclusions are offered in Sec. 9.4.

9.2. Spectral analysis of complex clustered networks

We consider the following general clustered network model [132, 134]: there are N nodes in a network which are divided into M clusters, and each cluster contains $n = N/M$ nodes. Nodes in the same cluster are connected with probability p_s, and the probability for two nodes, each belonging to a different cluster, to be linked is p_l. The clustered topology requires $p_l \ll p_s$. For typical clustered networks arising in different situations, the topology of the subnetworks in individual clusters is mostly random [1–6], which we shall assume for our analysis in this chapter.

For a given node dynamics, the values of the general coupling parameter that define the stable synchronization regime, K_1 and K_2, are fixed. The synchronizability of the oscillator network is then determined by its topology as characterized by the smallest and the largest nontrivial eigenvalues of the coupling matrix, λ_2 and λ_N, respectively. In the following, we shall consider two different coupling schemes and derive analytic formulas for λ_2 and λ_N.

9.2.1. Type-I coupling

In this case, the coupling matrix is defined as: for any $i (1 \leq i \leq N)$, $G_{ii} = k_i$, where k_i is the degree (the number of links) of node i, $G_{ij} = -1$ $(i \neq j)$ if there is a link between node i and j, and $G_{ij} = 0$ otherwise. This matrix is in fact the generalized Laplacian matrix.

To obtain an analytic estimate for λ_N, we make use of the relation between λ_N and the maximum degree of the network as derived in Ref. [133]:

$$\lambda_N \approx k_{\max} + 1. \tag{9.4}$$

Our goal is thus to obtain an expression for $k_{\max}$ for random clustered networks.

In a single random network with connection probability p, the degree k_i of a node i follows a Binomial distribution $B(N-1, p)$: $P(k_i = k) = C_{N-1}^k p^k (1-p)^{N-1-k}$, where $C_{N-1}^k = (N-1)!/[k!(N-1-k)!]$ is the Binomial coefficient. When N is large, a straightforward application of the law of large numbers yields

the following standard approximation:

$$P(k) \approx \frac{1}{\sqrt{Np(1-p)}}\phi(\frac{k-Np}{\sqrt{Np(1-p)}}),$$

where $\phi(x) = (1/\sqrt{2\pi})e^{-\frac{1}{2}x^2}$. For a clustered network, node i connects to the remaining $n-1$ nodes in the same cluster with probability p_s, and connects to the $N-n$ nodes in different clusters with probability p_l. Therefore, the degree distribution of the network consists of two parts: $B(n-1, p_s)$ for intra-cluster links and $B(N-n, p_l)$ for inter-cluster links. Using the approximation of normal distribution, we have

$$P_s(k) \approx \frac{1}{\sqrt{np_s(1-p_s)}}\phi(\frac{k-np_s}{\sqrt{np_s(1-p_s)}}),$$
$$P_l(k) \approx \frac{1}{\sqrt{(N-n)p_l(1-p_l)}}\phi(\frac{k-(N-n)p_l}{\sqrt{(N-n)p_l(1-p_l)}}).$$

Assuming that intra-cluster and inter-cluster links are independent of each other, we can sum the two distributions to obtain a new normal distribution for the degree distribution:

$$P(k) \approx \frac{1}{\sigma}\phi(\frac{k-\langle k\rangle}{\sigma}), \tag{9.5}$$

where the mean and the variance are given by

$$\langle k\rangle = np_s + (N-n)p_l,$$
$$\sigma^2 = np_s(1-p_s) + (N-n)p_l(1-p_l). \tag{9.6}$$

The maximum degree $k_{\max}$ of the network can be calculated by following the condition that the probability of a node to have a degree larger than or equal to $k_{\max}$ is $1/N$, i.e.,

$$\int_{k_{\max}}^{\infty} P(k)dk = 1/N.$$

Using Eq. (9.5), we obtain

$$k_{\max} = \mathrm{erf}^{-1}(1-2/N)\cdot\sqrt{2}\sigma + \langle k\rangle, \tag{9.7}$$

where $\mathrm{erf}^{-1}(x)$ is the inverse of the error function $\mathrm{erf}(x) = \frac{2}{\sqrt{\pi}}\int_0^x e^{-t^2}dt$. The largest eigenvalue λ_N can then be approximated as

$$\lambda_N \approx k_{\max} + 1 = \mathrm{erf}^{-1}(1-2/N)\cdot\sqrt{2}\sigma + \langle k\rangle + 1. \tag{9.8}$$

For λ_2, we have $\lambda_2 = \mathbf{e}_2^T \cdot \mathbf{G} \cdot \mathbf{e}_2 = \sum_{i,j=1}^{N} e_{2i} G_{ij} e_{2j}$, where $\mathbf{e}_2$ is the eigenvector associated with λ_2 and e_{2i} is the ith component of $\mathbf{e}_2$. A recent work [62] has revealed that for a clustered network, the components of the eigenvector $\mathbf{e}_2$ have approximately the same value within a cluster. Thus the eigenvector $\mathbf{e}_2$ can be written as: $\mathbf{e}_2 \approx [\tilde{e}_1, ..., \tilde{e}_1, \tilde{e}_2, ..., \tilde{e}_2, ..., \tilde{e}_M, ..., \tilde{e}_M]^T$, and for each index I, $1 \leq I \leq M$, there are n $\tilde{e}_I$'s in $\mathbf{e}_2$. We have

$$\lambda_2 \approx \sum_{i=1}^{N} e_{2i}\{G_{i1}\tilde{e}_1 + G_{i2}\tilde{e}_1 + \cdots + G_{in}\tilde{e}_1 + G_{i(n+1)}\tilde{e}_2 + \cdots + G_{iN}\tilde{e}_M\}. \tag{9.9}$$

For type-I coupling, the matrix elements are: (1) $G_{ii} = k_i$, (2) $G_{ii} = -1$ with probability p_s and $G_{ii} = 0$ with probability $1 - p_s$ if nodes i and j belong to the same cluster, and (3) $G_{ii} = -1$ with probability p_l and $G_{ii} = 0$ with probability $1 - p_l$ if nodes i and j belong to different clusters. Substituting these matrix elements into Eq. (9.9), we have

$$\lambda_2 \approx \sum_{i=1}^{N} e_{2i}\{-np_l\tilde{e}_1 - np_l\tilde{e}_1 + \cdots + k_i\tilde{e}_I - np_s\tilde{e}_I + \cdots - np_l\tilde{e}_M\},$$

where $\tilde{e}_I$ is the eigenvector component associated with the cluster that contains nodes i. For a random subnetwork, the degree distribution has a narrow peak centered at $k = np_s + (N - n)p_l$, which leads to $k_i \approx k$. We can thus write λ_2 as

$$\begin{aligned}\lambda_2 \quad &\approx \sum_{i=1}^{N} e_{2i}\{(N-n)p_l\tilde{e}_I - np_l\sum_{J\neq I}^{M}\tilde{e}_J\} = \sum_{i=1}^{N} e_{2i}\{Np_l\tilde{e}_I - np_l\sum_{J=1}^{M}\tilde{e}_J\} \\ &\approx \sum_{I=1}^{M} n\tilde{e}_I\{Np_l\tilde{e}_I - np_l\sum_{J=1}^{M}\tilde{e}_J\} = Np_l\sum_{I=1}^{M} n\tilde{e}_I^2 - (n\sum_{J=1}^{M}\tilde{e}_J)^2 p_l.\end{aligned}$$

Note that $\sum_{I=1}^{M} n\tilde{e}_I^2 \approx \sum_{i=1}^{N} e_{2i}^2 = 1$, and $n\sum_{J=1}^{M}\tilde{e}_J = \sum_{i=1}^{N} e_{2i} = 0$ ($\mathbf{G}$ is symmetric for this type of coupling). We obtain, finally,

$$\lambda_2 \approx Np_l, \tag{9.10}$$

for $p_l \ll p_s$ so that the clustered structure of the network is maintained.

9.2.2. Type-II coupling

Type-II coupling is defined by the following normalized Laplacian matrix: for any $i(1 \leq i \leq N)$, $G_{ii} = 1, G_{ij} = -1/k_i$ $(i \neq j)$ if there is a link between node i and j, and $G_{ij} = 0$ otherwise. For such a

matrix, if $N \geq 2$ and the network is connected, then $0 < \lambda_2 \leq N/(N-1)$ and $N/(N-1) \leq \lambda_N \leq 2$ [55, 135]. λ_2 is more crucial in determining network synchronizability than λ_N is, because a slight change in λ_2 could lead to drastic change in the eigenratio Q, while the change of λ_N will not. Therefore, in the following, we estimate λ_N in one way, and estimate λ_2 in another more accurate way.

For λ_N, note that $\mathbf{G} = \mathbf{I} - \mathbf{D}^{-1}\mathbf{A}$, where $\mathbf{I}$ is the unit matrix, $\mathbf{D} = diag\{k_1, \ldots, k_N\}$, and $\mathbf{A}$ is the adjacency matrix. For a random network, its spectrum follows the Wigner semicircle law [136]. The minimum eigenvalue of $\mathbf{A}$ is thus given by

$$\begin{aligned} \lambda_{\min}^{A} &= -2\sqrt{np_s(1-p_s) + (N-n)p_l(1-p_l)} \\ &\approx -2\sqrt{np_s + (N-n)p_l} = -2\sqrt{\langle k \rangle}. \end{aligned}$$

Because of the narrow degree distribution, we have $k_i \approx \langle k \rangle$, which leads to [55, 137]

$$\lambda_N \approx 1 - \lambda_{\min}^{A}/\langle k \rangle \approx 1 + \frac{2}{\sqrt{\langle k \rangle}}. \tag{9.11}$$

For the smallest nontrivial eigenvalue λ_2 can be obtained in a more precise manner from Eq. (9.9). In particular, recall that for type-II coupling, $G_{ii} = 1$, and if i and j belong to the same cluster, G_{ij} equals $-1/k_i$ with probability p_s and 0 with probability $1 - p_s$, while if they belong to different clusters, G_{ij} equals $-1/k_i$ with probability p_l and 0 with probability $1 - p_l$. Using $1 - np_s/k_i = (N-n)p_l/k_i$ and performing a similar analysis as for the case of type-I coupling, we obtain

$$\lambda_2 \approx \frac{Np_l}{np_s + (N-n)p_l} = \frac{Np_l}{\langle k \rangle}. \tag{9.12}$$

Numerical results show, indeed, that Eq. (9.12) predicts more accurately λ_2 than the random-matrix prediction $\lambda_2 \approx 1 - 2/\sqrt{\langle k \rangle}$.

9.3. Scalability of clustered networks: theory and numerical support

The synchronization-based scalability of a random clustered network can be analyzed by exploring how the key eigenvalues λ_N and λ_2 of the coupling matrix vary as the size of the network is increased. There are two ways by which the network size $N = nm$ can be increased: either n or m is increased. In addition, for a clustered network with fixed intra-cluster connecting probability p_s, there are two distinct situations. First,

the inter-cluster connection probability p_l is fixed. In this case, the average number of inter-cluster links per node μ increases with the network size $N = nm$. Second, μ is fixed. In this case, when N is increased, the probability p_l needs to be decreased accordingly. With the two types of coupling schemes treated here, there are *eight* distinct combinatorial cases of interest. In the following, we will analyze each case and provide numerical support. Our approach will be as follows. Recall that, insofar as $Q = \lambda_N/\lambda_2 < K_2/K_1$, there is a finite parameter interval $(\varepsilon_1, \varepsilon_2)$, where $\varepsilon_1 = K_1/\lambda_2$ and $\varepsilon_2 = K_2/\lambda_N$, within which the oscillator network is synchronizable. We shall then focus on λ_N and λ_2, investigate when the condition $Q < K_2/K_1$ is satisfied, and plot ε_1 and ε_2 as a function of N to reveal the synchronizable (scalable) regions in the two-dimensional parameter space (N, ε).

For numerical exploration, we shall use the chaotic Rössler oscillators for node dynamics, which is given by $\mathbf{F}(\mathbf{x}) = [-(y+z), x+0.2y, 0.2+z(x-9)]^T$. Parameters adopted here permit a funnel attractor in the phase space and the system is in the chaotic state. The coupling function is chosen to be $\mathbf{H}(\mathbf{x}) = x$. We obtain $K_1 \approx 0.2, K_2 \approx 4.62$, and the synchronization boundaries of the system are given by $\varepsilon_1 = 0.2/\lambda_2$ and $\varepsilon_2 = 4.62/\lambda_N$.

9.3.1. Scalability for fixed inter-cluster connecting probability

For each case below, we fix $p_s = 0.3$ and $p_l = 0.01 \ll p_s$ in numerical computations so as to ensure the clustered topology of the network.

9.3.1.1. Type-I coupling

Case 1. Fixing n and varying m. In this case, the size of individual clusters is fixed while the number of clusters is varied. Theoretical results for λ_N and λ_2 can be obtained from Eq. (9.8) and Eq. (9.10), as shown by the solid curves in Figs. 35(a) and 35(b). The data points are from numerical computations. There is a reasonable agreement between theory and numerics. In particular, as m is increased, both λ_N and λ_2 increase, but Q decreases, as shown in Fig. 35(c). This means that, insofar as $Q < K_2/K_1$ is satisfied, larger networks are more synchronizable. The synchronization region in the (m, ε) parameter plane can be determined by Eq. (9.2), as shown in Fig. 36 as the region between the top and the bottom curves (open triangles are numerical results). It can be seen that as the number of clusters is increased, there exists a finite interval $\Delta\varepsilon$ within which

the oscillator system can be synchronized. We thus see that for type-I coupling, random clustered networks with fixed cluster size are scalable with respect to synchronization.

Case 2. Fixing m and varying n. In this case, the number of clusters is fixed and the size of the network is controlled by n, the size of each individual cluster. Theoretical and numerical results show that the behaviors of Q and of the critical values of the coupling parameter are similar to those for case 1. We conclude that, for type-I coupling and fixed inter-cluster connecting probability, a clustered network is scalable with respect to synchronization.

We now provide analytic insights into the behaviors of ε for type-I coupling. For this type of coupling, the relevant eigenvalues λ_N and λ_2 are given by Eq. (9.8) and Eq. (9.10). Based on these formulas, we can write down the eigenratio Q as

$$Q = \lambda_N/\lambda_2 \approx \frac{\mathrm{erf}^{-1}(1-2/N)\sqrt{2}\sigma + \langle k\rangle + 1}{Np_l}.$$

We proceed by making use of the following series expansion for the inverse error function [138]:

$$[\mathrm{erf}^{-1}(x)]^2 \sim \eta - \frac{1}{2}\ln\eta + \eta^{-1}(\frac{1}{4}\ln\eta - \frac{1}{2}) + \ldots, x \to 1,$$

where $\eta = -\ln[\sqrt{\pi}(1-x)]$. This expansion is valid for $x \to 1$, which holds in our problem as $1-2/N \to 1$ for large N. Keeping only the first-order term, we have

$$\mathrm{erf}^{-1}(1-2/N) \approx \sqrt{-\ln(\sqrt{\pi}\cdot 2/N)} = \sqrt{\ln(N/2\sqrt{\pi})}.$$

Substituting this into the expression for Q and omitting irrelevant constants, we have

$$Q = \frac{\sqrt{2\ln(N/2\sqrt{\pi})}\sigma + \langle k\rangle + 1}{Np_l} \approx \frac{\sqrt{nS} + np_s + mnp_l}{mnp_l},$$

where $S = [p_s(1-p_s) + mp_l]\ln(mn)$. We see that Q is essentially independent of m and n when they become large. But when we fix n and increase m, for instance, in order to maintain the clustered structure, m should smaller than $m_{\max} = p_s/p_l + 1$ (see Sec. 9.4). Substituting this expression of $m_{\max}$ in Eq. (9.13), we get

$$Q \approx 2 + \sqrt{\frac{2-p_s}{np_s}\ln\frac{np_s}{p_l}}, \text{ for fixed } n.$$

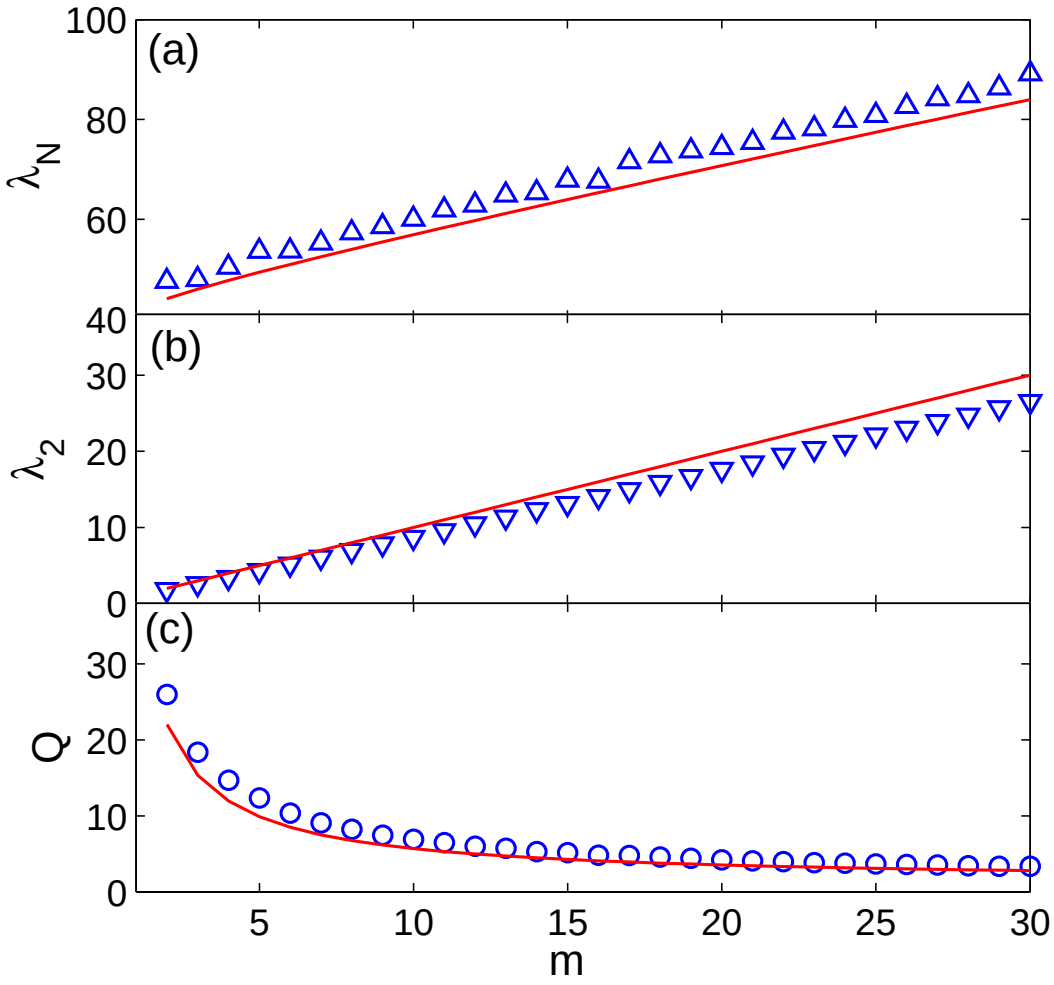

Fig. 35. (Color online) For type-I coupling, fixed cluster size, (a-c) λ_N, λ_2, and Q versus m, the number of clusters, respectively. Simulation parameters are $p_s = 0.3$, $p_l = 0.01$, and $n = 100$. The curves represent theoretical results and data points are numerical results averaged over 10 random network realizations.

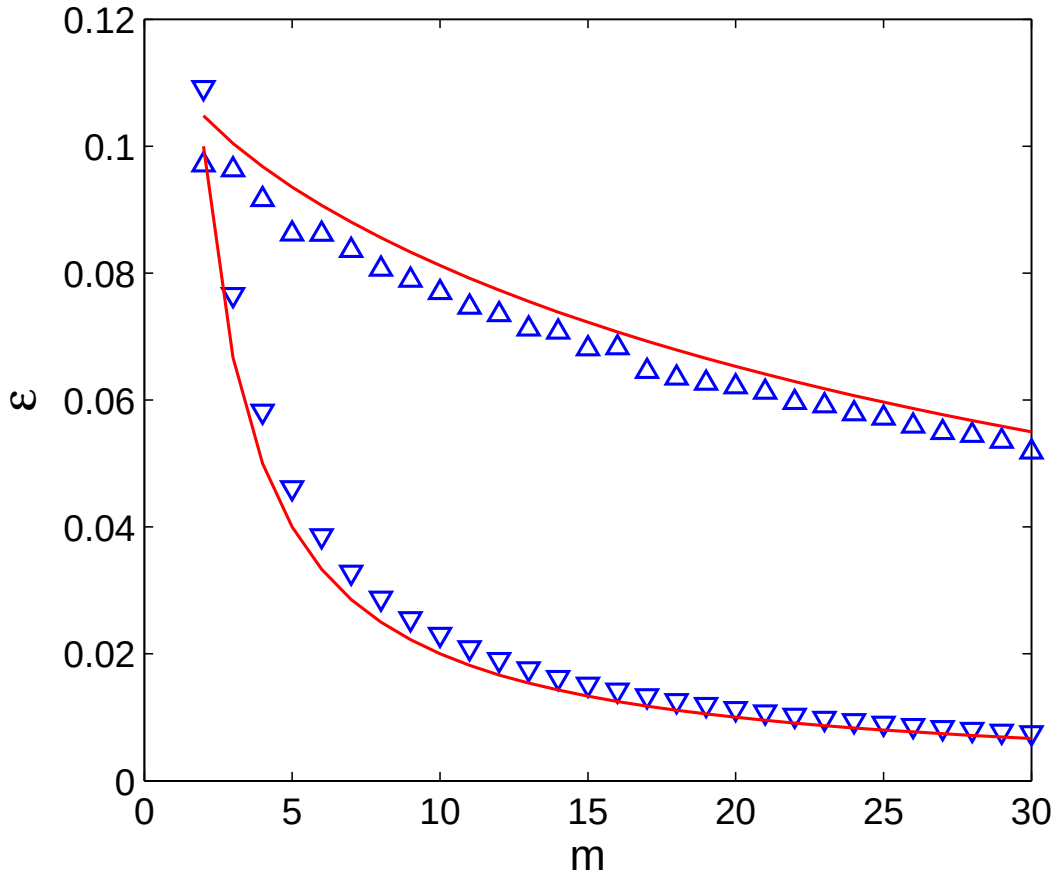

Fig. 36. (Color online) For the same setting as in Fig. 35, synchronizable region in the two-dimensional parameter plane (m, ε) as enclosed by the two curves. Data points are numerical results.

For fixed m, the asymptotical behavior of Q can be given as

$$Q \approx \frac{p_s}{mp_l} + 1, \text{ for fixed } m,$$

which does not depends on n and tends to a constant. The size $\Delta\varepsilon$ of the synchronizable region is then given by

$$\Delta\varepsilon \approx \frac{K_2 p_l - K_1(\sqrt{S/(m^2 n)} + p_s/m + p_l)}{p_l(\sqrt{nS} + np_s + mnp_l)}.$$

For fixed n, the leading term of $\Delta\varepsilon$ scales with m as m^{-1}. Making use of the expression for $m_{\max}$, we get

$$\Delta\varepsilon \approx \frac{K_2 np_s - K_1(\sqrt{np_s(1-p_s)\ln(np_s/p_l)} + 2np_s)}{np_s(\sqrt{np_s(1-p_s)\ln(np_s/p_l)} + 2np_s)}.$$

For fixed m we then have

$$\Delta\varepsilon \approx \frac{K_2 mp_l - K_1(p_s + mp_l)}{mnp_l(p_s + mp_l)},$$

which scales with n as n^{-1}.

9.3.1.2. Type-II coupling

Case 3. Fixing n and varying m. In this case, λ_N decreases as there are more clusters in the network, versus the cases associated with the type-I coupling where this eigenvalue increases as the network grows. Meanwhile, λ_2 increases with m, the eigenratio Q actually decreases with m, indicating that larger networks are more synchronizable. Both theoretical and numerical results show that the synchronizable coupling interval increases with m. Since the numerical results appear quite similar to those in Figs. 35 and 36, here we shall provide a scaling theory for type-II coupling.

Case 4. Fixing m and varying n. For the eigenvalues λ_N and λ_2 and the ratio Q, behaviors similar to those in $case3$ have been observed. As a result, the synchronizable region in the parameter plane (ε, n) shows a similar pattern too : the underlying oscillator network is scalable.

For type-II coupling, we have:

$$\begin{aligned} Q &= \frac{(1 + 2/\sqrt{\langle k\rangle})\langle k\rangle}{Np_l} \approx \frac{\langle k\rangle + 2\sqrt{\langle k\rangle}}{Np_l} \\ &\approx \frac{np_s + nmp_l + 2\sqrt{np_s + nmp_l}}{nmp_l} \end{aligned} \tag{9.13}$$

where $\langle k \rangle$ is the average degree of the network that can be calculated from Eq. (9.6). Apparently, Q depends neither on n nor on m when the system size becomes infinite. Let $m = m_{\max}$ be the critical value of the number of clusters above which the clustered structure cannot be maintained. We have

$$Q \approx 2(1 + \sqrt{2/(np_s)}), \text{ for fixed } n.$$

When we fix m and increase n, the asymptotic value of Q can be obtained as

$$Q \approx \frac{p_s}{mp_l} + 1, \text{ for fixed } m.$$

The synchronizable coupling-parameter interval $\Delta\varepsilon$ can then be calculated as

$$\Delta\varepsilon \approx K_2 - K_1 \frac{np_s + nmp_l}{nmp_l},$$

where the leading term is independent of n and m. For $m = m_{\max}$, we have

$$\Delta\varepsilon \approx K_2 - 2K_1, \text{ for fixed } n.$$

If m is fixed but n is increased, we have, asymptotically,

$$\Delta\varepsilon \approx K_2 - K_1 \frac{p_s + mp_l}{mp_l}.$$

For type-II coupling, when we fix m (or n) and increase n (or m), a finite interval in the coupling parameter always exists for which the network is synchronizable. The clustered networks are thus scalable. Combined with the results for type-I coupling, we can conclude that, for fixed inter-cluster connecting probability, the networks are scalable for both type-I and type-II coupling schemes. In particular, the eigenratio Q tends to constant values as the network grows, and the synchronizable parameter interval $\Delta\varepsilon$ is inversely proportional to the network size for type-I coupling but it tends to constant for type-II coupling as the system size N is increased.

9.3.2. Scalability for fixed average number of inter-cluster connections

The average number of inter-cluster connections is

$$\mu = \frac{n^2 m(m-1)p_l}{mn} = n(m-1)p_l.$$

When we fix μ to grow the network, the actual inter-cluster connection probability

$$p_l = \frac{\mu}{n(m-1)} \tag{9.14}$$

will be reduced, but our theoretical results in Sec. 9.2 for the eigenvalues are still applicable.

9.3.2.1. Type-I coupling

Cases 5 and 6. Fixing n (or m) and varying m (or n). In these cases, λ_N is still given by Eq. (9.8), except that σ and $\langle k \rangle$ now become

$$\sigma^2 = np_s(1-p_s) + \mu(1 - \frac{\mu}{n(m-1)}), \tag{9.15}$$
$$\langle k \rangle = np_s + \mu,$$

and λ_2 can be calculated from

$$\lambda_2 = \frac{m\mu}{m-1}. \tag{9.16}$$

When we fix μ, there is no required maximum value of m (see 9.3.3). We thus only need to discuss the behavior of Q as the network size is increased. From Eqs. (9.8), (9.15), and (9.16), we have

$$Q \approx \frac{1}{\mu}(\sqrt{(p_s(1-p_s) + mp_l)\ln(mn)} + np_s), \tag{9.17}$$

which scales as $\sqrt{m \ln m}$ for fixed n and as n for fixed m. Thus, for type-I coupling, when the network grows, Q always increases. As the network size increases through a critical value, there exists no interval in the coupling parameter for which the network can be synchronized, indicating a loss of scalability. These behaviors have been verified numerically.

9.3.2.2. Type-II coupling

Cases 7 and 8. Fixing n (or m) and varying m (or n). Substituting Eq. (9.14) into both Eq. (9.11) and Eq. (9.12), we get

$$\lambda_N \approx 1 + \frac{2}{\sqrt{\langle k \rangle}} = 1 + \frac{2}{\sqrt{np_s + \mu}}, \tag{9.18}$$

and

$$\lambda_2 \approx \frac{m\mu}{(m-1)\langle k \rangle} \approx \frac{m\mu}{(m-1)(np_s + \mu)}. \tag{9.19}$$

For large n (or m), the leading term of Q can be written as

$$Q \approx \frac{m-1}{m\mu}(np_s + 2\sqrt{np_s}),$$

which does not depend on m for sufficiently large values of m, but it increases with n as the network size is increased. Therefore, for fixed n, when m is increased, Q first increases and then approaches asymptotically a constant. But, for fixed m, the eigenratio increases linearly with n, indicating a quick loss of the network synchronizability as n becomes large. A representative example is shown in Fig. 37.

We see that n and m have different influence on Q for different cases. For example, when m is increased, Q increases as $\sqrt{m\ln(m)}$ for type-I coupling and as $(m-1)/m$ for type-II coupling. These increases are much slower than $Q \sim n$ when n is increased for fixed m. Thus, growing a clustered network by increasing the size of individual clusters can be much more effective to suppress synchronization than increasing the number of clusters.

From the above analysis, we can see that for the type of growing scheme defined by fixing μ, Q increases for both types of the coupling schemes [139]. Because of this, although small networks may be synchronizable, the synchronizability will be lost for larger networks. Clustered networks under the constraint of fixed μ are thus not scalable.

9.3.3. Scalability and deterioration of clustered characteristics

The above results are based on the assumption that the networks considered possess a clustered topology. An interesting question is whether the clustered structure can be retained when the network grows.

By definition, a clustered network requires that the intra-cluster connections be denser than the inter-cluster connections. Defining ν and μ as the average numbers per node of intra/inter-cluster connections, respectively, we need $\nu > \mu$. For our clustered network model, ν and μ are given by

$$\nu = (n-1)p_s,$$

$$\mu = n(m-1)p_l,$$

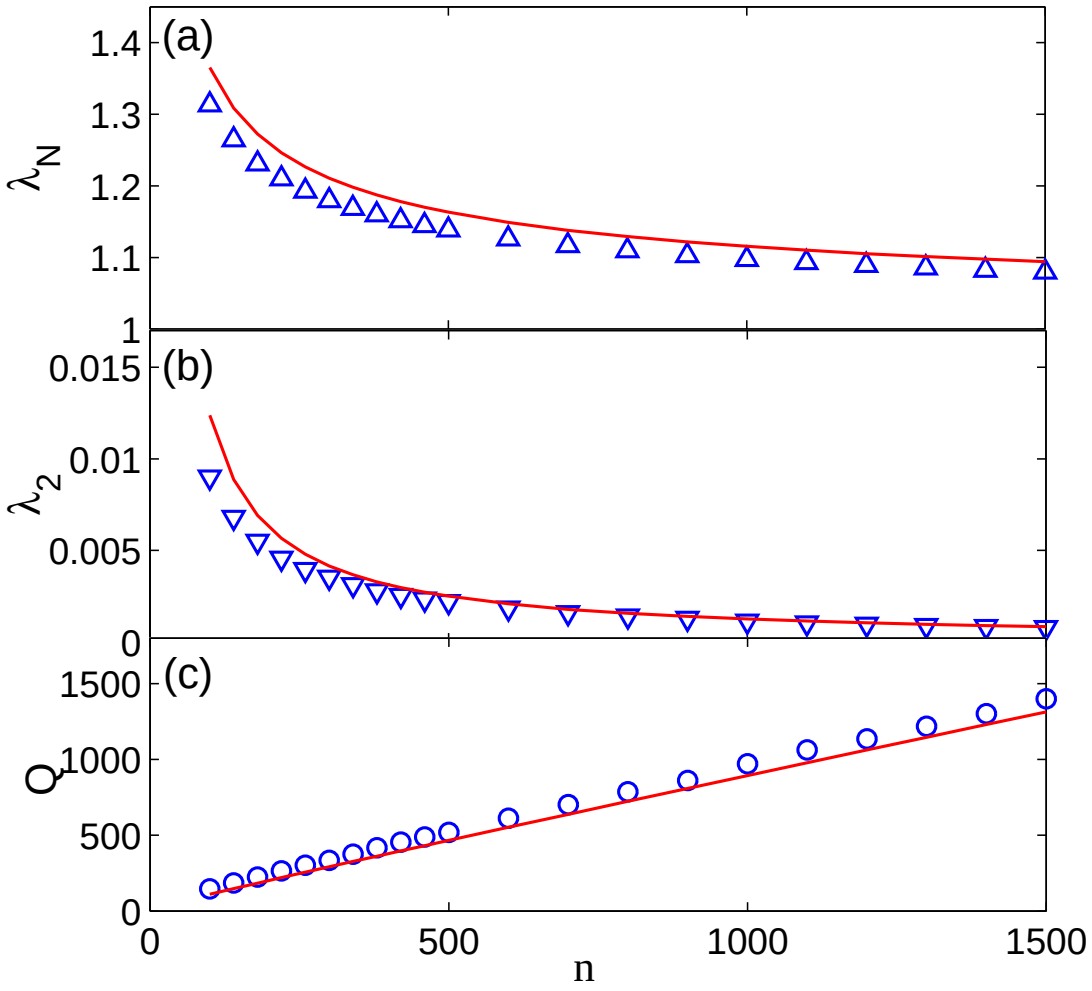

Fig. 37. (Color online) For fixed $\mu = 0.3$, type-II coupling, clustered networks of $m = 5$ clusters, (a-c) λ_N, λ_2 and Q versus n, respectively.

which leads the following condition for clustered structure:

$$\frac{\nu}{\mu} = \frac{(n-1)p_s}{n(m-1)p_l} > 1. \tag{9.20}$$

According to Eq. (9.20), the presence of the clustered topology depends on four parameters: n, m, p_l and p_s. (In this chapter p_s is fixed.)

First consider the setting where p_l is fixed. If we fix n and increase m, the condition guaranteeing a clustered network structure becomes

$$m < \frac{(n-1)p_s}{np_l} + 1 \approx \frac{p_s}{p_l} + 1,$$

which depends only on the ratio of p_s and p_l. For $m \geq p_s/p_l + 1$, the clustered structure no longer exists. For the typical numerical setting we have used, the parameters are $p_s = 0.3$ and $p_l = 0.01$. In order to ensure the clustered characteristics, the value of m should not exceed $p_s/p_l + 1 = 0.3/0.01 + 1 = 31$. This rule has been followed in all our numerical examples.

If we fix m and increase n, the clustered condition becomes

$$n[p_s - (m-1)p_l] > p_s.$$

Since Eq. (9.20) implies $(m-1)p_l < [(n-1)/n]p_s < p_s$, we have $p_s - (m-1)p_l > 0$ and, hence,

$$n > \frac{p_s}{p_s - (m-1)p_l},$$

which can usually be satisfied. For example, for $m = 5$, $p_s = 0.3$ and $p_l = 0.01$, the requirement is $n \gg 2$. (Typical values of n used in our simulations are two orders of magnitude larger.)

We remark, however, that for fixed p_l, the clustered topology can be maintained *if the number of clusters is small*. In realistic networked systems this number may be large. While networks generated for fixed value of p_l are scalable with respect to synchronization, the clustered topology is lost as the network becomes large if both the number of clusters and the number of nodes in each cluster grow.

Second, we consider the case where the average number of inter-cluster links μ is fixed. In this case, $p_l = \mu/[n(m-1)]$ decreases with network size. The condition for clustered structure is

$$\frac{\nu}{\mu} = \frac{(n-1)p_s}{\mu} > 1.$$

We see that ν/μ is independent of m. There is thus no requirement on m to ensure the clustered structure. If we fix m and increase n, the ratio of ν/μ will become larger. The condition becomes

$$n > \frac{\mu}{p_s} + 1.$$

For example, for the parameters used in our numerical examples ($\mu = 0.3$ and $p_s = 0.3$), the requirement is $n > 2$, which is always guaranteed. The conclusion is that, although the clustered topology can be maintained by fixing μ, the scalability is lost.

9.4. Discussions

We have addressed the scalability of complex clustered networks by investigating the size dependence of the network synchronizability. The general conclusion is that such networks are not scalable with respect to synchronization. In particular, if the probabilities of intra-cluster and inter-cluster connections are fixed, larger networks are actually more synchronizable. In this case, however, the number of inter-cluster links increases with the network size and, as such, a sufficiently large network may not exhibit the distinct feature of being clustered. On the other hand, if the average number of inter-cluster links is fixed, the network synchronizability deteriorates quickly as the network size becomes larger. A practical implication is that, for typical clustered networks, if synchronization is important for the system function, the clustered topology is undesirable [140]. We hope these results to be useful for the exploration of dynamics on complex clustered networks.

An important issue concerns possible time delay in the coupling function [141], as interactions between dynamical units in realistic physical systems cannot be instantaneous. When the coupling is time-delayed, the synchronization manifold still exists, so its stability can be analyzed. In particular, while the master-stability function needs to be determined from a set of variational equations that contain time delay, one can still define a generalized coupling parameter as the product between the original coupling parameter and the eigenvalues of the coupling (Laplacian) matrix. Hence, although a time delay can cause a shift or a change in the interval where the master-stability function is negative, the eigenratio is determined solely by the network topology

and can still be used to characterize the network synchronizability. We thus expect our results to hold for complex clustered networks where there is a time delay in the interactions among nodes.

10 . CONCLUDING REMARKS

Here we list the concluding remarks from the above studies:

1. We find that synchronization in complex, clustered networks tends to obey a different set of rules other than for a network without clustered structure. In particular, the synchronizability of such a network is determined by the interplay between inter-cluster and intra-cluster links.The network is most synchronizable when the numbers of the two types of links are approximately equal. In the presence of a mismatch, increasing the number of intra-cluster links, while making the network distance smaller, can counterintuitively suppress or even destroy the synchronization. We provide theory and numerical evidence to establish this phenomenon.

2. We have presented theory and numerical evidence that optimal synchronization of continuous-time oscillator clustered networks can be achieved by matching the probabilities of inter-cluster and intra-cluster links. That is, at a global level, the network has the strongest synchronizability when these probabilities are approximately equal. Overwhelmingly strong intra-cluster connection can counterintuitively weaken the network synchronizability. This can be better understood by the following considerations. Network synchronizability is usually characterized by the spread of the nontrivial eigenvalues. What our analytical formulae suggest is that spread becomes minimal when the two probabilities are approximately matched. For instance, when the inter-cluster linking probability p_l is fixed, increasing the intra-cluster connection probability p_s could result in desynchronization. On the other hand, for realistic clustered networks, p_l is always smaller than p_s, and is usually much smaller. Our analysis indicates that, insofar as the network is clustered ($p_s > p_l$), a larger p_l will lead to better synchronizability.

While our network model is somewhat idealized, we have argued that similar phenomena should persist in more general clustered networks. We have studied the synchronizability of clustered scale-free networks, where each cluster contains a scale-free subnetwork. We have carried out numerical simulations, and found that the patterns for the eigenvalues λ_N and λ_2 are essentially the same as that for the clustered network where each cluster contains a random subnetwork This indicates that optimization of synchronization by matching different types of links is a general rule.

3. For a typical locally regular clustered network, its synchronizability exhibits an alternating, highly non-monotonic behavior as a function of the intra-cluster link density. In fact, there are distinct regions of the

density for which the network synchronizability is maximized, but there are also parameter regions in between for which the synchronizability diminishes. We show that, while surprising, this phenomenon of *alternating synchronizability* can be fully explained theoretically based on analyzing the behavior of the eigenvalues and eigenvectors of the coupling matrix. A feature that makes our theoretical analysis feasible is that, due to the locally regular topology of the network, some key eigenvectors within each individual cluster exhibit periodic wave patterns. Both numerical eigenvalue calculations and direct simulation of the actual synchronization dynamics of the underlying oscillator network provide firm support for the theory.

4. We have found that the behavior of cascading breakdown in clustered networks is quite different to those in a single scale-free network. In particular, we find it convenient to classify nodes in the network as bridge nodes (nodes that are connecting different clusters), skeleton nodes (nodes within a cluster that connect the bridge nodes), and the non-essential nodes (the rest of the nodes). The bridge and skeleton nodes effectively constitute the backbone. We find that, unlike the case for a single-component network where the betweenness is correlated with the degree, for a complex clustered network, the load is rather determined by the specific node type. In general, bridge nodes have the largest loads, followed by the skeleton nodes, and then by the non-essential nodes. The population of the bridge nodes is generally small, but the load they carry can be quite substantial. Thus to alleviate traffic jams in the clustered networks, it is efficient to increase the capacity of the backbone nodes and in case of cascading, to intentionally remove some of the non-essential nodes. We have worked out a theory to estimate the amount of non-essential nodes that need to be removed and the remaining network size. Our theory agrees well with numerical simulations.

5. We have addressed the fundamental issue of scalability in both complex and regular networks, by focusing on their synchronizabilities. Our analysis indicates that random networks are scalable in the sense that they are synchronizable, regardless of their sizes, insofar as the coupling parameter is chosen properly. However, scale-free networks are scalable only for certain types of node dynamics. For the regular topology, globally coupled networks are scalable but locally coupled networks are not. Investigating network scalability not only can provide a better understanding of the workings of networks in nature, but also is important for designing technological networks, notably computer networks in information infrastructure.

APPENDIX A

MASTER STABILITY FUNCTIONS FOR TYPICAL CHAOTIC OSCILLATORS

Most existing works (including Chapters 3-6 and Chapters 8 and 9) dealing with synchronization of complex networks assume that the dynamical oscillator employed has a master stability function (MSF) that is negative in a finite region of K, say (K_1, K_2). However, when refer to real dynamical systems, most papers only use 11 coupling of Rössler oscillator. It is also known that other couplings of Rössler oscillator, say, 22, 33, do not have such master stability functions. Thus it becomes a big concern of the applicability of these studies. Here we carry out a comprehensive study to calculate the MSFs for all known, typical nonlinear oscillators under all commonly used coupling configurations. Our results show that for most nonlinear oscillators, there exist some couplings for which the MSFs have a finite negative region, thus assured the previous studies of synchronization properties of complex network systems.

Generally, for nonlinear oscillators, the Jacobian matrix $\mathbf{DF}$ depends on the trajectory $\mathbf{s}(t)$; while the Jacobian matrix for linear coupling function $\mathbf{H}$ is a constant matrix. Here, we only consider one component coupling. To be as general as possible, we consider all possible one component coupling, say, ith component coupled to jth component: $[\mathbf{H}(\mathbf{x})]_k = \delta_{jk} x_i$, where δ_{jk} is the Kronecker's delta such that $\delta_{jk} = 1$ if $j = k$ and zero otherwise, and i and j run over 1 to d. The Jacobian matrix $\mathbf{DH}$ thus only has one non-zero element: $H_{ji} = 1$, while all other elements are zero.

We have carried out a comprehensive study to calculate the MSFs for all known, typical nonlinear oscillators under all commonly used coupling configurations. For instance, for a three-dimensional system (x_1, x_2, x_3), there are nine commonly used, linear coupling configurations: 11, 12, 13, 21, 22, 23, 31, 32, and 33, and we have calculated the MSFs for all these configurations. [Here the notation ij $(i, j = 1, 2, 3)$ stands for the coupling scheme from ith component to the jth component.] The dynamical systems that we have tested include: Rössler oscillator, Lorenz oscillator, Chua's circuit, Chen's oscillator, HR neuron, Duffing's oscillator, and Van der Pol system. For all these oscillators, the parameters are chosen such that an isolated oscillator oscillates chaotically, corresponding to a positive Lyapunov exponent.

The Lyapunov exponents of variational equation (1.14) are calculated as follows. Define $\widetilde{\mathbf{DF}}(\mathbf{s}) =$

$\mathbf{DF}(\mathbf{s}) - K\mathbf{DH}(\mathbf{s})$. Then solve the matrix equation

$$\frac{d\mathbf{O}(t)}{dt} = \widetilde{\mathbf{DF}}(\mathbf{s})\mathbf{O}(t) \tag{A.1}$$

with initial condition $\mathbf{O}(0) = \mathbf{I}$, where $\mathbf{I}$ is the identical matrix of order d [142]. This matrix equation is solved together with Eq. 1.11, from which it gets the trajectory variables $\mathbf{s}(t)$. Both equations are integrated with the fourth-order Runge-Kutta (RK4) method (the calculated Lyapunov exponents will have systematic deviations if the system state is integrated using RK4 while the matrix equation is integrated using Eular method). Let $\lambda_i(t), i = 1, ..., d$ be the eigenvalues of $\mathbf{O}(t)$, then the Lyapunov exponents are given by

$$h_i = \lim_{t\to\infty} \frac{1}{t} \ln \lambda_i(t). \tag{A.2}$$

However, numerically integrate equation (A.1) is unpractical (it will quickly diverge if the system has a positive Lyapunov exponent or it will diminish to the round-off error if all Lyapunov exponents are negative). A reasonable way is to "normalize" and reset $\mathbf{O}(t)$ periodically and the Lyapunov exponents can be obtained from the normalization parameters. In our calculation, we use QR decomposition method to "normalize" $\mathbf{O}(t)$. Details can be found in pages 650-651 in Ref. [143]. 10^4 cycles of $\mathbf{s}(t)$ are calculated to allow the system reside on the attractor. Then 3×10^4 cycles are used to calculate Lyapunov exponents. Time step is $dt = 0.001$.

Rössler system [144]:

$$\begin{cases} \dot{x} = -y - z, \\ \dot{y} = x + \alpha y, \\ \dot{z} = \beta + (x - \gamma)z. \end{cases} \tag{A.3}$$

where the parameters are $\alpha = 0.2$, $\beta = 0.2$, $\gamma = 9$. The Jacobian matrix is

$$\mathbf{DF} = \begin{pmatrix} 0 & -1 & -1 \\ 1 & \alpha & 0 \\ z & 0 & x - \gamma \end{pmatrix}. \tag{A.4}$$

The Lyapunov exponents for the this system are $\lambda_1 \simeq 0.080$, $\lambda_2 \simeq 0$, and $\lambda_3 \simeq -8.716$. The master stability functions for various couplings are shown in Fig. 38.

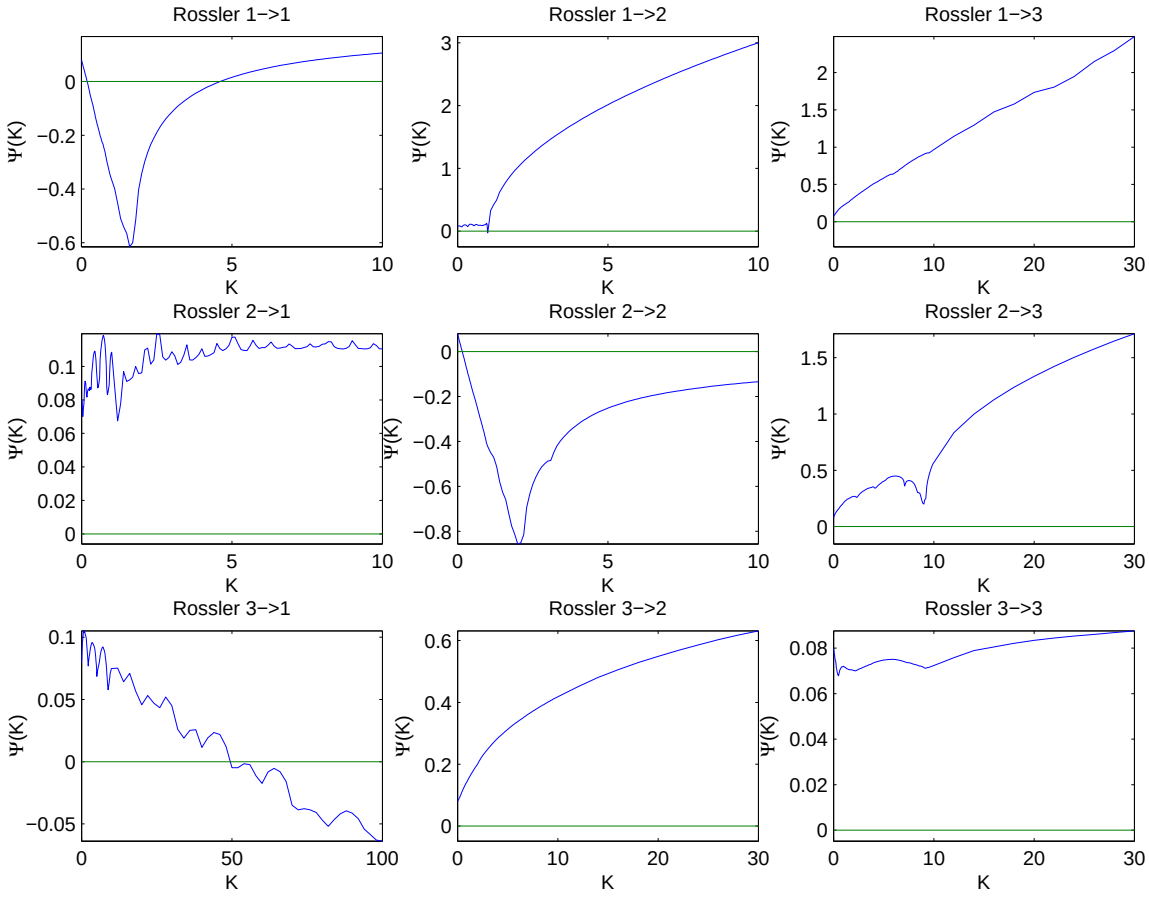

Fig. 38. MSFs versus the normalized coupling parameter K for Rössler system (A.3) with various coupling schemes. See text for the parameter values.

Lorenz system [145]:

$$\begin{cases} \dot{x} = \sigma(y - x) \\ \dot{y} = x(\rho - z) - y \\ \dot{z} = xy - \beta z \end{cases} \tag{A.5}$$

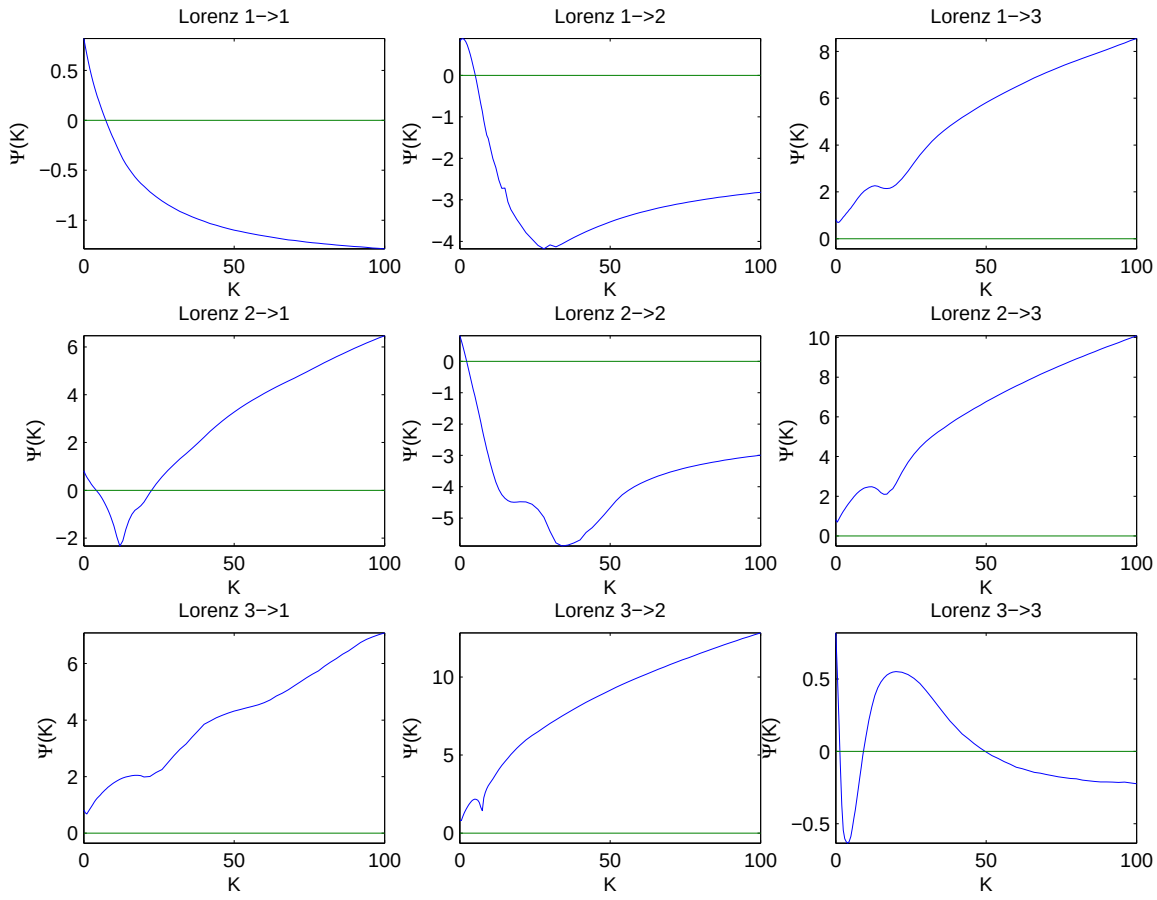

Fig. 39. MSFs versus the normalized coupling parameter K for Lorenz system (A.5).

where $\sigma = 10$, $\rho = 28$, $\beta = 2$. The Jacobian matrix is

$$\mathbf{DF} = \begin{pmatrix} -\sigma & \sigma & 0 \\ \rho - z & -1 & -x \\ y & x & -\beta \end{pmatrix}. \tag{A.6}$$

The Lyapunov exponents for the this system are $\lambda_1 \simeq 0.819$, $\lambda_2 \simeq 0$, and $\lambda_3 \simeq -13.819$. Since the diagonals of the Jacobian matrix are independent to the dynamical variables, the sum of the Lyapunov exponents should be equal the trace of the Jacobian matrix $\mathbf{DF}$. Indeed, we have $\lambda_1 + \lambda_2 + \lambda_3 \simeq -13$, and $\mathrm{Tr}(\mathbf{DF}) = -\sigma - 1 - \beta = 13$. The MSFs for different coupling schemes are plotted in Fig. 39.

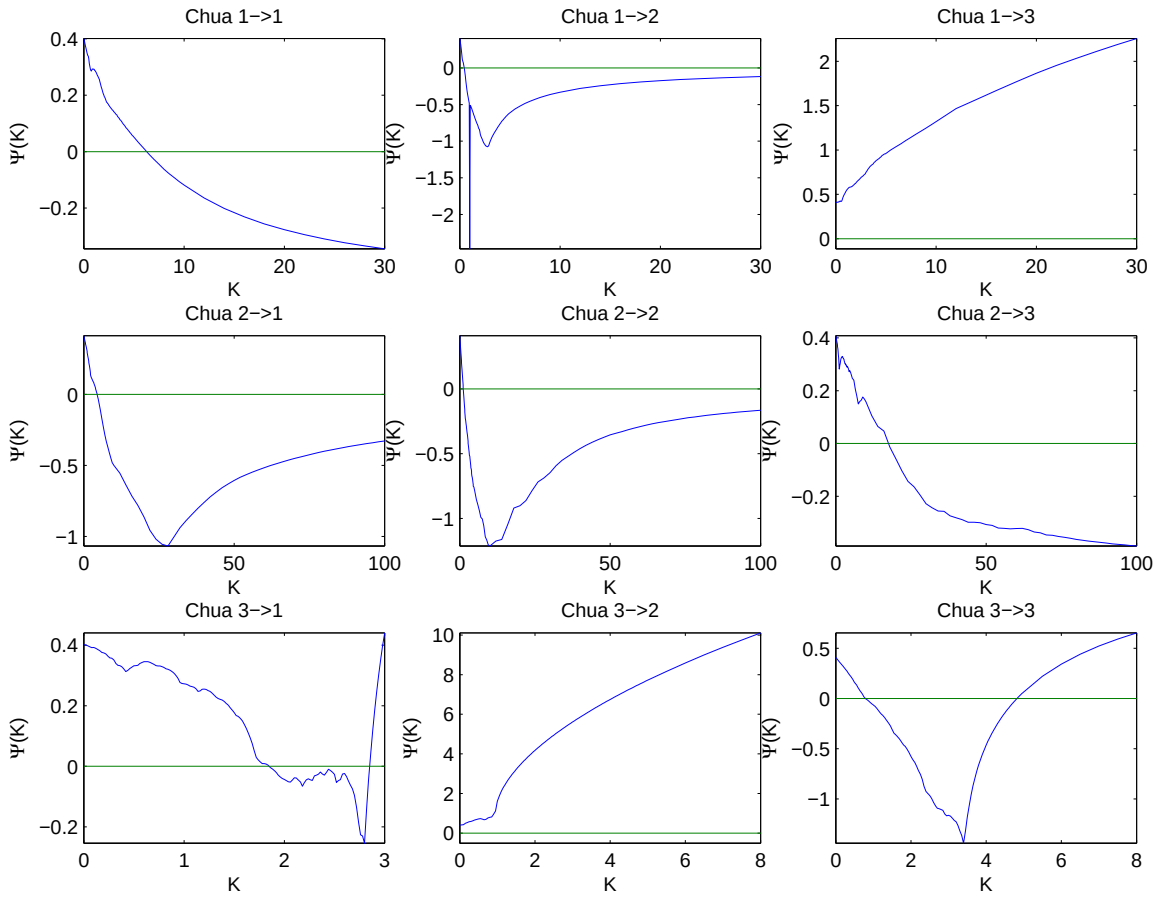

Fig. 40. MSFs for Chua system (A.7) with various coupling schemes.

Chua system [146]:

$$\begin{cases} \dot{x} = \alpha(y - x + f(x)) \\ \dot{y} = x - y + z \\ \dot{z} = -\beta y - \gamma z \end{cases} \tag{A.7}$$

where $\alpha = 10$, $\beta = 14.87$, $\gamma = 0$, and

$$f(x) = \begin{cases} -bx - a + b, & x > 1 \\ -ax, & |x| < 1 \\ -bx + a - b, & x < -1, \end{cases} \tag{A.8}$$

where $a = -1.27$, $b = -0.68$. The Jacobian matrix is

$$\mathbf{DF} = \begin{pmatrix} -\alpha - \alpha \times \begin{cases} b, & |x| > 1 \\ a, & |x| < 1 \end{cases} & \alpha & 0 \\ 1 & -1 & 1 \\ 0 & -\beta & -\gamma \end{pmatrix}. \tag{A.9}$$

The Lyapunov exponents for this system are $\lambda_1 \simeq 0.409$, $\lambda_2 \simeq 0$, and $\lambda_3 \simeq -3.859$. The MSFs are presented in Fig. 40.

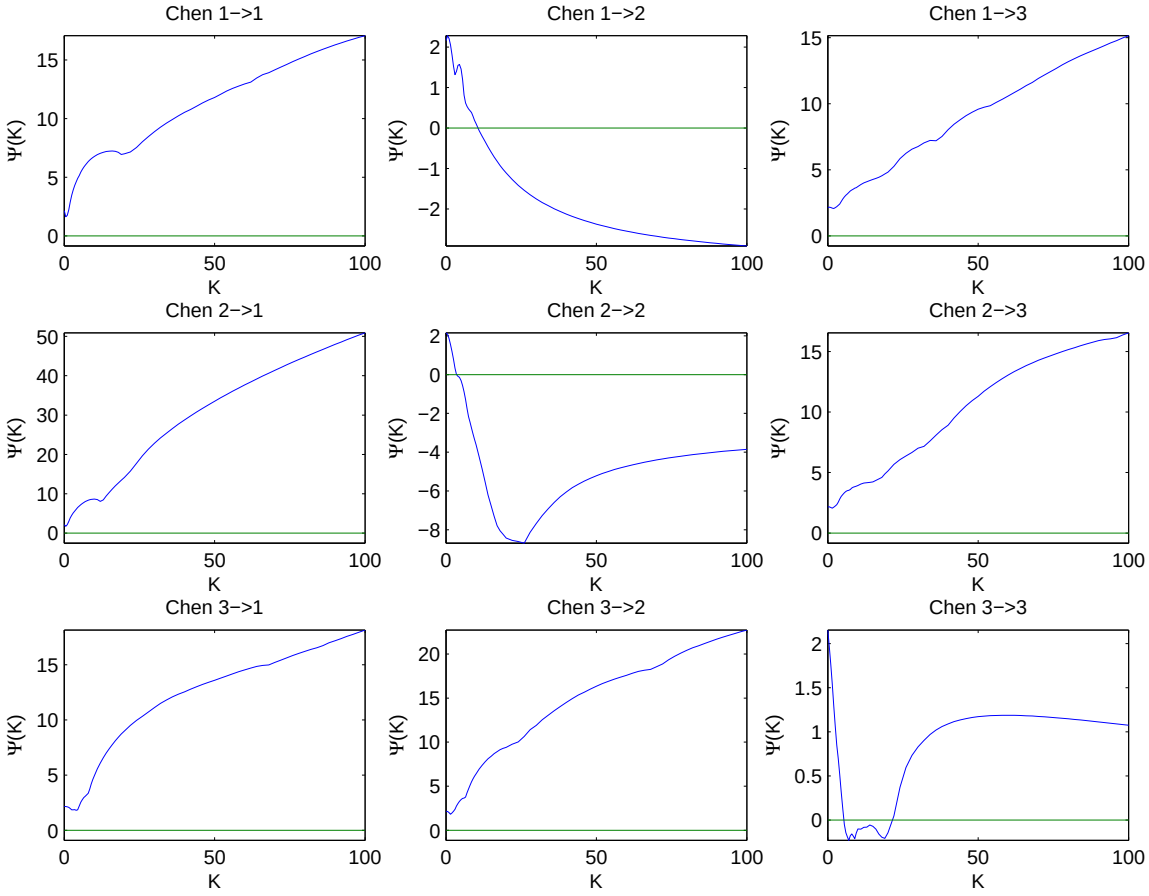

Fig. 41. MSFs for Chen system (A.10).

Chen system [147]:

$$\begin{cases} \dot{x} = a(y - x) \\ \dot{y} = (c - a - z)x + cy \\ \dot{z} = xy - \beta z \end{cases} \tag{A.10}$$

where $a = 35$, $c = 28$, $b = 8/3$. The Jacobian matrix is

$$\mathbf{DF} = \begin{pmatrix} -a & a & 0 \\ c - a - z & c & -x \\ y & x & -\beta \end{pmatrix}. \tag{A.11}$$

The calculated Lyapunov exponents for the this system are $\lambda_1 \simeq 2.154$, $\lambda_2 \simeq 0$, and $\lambda_3 \simeq -11.820$. The sum of the Lyapunov exponents should be equal $\text{Tr}(\mathbf{DF}) = -a + c - b \simeq -9.667$, which is approximately satisfied by the numerical results whose summation is -9.666. Note that for our calculation, Eq. (A.1) is integrated together with Eq. (1.11) using RK4 method. If Eq. (A.1) integrated using Eular method together with Eq. (1.11) integrated using RK4 method, the calculated Lyapunov exponents are $\lambda_1 \simeq 2.17$, $\lambda_2 \simeq 0.25$, and $\lambda_3 \simeq -11.96$. One can see there are systematic deviations. The results of MSFs of this system are shown in Fig. 41.

HR neuron [141]:

$$\begin{cases} \dot{x} = y + 3x^2 - x^3 - z + I \\ \dot{y} = 1 - 5x^2 - y \\ \dot{z} = -rz + rs(x + 1.6) \end{cases} \tag{A.12}$$

where $I = 3.2$ is the external current input, $r = 0.006$, $s = 4$. The Jacobian matrix is

$$\mathbf{DF} = \begin{pmatrix} 6x - 3x^2 & 1 & -1 \\ -10x & -1 & 0 \\ rs & 0 & -r \end{pmatrix}. \tag{A.13}$$

The Lyapunov exponents for the this system are $\lambda_1 \simeq 0.013$, $\lambda_2 \simeq 0$, and $\lambda_3 \simeq -8.610$. The MSFs of the above system are shown in Fig. 42.

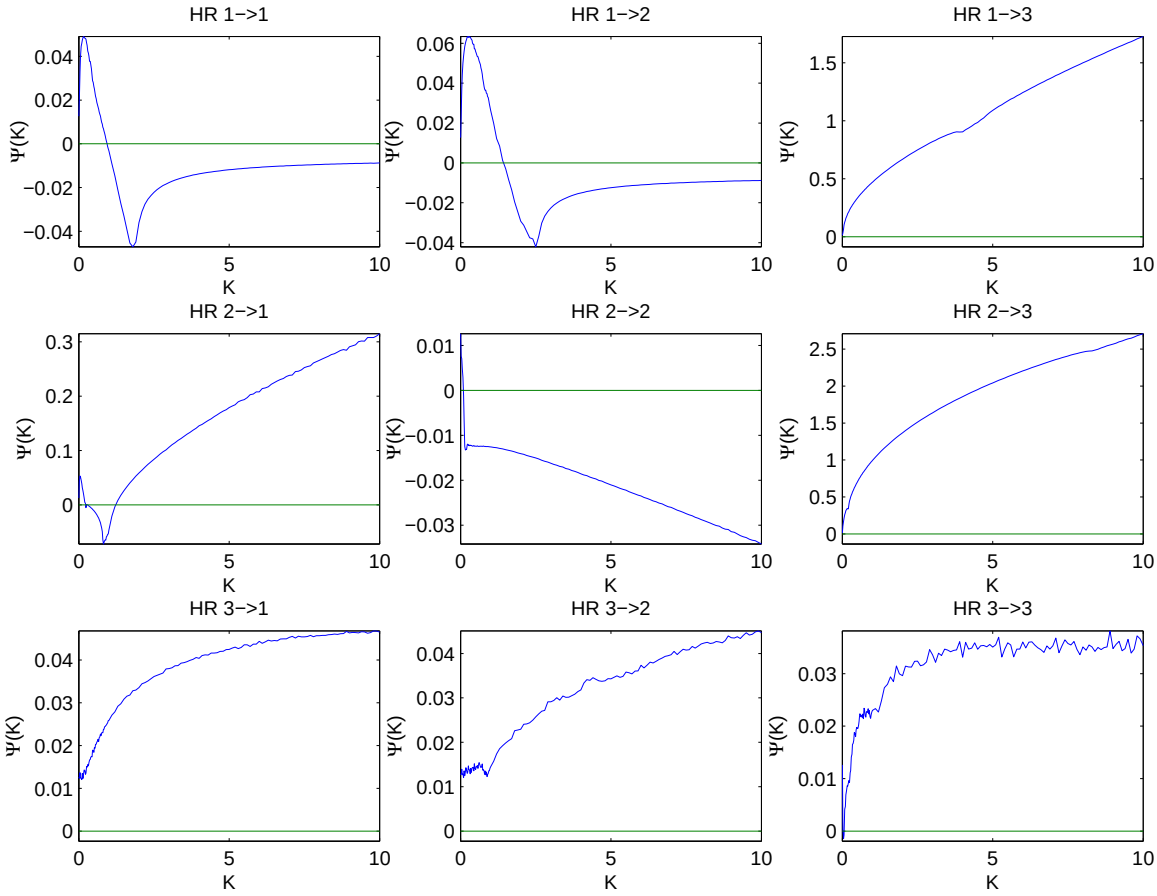

Fig. 42. MSFs for HR neuron (A.12).

Duffing system [148]:

$$\ddot{x} + h\dot{x} + x^3 = q\sin(\eta t), \tag{A.14}$$

or

$$\begin{cases} \dot{x} = y \\ \dot{y} = -hy - x^3 + q\sin(\eta t), \end{cases} \tag{A.15}$$

where $\eta = 1$, $h = 0.1$, $q = 5.6$. The Jacobian matrix is

$$\mathbf{DF} = \begin{pmatrix} 0 & 1 \\ -3x^2 & -h \end{pmatrix}. \tag{A.16}$$

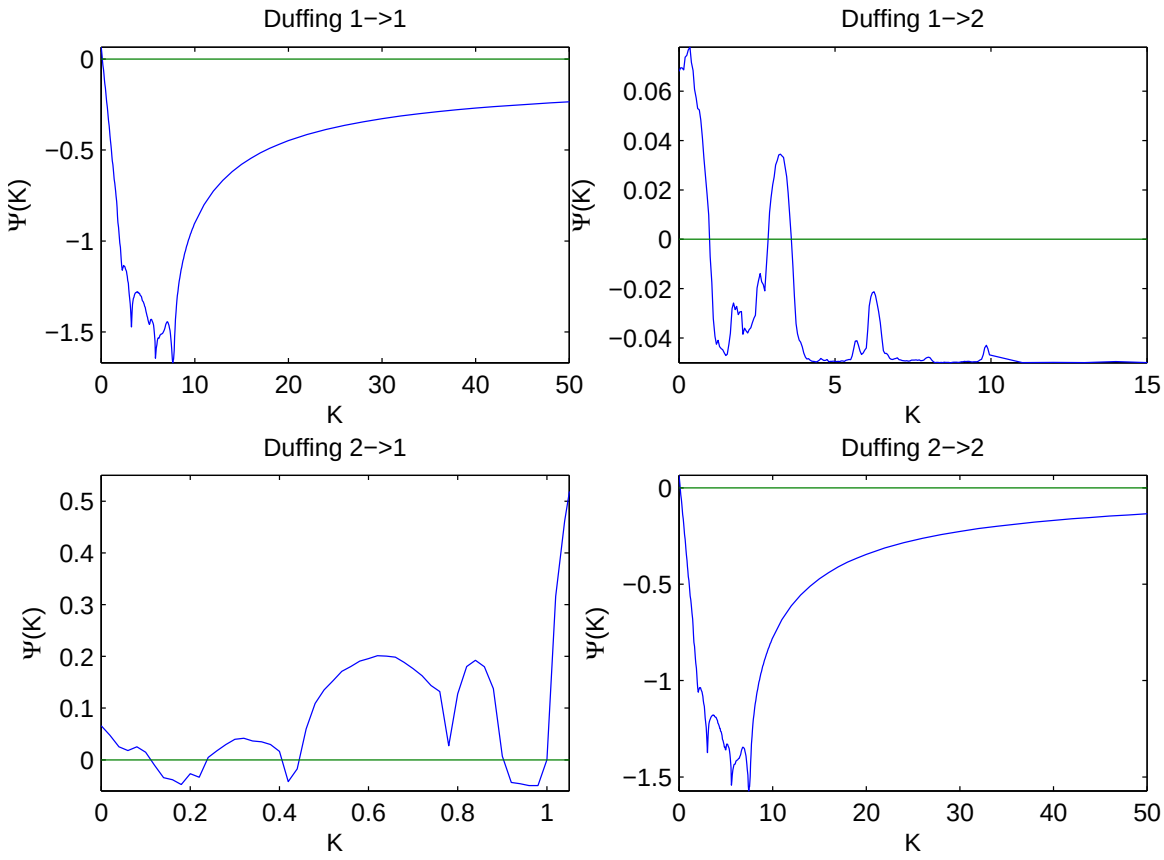

Fig. 43. MSFs for Duffing system (A.15) with various coupling schemes.

The Lyapunov exponents for the this system are $\lambda_1 \simeq 0.066$, and $\lambda_2 \simeq -0.166$. The sum of the exponents should be equal to $\mathrm{Tr}(\mathbf{DF}) = -h = 0.1$. This is approximately satisfied by the calculated Lyapunov exponents. The MSFs for this system are plotted in Fig. 43.

Van der Pol system [149]:

$$\ddot{x} - d(1 - x^2)\dot{x} + x = F\sin(\Omega t), \tag{A.17}$$

or

$$\begin{cases} \dot{x} = y \\ \dot{y} = -x + d(1 - x^2)y + F\sin(\Omega t), \end{cases} \tag{A.18}$$

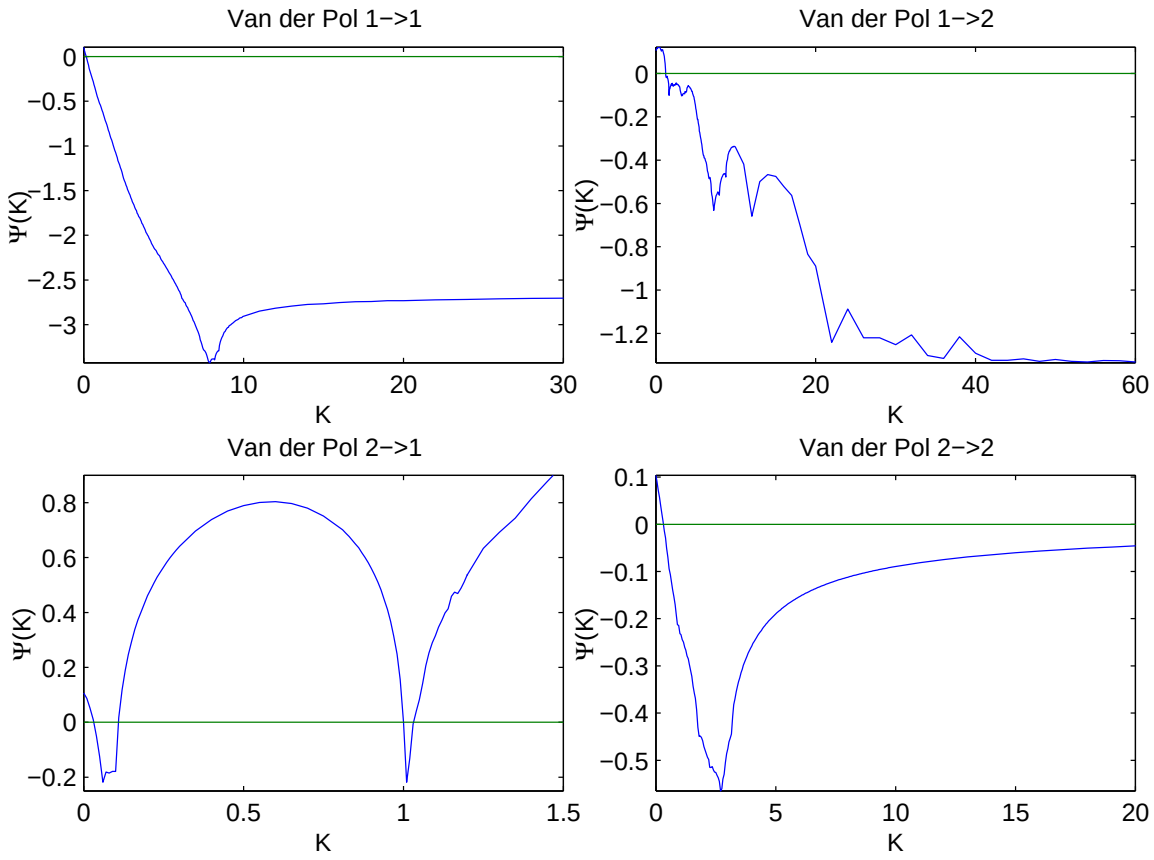

Fig. 44. MSF function for Van der Pol system (A.18) with various coupling schemes.

where we use $d = 3$, $F = 15$, $\Omega = 4.065$. The Jacobian matrix is

$$\mathbf{DF} = \begin{pmatrix} 0 & 1 \\ -1 - 2dxy & d(1 - x^2) \end{pmatrix}. \tag{A.19}$$

The Lyapunov exponents for the this system are $\lambda_1 \simeq 0.106$, and $\lambda_2 \simeq -2.774$. The MSFs are presented in Fig. 44.

Based on the above observation of MSFs, we classify the behavior of coupled dynamical systems into four categories based on the cross points of $\Psi(K)$ with the K-axis. Since we focus on chaotic oscillators, when $K = 0$, the master stability function $\Psi(0)$ is just the largest Lyapunov exponent of Eq. (1.11), which is positive, and it is the same for all $d \times d$ different coupling schemes. Class I: $\Psi(K)$ has two cross points, K_a,

K_b, with the K-axis; Class II: $\Psi(K)$ has only one cross point K_a with the K-axis; Class III: $\Psi(K)$ has three or more cross points with the K-axis; and Class IV: $\Psi(K)$ has no cross points with the K-axis. For Class I, $\Psi(K)$ becomes negative at, say, K_a, and as K is increased, $\Psi(K)$ becomes positive again at K_b, and remain positive thereafter. In this case, $\Psi(K)$ is negative in a finite interval (K_a, K_b). For Class II, after crossing the K-axis at K_a, $\Psi(K)$ remains negative for all $K > K_a$. That is, $\Psi(K)$ is negative in (K_a, ∞), or $K_b \to \infty$ in Class I. Class III is where $\Psi(K)$ is negative in several distinct stable regions, say (K_{a1}, K_{b1}), (K_{a2}, K_{b2}), ... , (K_{af}, K_{bf}), for which $\Psi(K)$ is negative, where $K_{a1} < K_{b1} < K_{a2} < K_{b2} < ... < K_{af} < K_{bf}$, and K_{bf} can be either finite or infinite. When a single finite interval (K_{ai}, K_{bi}) is of concern, the coupled dynamics is equivalent to a Class I dynamic [it is possible that K_i's ($\varepsilon\lambda_i$) reside in different stable intervals where the system can still be synchronized, this has been of particular interest for some authors [148]]. When K_{bf} is infinite and it is large K values are pertinent, then the system is equivalent to a class-II dynamic. For Class IV, since $\Psi(K)$ is always positive, the corresponding coupled system do not allow synchronization states.

The classification is summarized in Table 1. The most astonishing finding is that, regardless of the differences in the details of the oscillator dynamics, there always exists a coupling configuration for which the MSF is negative in a finite parameter interval.

TABLE 1

Classification based on master stability functions

	Rössler	Lorenz	Chua	Chen	HR	Duffing	Van der Pol
Class I	11	21	31,33	33	21		
Class II	22,31	11,12,22	11,12,21,22,23	12,22	11,12,22	11,22	11,12,22
Class III		33				12,21	21

APPENDIX B

ACHIEVEMENTS DURING PHD STUDIES

For integrity and clarity, the dissertation mainly consists of my works investigating properties of complex clustered networks. The relevant publications are:

1. L. Huang, K. Park, and Y.-C. Lai, "Information propagation on modular networks," Phys. Rev. E **73**, 035103(R) (2006). This paper has been selected for the April 1, 2006 issue of Virtual Journal of Biological Physics Research. (Chapter 2)

2. L. Huang, K. Park, Y.-C. Lai, L. Yang, and K. Yang, "Abnormal synchronization in complex clustered networks," Phys. Rev. Lett. **97**, 164101 (2006). (Chapter 3)

3. L. Huang, Y.-C. Lai, and R. A. Gatenby, "Optimization of synchronization in complex clustered networks," Chaos **18**, 013101 (2008). This paper has been selected for the January 15, 2008 issue of Virtual Journal of Biological Physics Research. (Chapter 4)

4. L. Huang, Y.-C. Lai, K. Park, X. Wang, C. H. Lai and R. A. Gatenby, "Synchronization in complex clustered networks," Frontiers of Physics in China, Volume **2**, Number 4 / October, pp. 446-459 (2007). (Chapters 3 and 4)

5. L. Huang, Y.-C. Lai, and R. A. Gatenby, "Alternating synchronizability of complex clustered networks with regular local structure," Phys. Rev. E **77**, 016103 (2008). This paper has been selected for the January 15, 2008 issue of Virtual Journal of Biological Physics Research. (Chapter 5)

6. X. Wang, L. Huang, Y.-C. Lai, and C. H. Lai, "Optimization of synchronization in gradient clustered networks," Phys. Rev. E **76**, 056113 (2007). This paper has been selected for the December 1, 2007 issue of Virtual Journal of Biological Physics Research. (Chapter 6)

7. L. Huang, Y.-C. Lai, and G.-R. Chen, "Understanding and preventing cascading breakdown in complex clustered networks," Phys. Rev. E, **78**, 036116 (2008). (Chapter 7)

8. L. Huang, Y.-C. Lai, and R. A. Gatenby, "Dynamics-based scalability of complex networks," Phys. Rev. E **78**, 045102(R) (2008). (Chapter 8)

9. X. Ma, L. Huang, Y.-C. Lai, Y. Wang, and Z. Zheng, "Synchronization-based scalability in complex clustered networks," Chaos, accepted. (Chapter 9)

10. L. Huang, Q. Chen, Y.-C. Lai, and L. M. Pecora, "Master stability functions for typical coupled chaotic oscillators," in preparation. (Appendix A)

The other works that I have involved in are listed as follows for completeness.

Works on general complex networks:

11. X.-G. Wang, L. Huang, S.-G. Guan, Y.-C. Lai, and C. H. Lai, "Onset of synchronization in complex gradient networks," Chaos, **18**, 037117 (2008).

12. R. Yang, L. Huang, and Y.-C. Lai, " Selectivity-based spreading dynamics on complex networks," Phys. Rev. E **78**, 026111 (2008).

13. L. Huang, Y.-C. Lai, K. Park, J. Zhang and Z. Hu, "Critical behavior of blind spots in sensor networks," Chaos **17**, 023132 (2007).

14. K. Park, L. Huang, and Y.-C. Lai, "Desynchronization waves in complex networks," Phys. Rev. E **75**, 026211 (2007).

15. L. Huang, Y.-C. Lai, K. Park, and J. Zhang, "Percolation and blind spots in complex networks," Phys. Rev. E **73**, 066131 (2006).

16. W.-X. Wang, L. Huang, and Y.-C. Lai, "Universal dynamics on complex networks," submitted to Phys. Rev. Lett.

17. L. Huang, Y.-C. Lai, and M. A. F. Harrison, "Probing complex networks from measured time series," submitted to Phys. Rev. Lett.

18. X. Ma, L. Huang, Y.-C. Lai, and Z. Zheng,"Emergence of loop structure in scale-free networks and dynamical consequences," submitted to Phys. Rev. E

19. R. Yang, L. Huang, and Y.-C. Lai, "Transient disorder in dynamically evolving networks," submitted to Phys. Rev. E

Dynamics and electron transport in graphene quantum dots:

20. L. Huang, Y.-C. Lai, D. K. Ferry, R. Akis, and S. M. Goodnick, "Transmission and scarring in graphene quantum dots," submitted to J. of Physics: Condensed Matter

21. L. Huang, Y.-C. Lai, D. K. Ferry, R. Akis, and S. M. Goodnick, "Quantum scars of graphene quantum dots," in preparation.

Nonlinear dynamics in MEMS devices:

22. Q. Chen, L. Huang, and Y.-C. Lai, "Chaos-induced intrinsic localized modes in coupled microcantilever arrays," Applied Physics Letters **92**, 241914 (2008). This paper has been selected for the June 30, 2008 issue of Virtual Journal of Nanoscale Science and Technology.

23. Q. Chen, L. Huang, and Y.-C. Lai, " Controlling bistability in microelectromechanical resonators," Chaos **18**, 013103 (2008). This paper has been selected for the January 28, 2008 issue of Virtual Journal of Nanoscale Science and Technology.

Bayesian estimation with applications to GPS

24. L. Huang and Y.-C. Lai, "Sequential Monte Carlo scheme for Bayesian estimation in the presence of data outliers," Phys. Rev. E **75**, 056705 (2007). This paper has been selected for the June 1, 2007 issue of Virtual Journal of Biological Physics Research.

Random matrix theory in synchrony characterization

25. Y.-C. Lai, M. G. Frei, I. Osorio, and L. Huang, "Characterization of Synchrony with Applications to Epileptic Brain Signals," Phys. Rev. Lett. **98**, 108102 (2007). This work was selected by the Virtual Journal of Biological Physics Research for the March 15, 2007 issue.

REFERENCES

[1] D. J. Watts, P. S. Dodds, and M. E. J. Newman, Science **296**, 1302 (2002).

[2] E. Ravasz, A. L. Somera, D. A. Mongru, Z. Oltvai, and A.-L. Barabási, Science **297**, 1551 (2002).

[3] V. Spirin and L. A. Mirny, Proc. Natl. Acad. Sci. USA **100**, 12123 (2003).

[4] A. E. Motter, T. Nishikawa, and Y.-C. Lai, Phys. Rev. E **68**, 036105 (2003).

[5] G. Palla, I. Derényi, I. Farkas, and T. Vicsek, Nature **435**, 814 (2005).

[6] E. Oh, K. Rho, H. Hong, and B. Kahng, Phys. Rev. E **72**, 047101 (2005).

[7] T. Ideker, Advances in Experimental Medicine and Biology **547**, 21 (2004).

[8] Y. Xia, H. Yu, R. Jansen, M. Seringhaus, S. Baxter, D. Greenbaum, H. Zhao, and M. Gerstein, Annual Review of Biochemistry **73**, 1051 (2004).

[9] M. Lappe, and L. Holm, Nature Biotechnology **22**, 98 (2004).

[10] B. P. Kelley, R. Sharan, R. M. Karp, T. Sittler, D. E. Root, B. R. Stockwell, and T. Ideker, Proc. Natl. Acad. Sci. USA **100**, 11394 (2003).

[11] A.-L. Barabási and Z. N. Oltvai, Nature Reviews—Genetics **5**, 101 (2004).

[12] R. Albert and A.-L. Barabási, Rev. Mod. Phys. **74**, 47 (2002).

[13] M. E. J. Newman, SIAM Rev. **45**, 167 (2003).

[14] S. N. Dorogovtsev and J. F. F. Mendes, *Evolution of Networks* (Oxford University Press, Oxford, 2003).

[15] R. Pastor-Satorras and A. Vespignani, *Evolution and Structure of the Internet* (Cambridge University Press, Cambridge, 2004).

[16] Y. Ho, A. Gruhler, A. Heilbut, G. D. Bader, L. Moore, *et al.*, Nature **415**, 180 (2002).

[17] E. Yeger-Lotem, S. Sattath, N. Kashtan, S. Itzkovitz, R. Milo, R. Y. Pinter, U. Alon, and H. Margalit, Proc. Nat. Acad. Sci. **101**, 5934 (2004).

[18] S.-H. Yook, Z. N. Oltvai, and A. L. Barabási, Proteomics **4**, 928 (2004).

[19] B. Grunenfelder and E. A. Winzeler, Nat. Rev. Genet. **3**, 653 (2002).

[20] S. Li *et al.*, Science **303**, 540 (2004).

[21] J.-D. J. Han *et al.*, Nature **430**, 88 (2004).

[22] R. A. Gatenby and B. R. Frieden, Cancer Research **62**, 3675 (2002); R. A. Gatenby and T. L. Vincent, *ibid* **63**, 6212 (2003); R. A. Gatenby and R. J. Gillies, Nature Rev. Cancer **4**, 891 (2004); R. A. Gatenby and B. R. Frieden, Bull. Math. Biol. **69**, 635 (2006).

[23] For example, a human liver typically contains 10^{12} cells and has the length scale of about 15 cm, which is equivalent to about 10^5 cell diameters.

[24] M. Lamboley, P. Pittet, M. Koenigsberger, R. Sauser, J. L. Beny, J. J. Meister. Cell Calcium. **37**, 311 (2005).

[25] Z. Toroczkai and K.E. Bassler, Nature **428**, 716 (2004).

[26] K. Park, Y.-C. Lai, L. Zhao, and N. Ye, Phys. Rev. E **71**, 065105 (2005).

[27] A. Sudbury, J. Appl. Prob. **22**, 443 (1985).

[28] R. Pastor-Satorras and A. Vespignani, Phys. Rev. Lett. **86**, 3200 (2001); Phys. Rev. E **63**, 066117 (2001); *ibid* **65**, 035108(R) (2002).

[29] A. L. Lloyd and R. M. May, Science **292**, 1316 (2001); R. M. May and A. L. Lloyd, Phys. Rev. E **64**, 066112 (2001).

[30] D. H. Zanette, Phys. Rev. E **64**, 050901(R) (2001); *ibid* **65**, 041908 (2002).

[31] M. Kuperman and G. Abramson, Phys. Rev. Lett. **86**, 2909 (2001).

[32] R. Pastor-Satorras and A. Vespignani, Phys. Rev. E **65**, 036104 (2002).

[33] Z. Dezsö and A. -L. Barabási, Phys. Rev. E **65**, 055103(R) (2002).

[34] Y. Moreno, R. Pastor-Satorras, and A. Vespignani, Eur. Phys. J. B **26**, 521 (2002).

[35] M. E. J. Newman, I. Jensen, R. M. Ziff, Phys. Rev. E **65**, 021904 (2002).

[36] V. M. Eguíluz and K. Klemm, Phys. Rev. Lett. **89**, 108701 (2002).

[37] R. Cohen, S. Havlin, and D. ben-Avraham, Phys. Rev. Lett. **91**, 247901 (2003).

[38] Z.-H. Liu, Y.-C. Lai and N. Ye, Phys. Rev. E **67**, 031911 (2003).

[39] J. Balthrop, S. Forrest, M. E. J. Newman, and M. M. Williamson, Science **304**, 527 (2004).

[40] M. Barthélemy, A. Barrat, R. Pastor-Satorras, and A. Vespignani, Phys. Rev. Lett. **92**, 178701 (2004).

[41] R. Pastor-Satorras, A. Vespignani, *Evolution and Structure of the Internet: A Statistical Physics Approach*, (Cambridge University Press, 2004)

[42] D. J. Watts and S. H. Strogatz, Nature **393**, 440 (1998).

[43] A.-L. Barabási and R. Albert, Science **286**, 509 (1999); A.-L. Barabási, R. Albert, and H. Jeong, Physica A **272**, 173 (1999).

[44] R. M. May and R. M. Anderson, Philos. Trans. R. Soc. London Ser. B **321**, 565 (1988).

[45] R. M. Anderson and R. M. May, *Infectious diseases of humans* (Oxford University Press, Oxford, 1992).

[46] L. Huang, K. Park, and Y.-C. Lai, Phys. Rev. E **73**, 035103(R) (2006).

[47] L. F. Lago-Fernandez, R. Huerta, F. Corbacho, and J. A. Siguenza, Phys. Rev. Lett. **84**, 2758 (2000).

[48] P. M. Gade and C.-K. Hu, Phys. Rev. E **62**, 6409 (2000).

[49] M. Barahona and L. M. Pecora, Phys. Rev. Lett. **89**, 054101 (2002).

[50] X. F. Wang and G. Chen, Int. J. of Bifur. Chaos **12**, 187 (2002).

[51] X. F. Wang and G. Chen, IEEE Trans. on Circ. Sys., Part I **49**, 54 (2002).

[52] H. Hong, M. Y. Choi, and B. J. Kim, Phys. Rev. E **65**, 026139 (2002).

[53] S. Jalan and R. E. Amritkar, Phys. Rev. Lett. **90**, 014101 (2003).

[54] T. Nishikawa, A. E. Motter, Y.-C. Lai, and F. C. Hoppensteadt, Phys. Rev. Lett. **91**, 014101 (2003).

[55] A. E. Motter, C. Zhou, and J. Kurths, Europhys. Lett. **69**, 334 (2005).

[56] A. E. Motter, C. Zhou, and J. Kurths, Phys. Rev. E **71**, 016116 (2005).

[57] C. Zhou, A. E. Motter, and J. Kurths, Phys. Rev. Lett. **96**, 034101 (2006).

[58] M. Chavez, D.-U. Hwang, A. Amann, H. G. E. Hentschel, and S. Boccaletti, Phys. Rev. Lett. **94**, 218701 (2005).

[59] F. M. Atay, T. Bıyıkoğlu, and J. Jost, IEEE Trans. on Circ. Sys., Part I **53**, 92 (2006).

[60] L. M. Pecora and T. L. Carroll, Phys. Rev. Lett. **80**, 2109 (1998).

[61] L. Huang, K. Park, Y.-C. Lai, L. Yang, and K. Yang, Phys. Rev. Lett. **97**, 164101 (2006).

[62] L. Huang, Y.-C. Lai, and R. A. Gatenby, Chaos **18**, 013101 (2008).

[63] L. Huang, Y.-C. Lai, and R. A. Gatenby, Phys. Rev. E **77**, 016103 (2008).

[64] X. Wang, L. Huang, Y.-C. Lai, and C. H. Lai, Phys. Rev. E **76**, 056113 (2007).

[65] P. Holme, Phys. Rev. E **66**, 036119 (2002).

[66] A. E. Motter and Y.-C. Lai, Phys. Rev. E **66**, 065102(R) (2002).

[67] Y. Moreno, J. B. Gómez, and A. F. Pacheco, Europhys. Lett. **58**, 630 (2002).

[68] X.-F. Wang and G.-R. Chen, IEEE Cir. Syst. Magazine **3**, 6 (2003); K-.I. Goh, D.-S. Lee, B. Kahng, and D. Kim, Phys. Rev. Lett. **91**, 148701 (2003); P. Crucitti, V. Latora, and M. Marchiori, Phys. Rev. E **69**, 045104(R) (2004).

[69] L. Zhao, K. Park, and Y.-C. Lai, Phys. Rev. E **70**, 035101(R) (2004).

[70] A. E. Motter, Phys. Rev. Lett. **93**, 098701 (2004).

[71] E. J. Lee, K.-I. Goh, B. Kahng, and D. Kim, Phys. Rev. E **71**, 056108 (2005); L. Zhao, K. Park, and Y.-C. Lai, and N. Ye, Phys. Rev. E **72**, 025104(R) (2005); D.-H. Kim, B. J. Kim, and H. Jeong, Phys. Rev. Lett. **94**, 025501 (2005); J. Xu and X.-F. Wang, Physica A **349**, 685 (2005); L. Huang, L. Yang, and K.-Q. Yang, Phys. Rev. E **73**, 036102 (2006); I. Simonsen, L. Buzna, K. Peters, S. Bornholdt, and D. Helbing, Phys. Rev. Lett. **100**, 218701 (2008).

[72] R. Albert, I. Albert, and G. L. Nakarado, Phys. Rev. E **69**, 025103(R) (2004); R. Kinney, P. Crucitti, R. Albert, and V. Latora, Euro. Phys. J. B - Cond. Mat. & Comp. Syst. **46**, 101 (2005).

[73] S. Strogatz, *Sync: The Emerging Science of Spontaneous Order* (New York, Hyperion, 2003).

[74] J. Jost and M. P. Joy, Phys. Rev. E **65**, 016201 (2001).

[75] B. Bollobas, *Random Graphs*, (Cambridge University Press, 2001).

[76] B Bollobas, O. Riordan, Combinatorica **24**, 5 (2004).

[77] W. W. Zachary, J. Anthropol. Res. **33**, 452 (1977).

[78] L. F. Lago-Fernandez, R. Huerta, F. Corbacho, and J. A. Siguenza, Phys. Rev. Lett. **84**, 2758 (2000); P.M. Gade and C.-K. Hu, Phys. Rev. E **62**, 6409 (2000); M. Barahona and L. M. Pecora, Phys. Rev. Lett. **89**, 054101 (2002); X. F. Wang and G. Chen, Int. J. Bifurcation Chaos Appl. Sci. Eng. **12**, 187 (2002), IEEE Trans. Circuits Syst. **49**, 54 (2002); H. Hong, M.Y. Choi, and B. J. Kim, Phys. Rev. E **65**, 026139 (2002); S. Jalan and R. E. Amritkar, Phys. Rev. Lett. **90**, 014101 (2003).

[79] A. E. Motter, C. Zhou, and J. Kurths, Europhys. Lett. **69**, 334 (2005) and Phys. Rev. E **71**, 016116 (2005); M. Chavez, D.-U. Hwang, A. Amann, H. G. E. Hentschel, and S. Boccaletti, Phys. Rev. Lett. **94**, 218701 (2005); C. Zhou, A. E. Motter, and J. Kurths, Phys. Rev. Lett. **96**, 034101 (2006).

[80] D. J. Watts, P. S. Dodds, and M. E. J. Newman, Science **296**, 1302 (2002); A. E. Motter, T. Nishikawa, and Y.-C. Lai, Phys. Rev. E **68**, 036105 (2003); E. Oh, K. Rho, H. Hong, and B. Kahng, Phys. Rev. E **72**, 047101 (2005).

[81] V. Spirin and L. A. Mirny, Proc. Natl. Acad. Sci. USA **100**, 12123 (2003); G. Palla, I. Derényi, I. Farkas, and T. Vicsek, Nature **435**, 814 (2005).

[82] R. Milo, S. Shen-Orr, S. Itzkovitz, N. Kashtan, D. Chklovskii, and U. Alon, Science **298**, 824 (2002); A. Vázquez, R. Pastor-Satorras, and A. Vespignani, Phys. Rev. E **65**, 066130 (2002); K. A. Eriksen, I. Simonsen, S. Maslov, and K. Sneppen, Phys. Rev. Lett. **90**, 148701 (2003).

[83] Our result does not depend on the details of the synchronized states. Consider two clustered networks where (A) the two types of links are approximately matched and (B) there is a substantial mismatch. Our theory would predict that network A is more synchronizable than network B. This statement is meaningful in a probabilistic sense, as whether or not a specific system may achieve synchronization is also determined by many other factors such as the choice of the initial condition, possible existence of multiple synchronized states, and noise, etc. Our result means that, under the influence of these random factors, there is a higher probability for network A to be synchronized than network B.

[84] A recent work [59] showed that statistical properties of a complex network are not sufficient to determine its synchronizability. In particular, it has been proved rigorously that degree distribution of a network does not suffice to characterize its synchronizability. Our result indicates that non-statistical properties of a network can have a significant effect on its ability to synchronize. This is consistent with the result in [59].

[85] K. Park, Y.-C. Lai, S. Gupte, and J.-W. Kim, Chaos **6**, 015105 (2006).

[86] J. B. Buck and E. Buck, Science **159**, 1319 (1968).

[87] C. Peskin, in *Physiology. Courant Inst. of Math. Sci. Publication* (New York, 1975).

[88] A. Sherman and J. Rinzel, Biophys. J. **59**, 547 (1991).

[89] J. Dye, J. Comp. Physiol. A **168**, 521 (1991).

[90] J. G. Restrepo, E. Ott, and B. R. Hunt, Phys. Rev. Lett. **93**, 114101 (2004).

[91] J. G. Restrepo, E. Ott, and B. R. Hunt, Phys. Rev. E **69**, 66215 (2004).

[92] B. Gong, L. Yang, and K. Yang, Phys. Rev. E **72**, 037101 (2005).

[93] E. P, Wigner, Ann. Math. **62**, 548 (1955).

[94] E. P, Wigner, Ann. Math. **65**, 203 (1957).

[95] M. L. Mehta, *Random Matrices, 2nd ed.* (Academic, New York, 1991).

[96] I. J. Farkas, I. Derényi, A.-L.Barabási, and T. Vicsek, Phys. Rev. E **64**, 026704 (2001).

[97] R. Milo, S. Shen-Orr, S. Itzkovitz, N. Kashtan, D. Chklovskii, and U. Alon, Science **298**, 824 (2002).

[98] A. Vázquez, R. Pastor-Satorras, and A. Vespignani, Phys. Rev. E **65**, 066130 (2002).

[99] K. A. Eriksen, I. Simonsen, S. Maslov, and K. Sneppen, Phys. Rev. Lett. **90**, 148701 (2003).

[100] L. F. Lago-Fernandez, R. Huerta, F. Corbacho, and J. A. Siguenza, Phys. Rev. Lett. **84**, 2758 (2000); M. Barahona and L. M. Pecora, Phys. Rev. Lett. **89**, 054101 (2002); X. F. Wang and G. Chen, Int. J. Bifurcation Chaos Appl. Sci. Eng. **12**, 187 (2002); S. Jalan and R. E. Amritkar, Phys. Rev. Lett. **90**, 014101 (2003).

[101] M. Chavez, D.-U. Hwang, A. Amann, H. G. E. Hentschel, and S. Boccaletti, Phys. Rev. Lett. **94**, 218701 (2005); C. Zhou, A. E. Motter, and J. Kurths, Phys. Rev. Lett. **96**, 034101 (2006); X.-G. Wang, Y.-C. Lai, and C. H. Lai, Phys. Rev. E **75**, 056205 (2007).

[102] M. Zhao, T. Zhou, B.-H. Wang, and W.-X. Wang, Phys. Rev. E **72**, 057102 (2005); L. Donetti, P. I. Hurtado, and M. A. Muñoz, Phys. Rev. Lett. **95**, 188701 (2005); S. Boccaletti, D.-U. Hwang, M. Chavez, A. Amann, J. Kurths, and L. M. Pecora, Phys. Rev. E **74**, 016102 (2006); J. G. Restrepo, E. Ott, and B. R. Hunt, Phys. Rev. Lett. **97**, 094102 (2006).

[103] P. Erdös and A. Rényi, Publ. Math. Inst. Hung. Acad. Sci. **5**, 17 (1960); B. Bollobaás, *Random Graphs* (Academic, London, 1985).

[104] D. J. Watts, P. S. Dodds, and M. E. J. Newman, Science **296**, 1302 (2002); R. Milo, S. Shen-Orr, S. Itzkovitz, N. Kashtan, D. Chklovskii, and U. Alon, Science **298**, 824 (2002); K. A. Eriksen, I. Simonsen, S. Maslov, and K. Sneppen, Phys. Rev. Lett. **90**, 148701 (2003); A. E. Motter, T. Nishikawa, and Y.-C. Lai, Phys. Rev. E **68**, 036105 (2003); E. Oh, K. Rho, H. Hong, and B. Kahng, Phys. Rev. E **72**, 047101 (2005).

[105] Let $\mathbf{b} = [1\ 1 \cdots]^T$, $(\mathbf{b}^T\mathbf{G}^T)_i = \sum_{j=1}^N G_{ij} = 0$, thus $\mathbf{b}^T\mathbf{G}^T = [0\ 0 \cdots]$. Therefore $\mathbf{b}^T\mathbf{G}^T\mathbf{e}_i = \lambda_i \sum_j^N e_{i,j} = 0$. If $\lambda_i \neq 0$, then $\sum_j^N e_{i,j} = 0$ (λ_i and $e_{i,j}$ could be complex).

[106] D. S. Friend and N. B. Gilula, J. Cell Biol. **53**, 758 (1972).

[107] N. DePaola, P. F. Davies, W. F. Pritchard, L. Florez, N. Harbeck, and D. C. Polacek, Proc. Natl. Acad. Sci. USA **96**, 3154 (1999).

[108] F. Lu, J. Gao, R. Ogawa, and H. Hyakusoku, Plast. & Reconstr. Surg. **119**, 844 (2007).

[109] B. P. Kelley, R. Sharan, R. M. Karp, T. Sittler, D. E. Root, B. R. Stockwell, and T. Ideker, Proc. Natl. Acad. Sci. USA **100**, 11394 (2003); T. Ideker, Advances in Exp. Med. and Biol. **547**, 21 (2004); Y. Xia, H. Yu, R. Jansen, M. Seringhaus, S. Baxter, D. Greenbaum, H. Zhao, and M. Gerstein, Ann. Rev. Biochem. **73**, 1051 (2004); M. Lappe, and L. Holm, Nature Biotechnology **22**, 98 (2004); A.-L. Barabási and Z. N. Oltvai, Nature Rev. - Genetics **5**, 101 (2004).

[110] Y. Ho, A. Gruhler, A. Heilbut, G. D. Bader, L. Moore, Nature **415**, 180 (2002).

[111] X. F. Wang and G. Chen, Int. J. Bifurcation Chaos Appl. Sci. Eng. **12**, 187 (2002); M. Barahona and L. M. Pecora, Phys. Rev. Lett. **89**, 054101 (2002); T. Nishikawa, A. E. Motter, Y.-C. Lai, and F. C. Hoppensteadt, Phys. Rev. Lett. **91**, 014101 (2003); A. E. Motter, C. S. Zhou, and J. Kurths, Europhys. Lett. **69**, 334 (2005); D.-U. Hwang, M. Chavez, A. Amann, and S. Boccaletti, Phys. Rev. Lett. **94**, 138701 (2005); C. Zhou and J. Kurths, Chaos **16**, 015104 (2006).

[112] R. Milo, S. Shen-Orr, S. Itzkovitz, N. Kashtan, D. Chklovskii, and U. Alon, Science **298**, 824 (2002).

[113] K. A. Eriksen, I. Simonsen, S. Maslov, and K. Sneppen, Phys. Rev. Lett. **90**, 148701 (2003).

[114] A. Arenas, A. Díaz-Guilera, and C. J. Pérez-Vicente, Phys. Rev. Lett. **96**, 114102 (2006); S. Boccaletti, M. Ivanchenko, V. Latora, A. Pluchino, and A. Rapisarda, Phys. Rev. E **75**, 045102 (2007).

[115] T. Nishikawa and A. E. Motter, Phys. Rev. E **73**, 065106 (2006); *ibid*, Physica D **224**, 77 (2006).

[116] X.G. Wang, Y.-C. Lai, and C.-H. Lai, Phys. Rev. E **75**, 056207 (2006).

[117] G. Hu, J. Yang, and W. Liu, Phys. Rev. E **58**, 4440 (1998).

[118] Let $\hat{b} = [1\ 1 \cdots]$, $(\hat{b}C^T)_i = \sum_{j=1}^N b_j C^T_{j,i} = \sum_{j=1}^N C_{ij} = 0$, thus $\hat{b}C^T = [0\ 0 \cdots]$. Therefore $\hat{b}C^T\hat{e}_i = \hat{b}\lambda_i\hat{e}_i = \lambda_i \sum_j^N \hat{e}_{i,j} = 0$. If $\lambda_i \neq 0$, then $\sum_j^N \hat{e}_{i,j} = 0$.

[119] J.W. Scannell *et al.*, Cereb. Cortex **9**, 277 (1999)

[120] C. C. Hilgetag *et al*., Phil. Trans. R. Soc. B **355**, 91 (2000); O. Sporns and J. D. Zwi, Neuroinformatics **2**, 145 (2004); C. C. Hilgetag and M. Kaiser, Neuroinformatics **2**, 353 (2004); and C. Zhou, L. Zemanova *et al*., Phys. Rev. Lett. **97** 238103 (2006).

[121] Denoting g_{ij} and g_{ji} the weights of the directed couplings on inter-cluster link (i, j), $i \in V_i$ and $j \in V_j$, and n_i (n_j) the size for cluster V_i (V_j). The average gradient of the cat brain network is calculated as $g_{ave} = \frac{1}{L}\sum_l^L (g_{ij} - g_{ji})$, with L the number of inter-cluster links.

[122] D. J. Watts, P. S. Dodds, and M. E. J. Newman, Science **296**, 1302 (2002); E. Ravasz, A. L. Somera, D. A. Mongru, Z. Oltvai, and A.-L. Barabási, Science **297**, 1551 (2002); V. Spirin and L. A. Mirny, Proc. Natl. Acad. Sci. USA **100**, 12123 (2003); A. E. Motter, T. Nishikawa, and Y.-C. Lai, Phys. Rev. E **68**, 036105 (2003); G. Palla, I. Derényi, I. Farkas, and T. Vicsek, Nature **435**, 814 (2005); E. Oh, K. Rho, H. Hong, and B. Kahng, Phys. Rev. E **72**, 047101 (2005).

[123] See, for example, L. F. Lago-Fernandez, R. Huerta, F. Corbacho, and J. A. Siguenza, Phys. Rev. Lett. **84**, 2758 (2000); X. F. Wang and G. Chen, Int. J. of Bifur. Chaos **12**, 187 (2002); X. F. Wang and G. Chen, IEEE Trans. Circuits Syst. I **49** 54, 2002; M. Barahona and L. M. Pecora, Phys. Rev. Lett. **89**, 054101 (2002); T. Nishikawa, A. E. Motter, Y.-C. Lai, and F. C. Hoppensteadt, Phys. Rev. Lett. **91**, 014101 (2003); A. E. Motter, C. Zhou, and J. Kurths, Europhys. Lett. **69**, 334 (2005); M. Chavez, D.-U. Hwang, A. Amann, H. G. E. Hentschel, and S. Boccaletti, Phys. Rev. Lett. **94**, 218701 (2005).

[124] We address network scalability by focusing on the network's ability to synchronize, not on actual synchronization. If one were to consider actual synchronization, it would be difficult to obtain general results as the synchronization would depend on many specific details such as initial conditions. Thus, when we say that a type of networks is scalable in the sense of synchronization, we mean only that a network can be synchronized, regardless of its size, if the coupling parameter and initial conditions can be adjusted. In contrast, if a class of networks is not scalable, a network absolutely cannot be synchronized if its size exceeds a critical value, regardless of how coupling or initial conditions are adjusted. It is in this sense of scalability which makes the MSF formalism meaningful.

[125] A. Pikovsky, A. Zaikin, and M. A. de la Casa, Phys. Rev. Lett. **88**, 050601 (2002).

[126] E. P. Wigner, Ann. Math. **53**, 36 (1951); T. A. Brody, J. Flores, J. B. French, P. A. Mello, A. Pandey, and S. S. M. Wong, Rev. Mod. Phys. **53**, 381 (1981).

[127] An underlying assumption in our study, as in any previous studies on network synchronization, is that the network must remain connected. The connectedness of a network can be characterized by its eigenvalue spectrum. In particular, a network is connected if λ_2 of the associated coupling matrix is not zero. Thus, insofar as $\lambda_2 > 0$, a typical network is connected. This in turn provides a criterion for connectivity of large random networks: $p > 4/(N+4) \approx 4/N$, which is consistent with the result by Erdös and Rényi [103].

[128] D.-H. Kim and A. E. Motter, Phys. Rev. Lett. **98**, 248701 (2007).

[129] L. F. Lago-Fernandez, R. Huerta, F. Corbacho, and J. A. Siguenza, Phys. Rev. Lett. **84**, 2758 (2000).

[130] L. Donetti, P. I. Hurtado, and M. A. Muñoz, Phys. Rev. Lett. **95**, 188701 (2005).

[131] S. H. Strogatz, Nature (London) **410**, 268 (2001).

[132] M. Girvan and M. E. J. Newman, Proc. Natl. Acad. Sci. USA **99**, 7821 (2002).

[133] D.-H. Kim and A. E. Motter, Phys. Rev. Lett. **98**, 248701 (2007).

[134] L. F. Costa, F.A. Rodrigues, G. Travieso, P. R. Villas Boas, Adv. Phys. **56**, 167 (2007).

[135] F. R. K. Chung, *Spectral Graph Theory* (AMS, Providence, 1994).

[136] E. P. Wigner, Ann. Math. **53**, 36(1951).

[137] F. Chung, L. Lu, and V. Vu, Proc. Natl. Acad. Sci. USA **100**, 6313 (2003).

[138] J. M. Blair, C. A. Edwards, and J. H. Johnson, Math. Comp. **30**, 827 (1976).

[139] For type-II coupling and fixed n, although our theory predicts that Q tends to a constant value for sufficiently large m, Q increases for small values of m.

[140] In a typical situation, the increase of the total size (N) of a clustered network is accompanied by the growth both of the number of clusters and of the number of nodes in individual cluster.

[141] M. Dhamala, V. K. Jirsa, and M. Ding, Phys. Rev. Lett. **92**, 074104 (2004).

[142] E. Ott, *Chaos in Dynamical Systems*, (Cambridge University Press, 1993.)

[143] J. -P. Eckmann and D. Ruelle, "Ergodic theory of chaos and strange attractors," Rev. Mod. Phys. **57**, 617 (1985).

[144] O. E. Rössler, Physics Letters A **57**, 397 (1976).

[145] E. N. Lorenz, J. Atmos. Sci. **20**, 130 (1963).

[146] L. O. Chua, T. Matsumoto, and M. Komuro, IEEE Transactions on Circuits and Systems **32**, 798 (1985).

[147] G. Chen, T. Ueta, Int. J. of Bifurcation and Chaos **9**, 1465 (1999).

[148] A. Stefański, P. Perlikowski, and T. Kapitaniak, Phys. Rev. E **75**, 016210 (2007).

[149] R. Mettin, U. Parlitz and W. Lauterborn, Int. J. of Bifurcation and Chaos **3**, 1529 (1993).